SAPIENZA
UNIVERSITÀ DI ROMA

Human Protein DDX3X: Design, Synthesis and Biological Evaluation of ATPase and RNA-helicase Inhibitors

Dipartimento di Chimica e Tecnologie del Farmaco
PhD. School in Pharmaceutical Sciences

Cycle XXXII

Author

Stefania Ronzini

Supervisor

Prof. Bruno Botta

A.A. 2018-2019

To Professor Maurizio Botta

Abstract

The human ATPase/RNA helicase X-linked DEAD-box polypeptide 3 (DDX3X) emerged as a novel therapeutic target in the fight against infectious disease.

The aim of this work was the study of two new families of DDX3X inhibitors.

The new compounds have been designed starting from the first ATPase DDX3X inhibitors discovered in 2008 from Prof. M. Botta's research group and characterized by a rhodanine scaffold. Replacing their rhodanine moiety, already reported in the list of PAINS, with the 1,3,4-thiadiazole ring a new family of inhibitors was designed, synthesized and tested for its inhibitory action on the ATPase activity of the enzyme. The most promising derivatives has been investigated by evaluating their anti-HIV-1 effects revealing inhibitory activities in the low micromolar range. ADME analysis demonstrated high metabolic stability and aqueous solubility. All the results make these novel compounds a very good starting point for further development.

When the inhibitors of RNA helicase were first discovered they showed activity against HIV-1 drug-resistant strains but their aqueous solubility limited bioavailability in preclinical models, causing its accumulation in fat tissues. A homology model-based virtual screening led to the identification of a new class characterized by sulfonamide moiety with better profile of aqueous solubility and specifically target the helicase activity of DDX3X, accordingly they were inactive in the ATPase assay.

Index

Index of figures

Index of Scheme

Index of table

Chapter 1

INTRODUCTION

RNA Helicase: functions and structure

Helicase protein are a class of highly conserved enzymes essential to all organisms. Discovered for the first time in *Escherichia coli* in 1976[1], the last few years have seen a notable increase in the number of cell biological, genetic, molecular biological, biochemical, biophysical and structural studies on them[2]. The number of helicases expressed in eukaryotic genomes is approximately 1% of the genes. They are involved in all aspects of nucleic acid metabolism, including replication, repair, recombination, transcription, chromosome segregation, and telomere maintenance[3].

Based on the substrates they bind or remodel, helicases can be classified as:

- DNA helicases;
- RNA helicases;
- helicases with functions on both DNA and RNA molecules[4].

The human genome encodes for 95 helicase proteins, of which 64 are RNA helicases and 31 are DNA helicases[5]. All biological processes involving DNA or RNA employ one or more helicases[6,7]; defects in their function as well as deregulated expression of these proteins have been linked to numerous diseases including cancers, developmental defects, and neurodegenerative diseases[8,9].

All the helicases can be classified into six super-families (SFs) based on two structural features: the ring forming helicases comprise SFs 3 to 6, and those not forming rings comprise SFs 1 and 2[10,11].

Most of the helicases belong to the super-families SF1 and SF2, both characterized by a conserved helicase core consisting of two similar protein domains. The helicase core contains characteristic sequence motifs, based on which the original subdivision of helicases in SFs was accomplished. Both SF1 and SF2 encompass defined protein families with distinct sequence, structural, and mechanistic features such as the DEAD-box families in

SF2, or the Pif1-like family in SF1. No comprehensive classification of these families has been reported for either SF.

To date, according to general classification were identified nine families and one group of proteins belonging to SF2, and three families to the SF1 (**Figure 1**). Several proteins (e.g. Suv3) do not fall into a family or group, despite a high level of conservation in eukaryotes or bacteria. The families were named according to terms in use (e.g. DEAD-box), or according to a prominent member (e.g. Ski2-like).

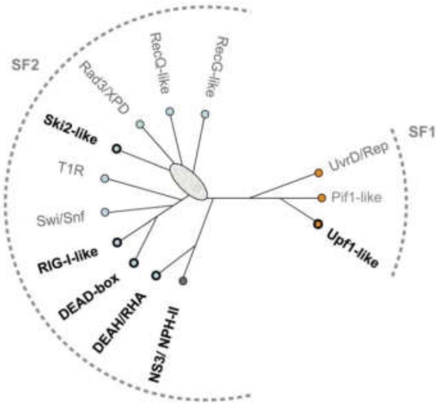

Figure 1
The families of the SF1 and SF2 helicases. Cladogram shows the three identified families of the SF1 (right), and the nine families and one group of the SF2 (left). Branch lengths are not to scale. The oval indicates significant uncertainty in the tree topology in this region.

DEAD-Box

Similarly to all SF2 helicases, DEAD box proteins differ in the amino acid (aa) sequence in their extreme N- and C- terminal parts. They all contain a core helicase domain, which is composed of two covalently linked globular domains, that resemble the bacterial recombination protein recombinase A (RecA), each consisting of five β-strands and five α-helices connected by a flexible linker.

The central catalytic core of helicase is composed of 12 highly conserved motifs that are responsible for the RNA-dependent ATPase and helicase activities. According to the classification of Gorbalenya and Koonin[11] the name "DEAD-box" originates from the single letter amino acid code Asp (D)-Glu (E)-Ala (A)-Asp (D) that is present in the highly conserved motif II (Walker B motif)[12].

Considered as molecular motors, these proteins bind or remodel RNA or RNA–protein complexes (ribonucleoprotein (RNP) complexes) in an ATP-dependent fashion[13].

Each helicase in vivo requires a specific structure of the substrate, interaction with specific proteins in order to participate in a very specific pathway of nucleic acid metabolism. Thus, each helicase must be meticulous in selecting those proteins and substrates with which it will interact. Helicases act in coordination with other proteins/factors and provide molecular motor function.

Like all helicases, they are essential for all aspects of nucleic acid metabolism in both prokaryotes and eukaryotes and have a central and, in many cases, essential physiological roles in the regulation of RNA metabolic processes such as transcription, ribosome biogenesis, translation, RNA splicing, RNA editing, RNA transport and RNA degradation.

The roles that the different DEAD-box proteins can play in a cell are shown in **Figure 2**:

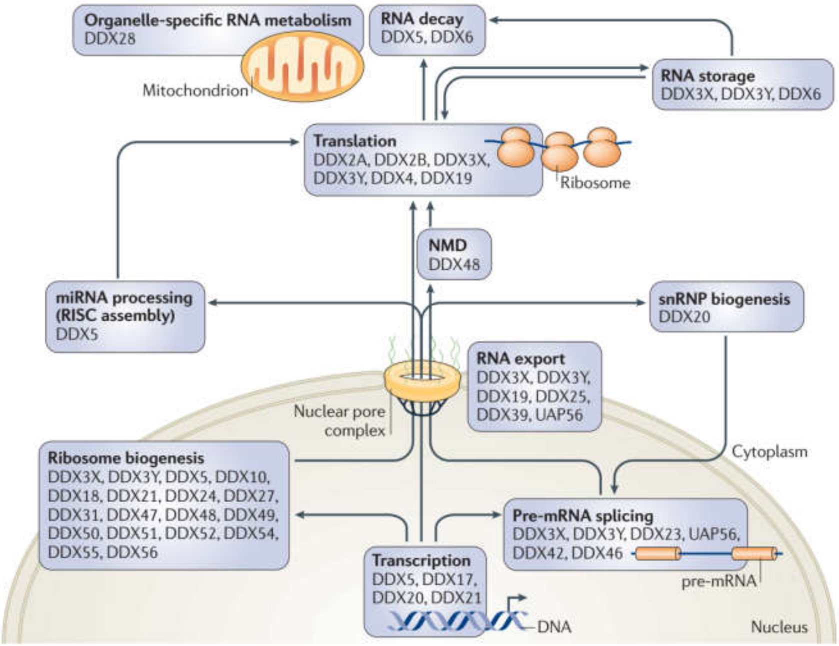

Figure 2

Human DEAD-box proteins that are involved in different steps of RNA metabolism. In the nucleus their presence is crucial for ribosome biogenesis, transcription and pre-mRNA splicing. In the cytoplasm, meanwhile, for processes like microRNA (miRNA) processing, nonsense-mediated decay (NMD) and protein translation, as well as organelle-specific RNA metabolism. At the interface between the nucleus and the cytoplasm, these enzymes are required for the directional transport of mRNA molecules.

The nuclear processes for which the presence of RNA helicase is crucial are:

- transcription. Only few DEAD-box proteins are associated with transcription; DDX20 was shown to be essential for repression of transcription[13,14]. DDX5 and DDX17 were found to act as co-repressors or co-activators of transcription and to interact with different transcription factors and nuclear receptors. DDX5 was recently found to be a co-activator of the transcriptional function of the tumour suppressor p53 in response to DNA damage. The results show that some helicases do not always need their enzymatic activities and that the requirement for enzymatic activities depends on the context helicases are in and the partners they interact with.

- RNA splicing. Necessary to create a mRNA molecule that can be translated into protein. It is a multistep process that requires two trans-esterification which are catalysed by the spliceosome, a complex of small nuclear ribonucleo proteins (snRNPs). Several DEAD-box proteins play crucial roles in the early events of pre-spliceosome assembly and in its progression toward the active spliceosome [15].
- Ribosome biogenesis. In eukaryotes it starts in the nucleolus, continues in the nucleoplasm and ends in the cytoplasm. Many DEAD-box proteins are associated with the process, even if their precise role is still unclear.
- RNA export. Export of mRNA through the nuclear pore requires dedicated proteins to bind mRNA[16]. Several factors have been identified that are associated with this process, and notably the DEAD-box protein DDX19 is one of them[17].

In the cytoplasm their presence is crucial for:

- RNA-induced silencing complex (RISC). It is multiprotein complex, which incorporates one strand of a single-stranded RNA (ssRNA) fragment, such as microRNA (miRNA) or double-stranded small interfering RNA (siRNA). RISC can degrade double-stranded RNA molecules of viral origin, for this process only DDX5 is involved.
- Nonsense-mediated decay (NMD). It is a surveillance pathway that exists in all eukaryotes. Its main function is to reduce errors in gene expression by eliminating mRNA transcripts that contain premature stop codons. DDX48 plays a predominant role for this process.
- Protein translation. DEAD box proteins DDX2A, and their homologues in higher eukaryotes are essential for translation initiation. DDX19 removes proteins from mRNA, after exiting the nucleus.
- Organelle-specific RNA metabolism. Recent reports also suggest that DDX28 resides in RNA granules, and function in assembly of mitochondrial ribosomes (mitoribosomes).
- RNA storage. In the P-bodies untranslated mRNAs are stored for later release. DDX6 is abundant in P-bodies. After formation of translational repressor complex,

DDX6 catalyzes ATP-dependent mRNA unwinding which leads to sequence-independent association with multiple DDX6 molecules. Thereafter, the silenced mRNP is localized to P-bodies and the transcript is either stored and subsequently released for translation or targeted to decapping and degradation.

- RNA decay. In mammalian cells, proteins involved in mRNA silencing and degradation localize to specific cytoplasmic foci called processing or P-bodies. DDX6 present in the P-bodies activates decapping by remodelling mRNPs. They are also required for the accumulation of the mRNA degradation factors in P-bodies. Spliced mRNAs harbouring a premature termination codon (PTC) are degraded by nonsensemediated decay (NMD). In mammals, the termination codon is located at least 50–55 nucleotides upstream of an exon–exon junction. Some mRNAs also possess uORFs or alternative splicing introducing non-sense codons or frameshifts, are also targeted to NMD as well. Degradation is triggered by the exon junction complex (EJC) through recruitment of upstream frame shifting (Upf) proteins forming Upf complex. Several DEAD box proteins are part of NMD. DEAD box protein DDX48 is an integral part of EJC. DDX5 participates in NMD by binding to the Upf complex.
- snRNP biogenesis. snRNPs combines with pre-mRNAs to form spliceosomes. DDX20/Gemin3 plays essential roles in the biogenesis of snRNPs.

DDX3

DDX3, an adenosine 5′-triphosphate (ATP) dependent RNA helicase, is a highly conserved subfamily of the DEAD-box proteins. Known homologues of DDX3 include yeast (Ded1p), Xenopus laevis (An3) and mouse (PL10).

In humans, there are at least two pseudo genes and two DDX3 homologs, DDX3X and DDX3Y[18]. Although DDX3X and DDX3Y share 92% protein sequence identity, they have very different functions and expression patterns in various organs. DDX3Y is located in the azoospermia factor a (AZFa) region of the Y-chromosome, is only expressed in the testes, and plays an important role in male fertility. Deletion of DDX3Y causes azoospermia and cannot be rescued by the DDX3X homologue in humans[19,20]. DDX3X is located on the X chromosome bands p11.3–> p11.23 and is ubiquitously expressed in all human tissues. Functionally, DDX3X appears to be one of the most multifaceted helicases, associated with several roles in immunology and cancer.

DDX3X structure

Structurally DDX3X consists of two recA-like domains (named 1 and 2), connected by a flexible linker, and twelve motifs.

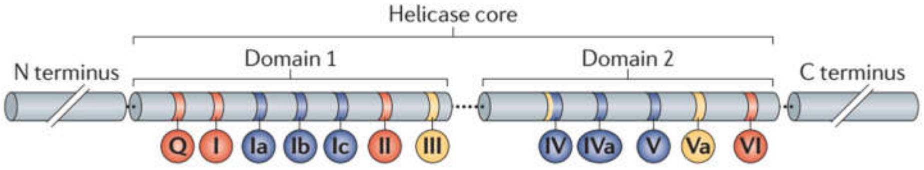

Scheme 1

Schematic representation of RNA helicase DDX3X and conserved motifs. In grey the two domains. The motifs include Q (^{182}F-^{200}YTRPTPVQ), I (^{226}TGSGKT), Ia (^{274}PTRELA), Ib (^{302}GG), Ic (323TPGR), II (^{347}DEAD), III (^{382}SAT), IV (^{445}LVFVET), IVa (^{477}QRDR–^{487}F), V (^{494}ILVAT), Va (^{502}ARGLD), VI (^{527}HRIGRTGR). Conserved amino acid sequences are indicated in parenthesis. Colours coding corresponds to the primary function of the domain: red for ATP binding and hydrolysis, blue for RNA binding, yellow for communication between ATP-binding and RNA-binding sites[21].

Both domains have been shown to possess ATPase and helicase activities experimentally.

The N-terminal domain 1, also known as ATPase domain, is characterized by the presence of motifs Q, I (Walker A), II (Walker B), involved in ATP binding. Motifs Ia, Ib, Ic are implicated in the RNA binding.

The C-terminal domain 2, or helicase domain, contains motifs IV, IVa and V implicated in the RNA-binding. Motif VI is strictly for ATP binding. Motif III of domain 1 and motif Va of domain 2 are crucial for communication between ATP-binding and RNA-binding sites.

In solution DDX3X exists in open or closed conformation, the transition between the two states at each catalytic cycle depends on ATP and RNA binding. The mechanism of activation of the RNA binding site was first described by Schütz et al[22]. They proposed the activation mechanism is characterized by three distinct conformational states named: open, pre-RNA binding and closed conformation.

The DDX3X open conformation (**Figure 3A**) is not able to bind the RNA substrate because the α-helix 8 of the DEAD-motif partially blocks the helicase pocket and domains 1 and 2 are separated each other. After ATP binding the helicase domain 2 rotates by about 180° with respect to domain 1 generating a compact pre-RNA binding conformation (**Figure 3B**). Next, RNA binding to the DEAD-domain completes cleft closure allowing the placement of α-helix 8 out of the RNA binding site (**Figure 3C**). The closed conformation is stabilized by a salt-bridge between the conserved arginine of motif V (Arg 503) and the aspartic acid of the DEAD motif (Asp 350), which is the terminal residue of α-helix 8. ATP hydrolysis and phosphate release switches the α-helix 8 back to the original conformation, allowing the release of the RNA substrate.

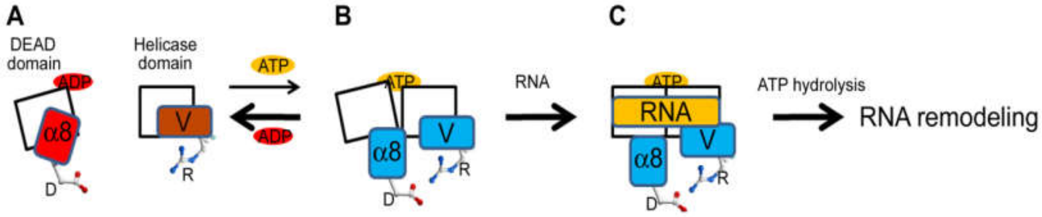

Figure 3
Schematic model for the regulation of RNA binding by a-helix 8 of DEAD-box helicases.
(A) In the isolated domains, reflecting the open and substrate free states, the RNA binding sites are partially blocked by α-helix 8 in the DEAD-domain and motif V in the helicase

domain. The aspartate indicated in the DEAD-domain is the second D of the DEAD sequence in motif II. The arginine indicated in the helicase domain is a conserved residue in motif V. **(B)** Binding of ATP favours closure of the cleft, facilitating interaction of a helix 8 with motif V across the cleft, thereby removing the blockage of the RNA binding site. **(C)** The closed cleft conformation is stabilized by RNA substrate to the competent site, allowing ATP hydrolysis to proceed[22].

DDX3X typically bind ADP with higher affinity than ATP, and binding of ATP and RNA are cooperative. Thus, the binding energy of the RNA protein interaction likely stabilizes a strained conformation that is competent for ATP hydrolysis. Conversely, relief of this strain upon ATP hydrolysis and phosphate release likely drives RNA substrate remodeling. ATP hydrolysis and phosphate release would allow α-helix 8 to move back into its original position, releasing the RNA substrate and switching back to a binding incompetent RNA site on the DEAD domain.

The three-dimensional crystal structure of the human RNA-free conformation of DDX3X has been solved in complex with AMP (**Figure 4, Figure 5**)[23] in 2006, in open conformation.

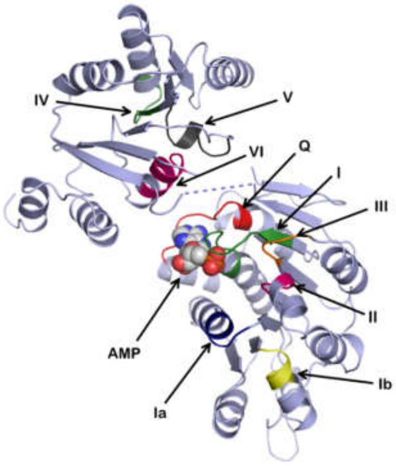

Figure 4
Crystallography structure of DDX3X (V168-G582) (PDB: 2I4I) with AMP as the substrate (12 conserved motifs are indicated with colours).

The interaction of AMP with amino acid residues in the nucleotide-binding pocket of DDX3X (V168-G582) is shown in **Figure 5**. Purine nucleobase stacks over phenyl group of Tyr 200. The adenine moiety of AMP interacts with amino acids in the Q motif (Arg 202 and Gln 207), whereas residues in the P-loop in motif I interact with the phosphate group (Gly 227, Ser228, Gly 229, Lys 230 and Thr 231).

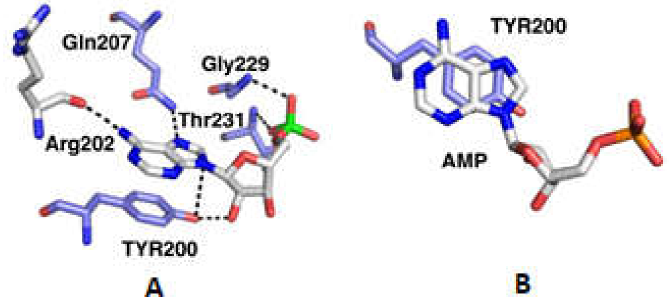

Figure 5

DDX3X interactions with AMP. **(A)**. Hydrogen bond interactions between AMP and amino acid residues of DDX3X ATP binding pocket: the C6 amino group of AMP as a hydrogen bond donor (HD) and the backbone carbonyl oxygen of Arg202 as a hydrogen bond acceptor (HA); the 2′-OH group as well as N9 of AMP (both act as HA) and the phenolic oxygen of Tyr200 (HD); N7 of AMP (HA) and the side chain NH2 group of Gln207 (HD); two phosphate oxygens of AMP (HA) and the backbone NH groups of Gly229 and Thr 231 (HD). **(B)**. π-π stacking interaction between the aromatic ring of AMP and the phenol side chain of Tyr200.

Cellular localization

Is difficult to establish the exact localization of DDX3X protein; several studies have described DDX3X as a protein that constantly shuttles between the cytoplasm and the nucleus, so it is influenced by the balance of import and export[24].

Export from the nucleus is mediated by the importin-β family shuttling factor CRM1 (chromosome maintenance region-1), that contains a leucine-rich nuclear export signal (NES). Recently it has been demonstrated that the export of DDX3X can go also via the tip-associated protein (TAP)-dependent export pathway, the major nuclear mRNA export receptor[25].

Studies based on the inhibition of CRM1[26,27,28] or TAP[29] results high level of DDX3X in the nucleus, suggesting that it can be exported through both pathways. Unfortunately, it is not clear if these two pathways are involved in equal measure in nuclear export of DDX3X, or if one pathway is favoured over the other, possibly it depends on additional co-factors associated with DDX3X or on the cell type.

Presumably due to the high rate of nuclear export, most studies revealed that DDX3 localisation is mainly or exclusively cytoplasmic[30,27]. In contraposition, Chao et al.[30]demonstrated that the localization is mainly nuclear in healthy primary epidermis cells, but largely cytoplasmic in skin tissue from cutaneous squamous cell carcinomas. It suggests discrepancies between transformed and non-transformed cells.

Cellular roles of DDX3X

Although the precise biological function of DDX3X remains elusive, it is involved in various aspects of RNA metabolism, including transcription, translation, unwinding of RNA splicing, RNA transport and RNA degradation, cell cycle regulation, immune response regulation.

Several studies were carried out to clarify the exact role of DDX3X in the mechanism of unwinding of RNA. Studies carried on yeast homologue Ded1p revealed a different mechanism from other translocating helicases[31]. Translocating helicases, e.g. DNA helicases, move along one strand of RNA or DNA directionally and in an energy-dependent manner. In the process, they displace complementary nucleic acid strands and/or interacting proteins. Ded1p unwinds substrates without strict polarity. A new mechanism was proposed in which the separation of the duplex is based on local destabilization of RNA helical regions, meaning that the helicase sitting on the duplex RNA 'switches' the two strands apart. This would be a suitable mechanism for DEAD-box helicases, since they mainly appear to be involved in local structural changes of RNA and ribonucleoprotein (RNP) complexes, involving only a small number of base pairs[31].

Splicing is a fundamental step in eukaryotic gene expression during which introns are excised from pre-mRNA and exons are ligated together to form a continuous reading frame.

It is still unclear whether DDX3X contribute to splicing[32]: several studies revealed that the C-terminus of DDX3X contains a region which resembles arginine-serine rich (RS) domains of splicing factors[33]. The mRNA product generated by splicing is complexed with a currently unknown number of proteins. Splicing is catalysed by the spliceosome. Each spliceosome is composed of five small nuclear RNAs (snRNA) and a range of associated protein factors. When these small RNAs are combined with the protein factors, they make RNA-protein complexes called snRNPs (small nuclear ribonucleo proteins). The snRNAs that make up the major spliceosome are named U1, U2, U4, U5, and U6, so-called because they are rich in uridine, and participate in several RNA-RNA and RNA-protein interactions. DDX3X was reported to be present in functional spliceosomal complexes[34]. The spliceosome is assembled from small nuclear RNAs (snRNA) and approximately 80 proteins. The spliceosome removes introns from a transcribed pre-mRNA, a type of primary transcript. However, DDX3X have been detected with spliced mRNA as part of mRNPs (messenger ribonucleoprotein particles) and it has been demonstrated that it is only associated with spliced mRNAs in an Exon junction complex (EJC)-dependent manner[34]. This suggests that DDX3X does not have an active role in splicing but associates with mRNPs after splicing for roles such as RNA transport. The fact elements of the RNA export machinery associate with mRNPs after splicing gave credence to this hypothesis.

Human protein DDX3X facilitates translation initiation. Studies demonstrated that it interacts with several translation initiation factors, namely eIF4e[35], eIF4a, eIF2a, PABP[29] and eIF3[36].

Several experiments showed an increasing evidence that DDX3X can function in transcriptional regulation of gene promoters. DDX3X up-regulates the interferon (IFN) β promoter and the $p21^{waf1/cip1}$ promoter, respectively. DDX3X binds to the transcription factor Sp1 and enhance the p21waf1/cip1 promoter. On the other hand, DDX3X down-regulates the E-cadherin promoter. *In vivo* association of DDX3X with the E-cadherin or the IFNβ promoter was demonstrated by chromatin immunoprecipitation assay. It is therefore possible that DDX3X regulates individual promoters in different ways and future studies should reveal the exact mechanisms by which DDX3X regulates gene promoter activation and/or suppression.

In eukaryotic cells, RNAs are transcribed in the nucleus and exported to the cytoplasm through the nuclear pore complex (NPC). The NPC is one of the largest protein complexes in eukaryotic cells, penetrating the inner and outer nuclear membrane. The RNA molecules that are exported from the nucleus into the cytoplasm include messenger RNAs (mRNAs), ribosomal RNAs (rRNAs), transfer RNAs (tRNAs), small nuclear RNAs (snRNAs), micro RNAs (miRNAs), and viral mRNAs. Each RNA is transported by a specific nuclear export receptor. The major export pathway of each type of RNA through the NPC are indicated in **Figure 6:**

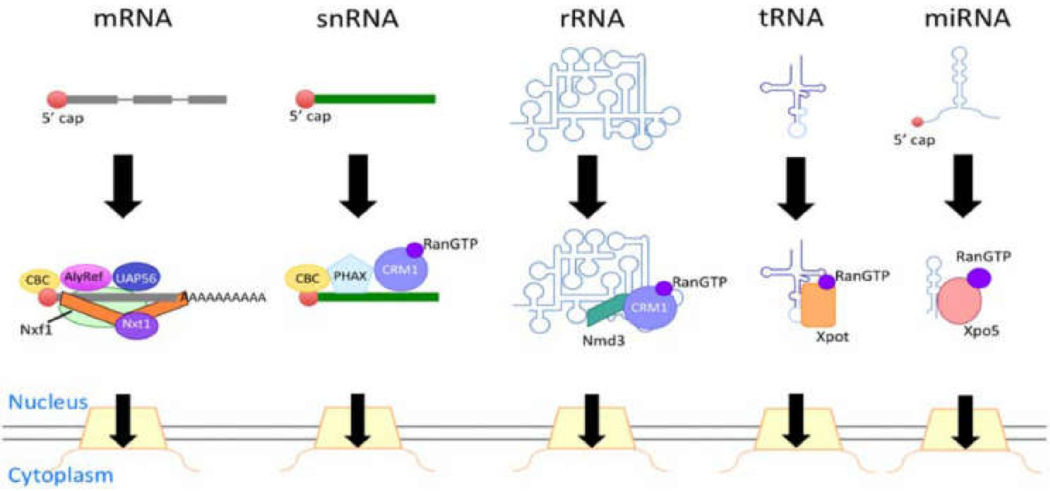

Figure 6

The major routes of RNA export. The transcripts undergo processing and associate with export receptors. This figure shows the representative export receptors for each RNA. CBC: cap-binding complex.

The proteins that compose the NPC are called nucleoporins (Nups). Ions and small molecules can freely diffuse through the pore, but molecules larger than 40–60 kDa pass through the NPC central channel by association with an export receptor such as Nxf1, CRM-1, or other karyopherins. Various RNAs and proteins are exported through the NPC in association with a specific export receptor

DDX3X interacts with two of these export shuttle proteins: CRM-1, the receptor that exports proteins containing a leucine-rich NES, and TAP, the main mRNA exporter. Ribosomal

RNAs and small nuclear RNAs (snRNAs) are exported in a CRM1-dependent manner[37]. The interaction between DDX3X and TAP involved the C-terminus of DDX3X (aa 536–661)[29]. It is still possible that DDX3X participates in the nuclear export of a specific subset of mRNAs via TAP. The CRM1–DDX3X interaction is exploited by HIV which seems to 'tag' its incompletely spliced RNAs to the CRM-1/DDX3X complex for export out of the nucleus. This is mediated via an interaction between the viral RNA-binding protein rev and DDX3X. Hence, DDX3X was shown to be required for the export of HIV RNAs from the nucleus[26]. However, the functional relevance of the CRM1–DDX3X interaction in uninfected cells remains unclear[26], therefore DDX3X does not seem to be a general cofactor of CRM1, the authors postulated that DDX3X is not CRM-1 cargo, but an effector molecule of the pathway. This was based on their finding that DDX3X binding to CRM-1 was Ran-GTP independent and did not require the NES of DDX3X. Rather, the CRM-1 interaction was mediated by aa 260–517 of DDX3[26]. One possibility is that DDX3X mediates the export of specific RNAs through the CRM1 pathway. If DDX3X was needed for the export of snRNA via CRM1 it could indirectly influence splicing by affecting the maturation of snRNAs, which are exported from and re-imported into the nucleus before they assemble with other splicing factors into a functional spliceosome[38]. Given its recently identified role in anti-viral gene expression[27], is clear that DDX3X have a role in mediating the export of these and other immuno-relevant mRNAs.

Several studies were carried out in order to clarify the role of DDX3X also in innate immune response but today the mechanism is still unclear.

DDX3X and viruses

Given the apparent multifunctional nature of DDX3X in the cell, it is thus no surprise to learn that DDX3X appears to be a prime target of viral manipulation, with numerous different viruses known to encode proteins that interact with the helicase and modulate its function.

Viruses are small parasites that cannot grow through cell division or replicate apart because they are acellular, they only produce multiple copies of themselves inside the living cells of an organism. A virus invades living cells and uses their chemical machinery to keep itself alive and to replicate itself.

The lifecycle of viruses differs between species, but there are six common stages in the life cycle of viruses (**Figure 7**):

1. Attachment is a specific binding between viral capsid proteins and specific receptors on the host cellular surface.
2. Penetration follows attachment. In this step virions enter in the host cell through receptor-mediated endocytosis or membrane fusion. This is often called viral entry.
3. Uncoating is the process when the viral capsid is removed: This removal may via degradation by viral enzymes or host enzymes or via simple dissociation. In the end of the process the viral genomic nucleic acid is released.
4. Replication of viruses involves primarily multiplication of the genome. Replication involves synthesis of viral messenger RNA (mRNA) from "early" genes, viral protein synthesis, possible assembly of viral proteins, then viral genome replication mediated by early or regulatory protein expression.
5. Assembly. Following the structure-mediated self-assembly of the virus particles, some modification of the proteins often occurs. In viruses such as HIV, this modification (sometimes called maturation) occurs after the virus has been released from the host cell.
6. Release. Viruses can be released from the host cell by lysis, a process that kills the cell by bursting its membrane and cell wall if present.

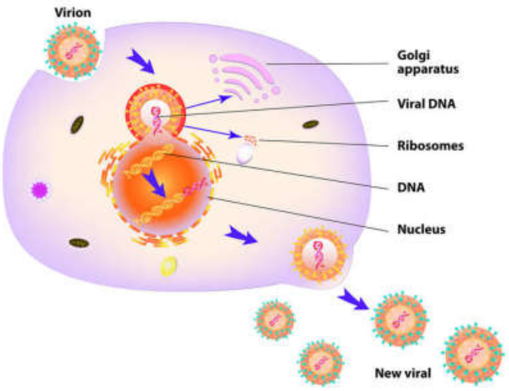

Figure 7
Typical virus replication cycle.

Virus may reproduce with fidelity or with errors (mutations); its ability to mutate is responsible for the faculty of some viruses to change slightly in each infected person, making treatment difficult. Viruses cause many common human infections and are also responsible for several rare diseases. Examples of viral diseases from the common cold, which can be caused by one of the rhinoviruses, to AIDS, which is caused by HIV.

Viruses may contain either DNA or RNA as their genetic material. RNA viruses have an enzyme called reverse transcriptase that permits the usual sequence of DNA-to-RNA to be reversed so that the virus can make a DNA version of itself.

DDX3X plays an important role in the replication of many viruses (**Figure 8**), which can encode one or more of these proteins[11,39.].

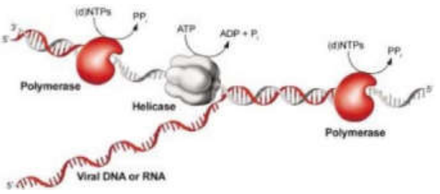

Figure 8

Role of helicase in viral replication. Helicases unwind duplex DNA or RNA intermediates formed during viral replication in a reaction driven by energy derived from the hydrolysis of nucleoside triphosphates.

Because of their limited genome sizes, viruses tend to target key regulators within the host cell machinery to help them replicate. The role of DDX3X in viral replication is exerted at two focal points: **(1)** ATPase-dependent catalytic cofactor for viral replication; **(2)** cellular sensor to trigger or antagonize the antiviral state[40].

Some larger entities can self-encode helicases, whereas size-constrained, smaller viruses can adapt to use a host cellular helicase. In general, RNA viruses that replicate in the cytoplasm mostly self-encode a helicase, whereas those that replicate in the nucleus often utilize a cellular helicase[41]. On these bases human helicases are considered promising targets for the development of new antiviral agents[7].

Considering the multifunctional nature of DDX3X in the cell, it is clear that DDX3X appears to be a prime target of viral manipulation, with numerous different viruses known to encode proteins that interact with the helicase and modulate its function[42].

DDX3X & HIV-1

HIV continues to be a major global public health issue. In 2017 an estimated 36.9 million people were living with HIV. The vast majority of people living with HIV are located in low and middle income countries, with an estimated 66% living in sub-Saharan Africa. Among this group 19.6 million are living in East and Southern Africa which saw 800,000 new HIV infections in 2017.

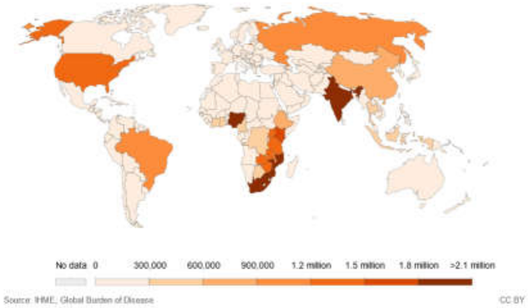

Source: IHME, Global Burden of Disease

CC BY

Figure 9

Number of people living with HIV, 2017

The human immunodeficiency viruses (HIV) are two species of *Lentivirus* (a subgroup of retrovirus) that causes HIV infection and over time acquired immunodeficiency syndrome (AIDS). Following initial infection, a person may not notice any symptoms, as the infection progresses, it interferes more with the immune system, increasing the risk of developing common infections such as tuberculosis, as well as other opportunistic infections, and tumours that rarely affect people who have uncompromised immune systems.

Without treatment, average survival time after infection with HIV is estimated to be 9 to 11 years, depending on the HIV subtype. In most cases, HIV is a sexually transmitted infection and occurs by contact with or transfer of blood, pre-ejaculate, semen. Non-sexual transmission can occur from an infected mother to her infant during pregnancy, during childbirth by exposure to her blood or vaginal fluid, and through breast milk[43,44]. Within these bodily fluids, HIV is present as both free virus particles and virus within infected immune cells.

DDX3X is an essential host factor for HIV replication. HIV-1 gene expression is substantially governed post-transcriptionally by Rev-regulated export of unspliced and partially spliced RNAs from the nucleus into the cytoplasm. The Rev protein binds a highly structured RNA element called the Rev responsive element (RRE) that is present in all unspliced and partially spliced HIV transcripts. This binding distinguishes, for purposes of nuclear export, viral transcripts from cellular RNAs. While performing this RNA transportation role, Rev interacts with the nuclear export receptor CRM1 (chromosome maintenance region 1)[26]. Knockdown of DDX3X inhibited the export of these unspliced and partially spliced HIV RNAs from the nucleus, resulting in impaired HIV replication. The function of DDX3X in this process was dependent on its helicase activity and that DDX3X interacted with nucleoporins and localised with the cytoplasmic side of nuclear pores. Following the initial delivery of the HIV RNAs by Rev/CRM1 into the nuclear pore, the enzymatic unwinding action of DDX3 facilitates the final release of the HIV-1 RNAs from the cytoplasmic side of the pore[26]. Confirmations that knockdown of DDX3X in cells inhibits HIV replication without affecting cell viability arrived[45]. These results revealed that DDX3X exhibited a positive regulatory function in Rev-independent gene expression and HIV-1 IRES-mediated translation, implying other roles for the helicase in the viral lifecycle[45] (**Figure 10**).

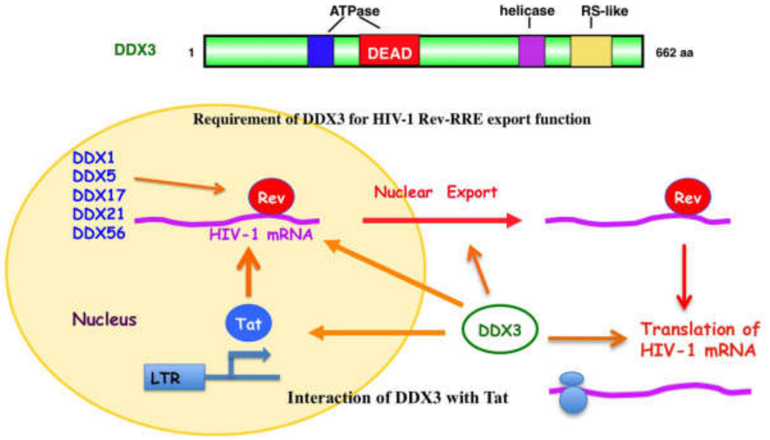

Figure 10

Role of DDX3X in the HIV-1 gene expression. DDX3 interacts with HIV-1 Rev and facilitates the Rev-dependent nuclear export of HIV-1 mRNA. DDX3 interacts with Tat and contributes to the translation of HIV-1 mRNA. Other DEAD-box RNA helicases, including DDX1, DDX5, DDX17, DDX21, and DDX56, also interact with HIV-1 Rev and facilitate its function

The importance of DDX3X in the HIV lifecycle encouraged many research groups to target the helicase with antiviral compounds. The first small-molecule inhibitors directed at the ATPase activity of DDX3X which inhibit HIV replication were successfully developed[26,46], then later the identification of the first small-molecules specifically designed to inhibit HIV-1 replication by targeting the RNA binding site of DDX3X arrived in 2012[47].

DDX3X & Flavivirus

In the general classification of flaviviruses (family *Flaviviridae*; genus *Flavivirus*) there are two main groups of viruses: those transmitted by ticks and those transmitted by mosquitoes. The tick-borne flaviviruses are a closely related, monophyletic group consisting of a single "serocomplex", despite distinct differences in the disease caused by representative viruses. On the contrary several mosquito-borne viruses are known, among them West Nile virus (WNV), Dengue virus (DENV), Japanese Encephalitis virus (JEV), Yellow Fever virus (YFV)[48].

Flaviviruses are considered as major human pathogens (**Figure 11**) and the diseases they cause have been recognized for many years. The tick-borne flaviviruses cause of number of significant diseases in humans associated with neurological symptoms, although some of these viruses are associated with haemorrhagic manifestations following infection. The variability of arthropod vectors, disease characteristics and the wide geographic distribution of the flaviviruses makes these viruses especially interesting, particularly if one considers that most people throughout the world live in a flavivirus endemic region. The ease with which these viruses can be introduced into new environments highlights the need for extensive additional research on them.

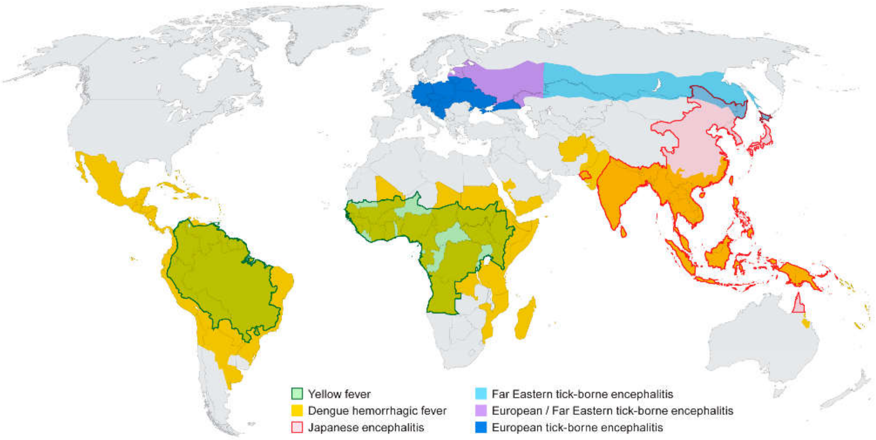

Figure 11

Distribution of major flaviviruses. Information was adapted from data and figures provided on Centres for Disease Control and Prevention (CDC) and World Health Organization (WHO) websites.

Flaviviruses are characterized by similar structural and functional aspects: common size (40–65nm), symmetry (enveloped, icosahedral nucleocapsid), nucleic acid (positive-sense, single-stranded RNA), and appearance in the electron microscope. In general, the genome encodes 3 structural proteins (Capsid, prM, and Envelope) and 7 non-structural proteins (NS1, NS2A, NS2B, NS3, NS4A, NS4B, NS5)[49](**Figure 12**).

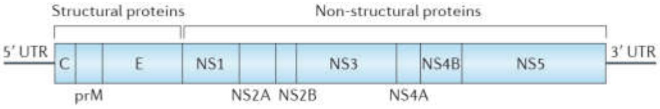

Figure 12

Flavivirus genome organization. At the 5′ end of the ORF (open reading frame) there are the core (C; encoding the capsid), pre-membrane (prM) and envelope (E) proteins, which together make up the viral particle and are referred to as structural proteins. The remaining nonstructural (NS) proteins are expressed during replication.

Most of these viruses are classified as arboviruses because they are transmitted by the bite from an infected arthropod (mosquito or tick). Other virus transmission routes for arboviruses include handling infected animal carcasses, blood transfusion, childbirth and consumption of unpasteurised milk products. Transmission from nonhuman vertebrates to humans without an intermediate vector arthropod is thought to be unlikely. For example, early tests with yellow fever showed that the disease is not contagious.

DDX3X & West Nile virus (WNV)

West Nile virus (WNV) is a neurotropic arbovirus member of Flaviviridae family. Since its introduction in Europe and America the number of novel infections is increasing, counting during 2017, 204 novel reported cases in Europe and 2002 in America. The number is impressive considering that about 80% of WNV infections is usually asymptomatic and only the remaining 20% may cause meningitis, encephalitis, or rarely death in 1%. In addition, probably due to climate warming, the number of novel human cases sharply increased in EU member states during the current year, reaching 710 infections and 63 deaths as of 30 August. The rapid diffusion of WNV is dependent on its zoonotic life cycle, which involves migratory birds, Culex and Aedes mosquitos, and mammals including horses and humans. In this context, inadequate vector control, globalization, and human travel networks are only a few factors that are contributing to this and other arboviruses spreading. Despite continuous efforts being made to identify new drugs or vaccines, no specific therapy or prophylaxis is actually available on the market and the treatment remains symptomatic. In this context, a drug repurposing strategy provided new drug candidates to fight emerging and re-emerging viruses but often the antiviral compounds are poorly active or are directed on viral enzymes and are thus generally characterized by a low genetic barrier to resistance. In the last few years DDX3X protein has been identified as a component of critical host-cell pathways, hijacked by several pathogenic human viruses. DDX3X, an adenosine 5′-triphosphate (ATP)-dependent RNA helicase, is involved in many aspects of RNA metabolism, such as transcription, translation, and RNA decay. It localizes to P-bodies, cytoplasmic foci related to mRNA turnover that are disrupted in response to the infection of viruses such as WNV. Furthermore, after WNV infection, DDX3X was released from P-bodies and co-localized at a perinuclear region with viral NS3. It was found moreover, that DDX3X knockdown strongly decreased WNV replication, suggesting an important implication not yet completely understood. Although its role in the life cycle of different viruses was extensively studied, only few DDX3X inhibitors have been published as antiviral agents and the mechanism of action is clearly described only for HIV-1[50].

DDX3X & Dengue virus

Dengue virus (DENV) is the cause of dengue fever. It is a mosquito-borne, virus of the family Flaviviridae; genus Flavivirus. Five serotypes of the virus have been found[51], all of which can cause the full spectrum of disease[52].

Dengue virus has increased dramatically within the last 20 years, becoming one of the worst mosquito-borne human pathogens with which tropical countries must deal. Current estimates indicate that as many as 390 million infections occur each year, and many dengue infections are increasingly understood to be asymptomatic or subclinical[53].

The structure of the dengue virus is roughly spherical, with a diameter of approximately 50 nm (**Figure 13**). The core of the virus is the nucleocapsid, that it is surrounded by a membrane called viral envelope, a lipid bilayer that is taken from the host. In the viral envelope there are 180 copies of the E and M proteins forming a protective outer layer that controls the entry of the virus into human cells.

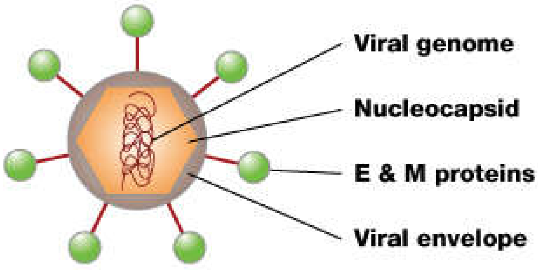

Figure 13
Dengue virus structure.

Recent studies revealed the plausible mechanism of interaction of DDX3X and dengue viruses: it was demonstrated that the N-terminal region of capsid is important for interaction with DDX3X, while the N-terminal domain of DDX3X seems to be involved in interaction with dengue capsid[54]. DDX3X was down regulated in dengue virus infected cells at later stages of infection. The results show that DDX3X is an antiviral protein as suppression of DDX3X expression by siRNA led to an increase in viral titers and overexpression of DDX3X led to inhibition of viral replication. Knock-down of DDX3X did not affect induction of type I interferon response upon infection suggesting that the effect of DDX3X knock-down is independent of the interferon-dependent pathways that DDX3X modulates under normal conditions. This study identifies DDX3X as a dengue virus capsid interacting protein and indicates a potential link between the antiviral functions of DDX3X and dengue capsid at later stages of dengue infection.

DDX3X & Japanese Encephalitis virus (JEV)

Japanese encephalitis is the most commonly diagnosed epidemic encephalitis in the world. The most comprehensive estimate of incidence within the past decade suggests that 69,000 cases of Japanese encephalitis occur every year. Japanese encephalitis is caused by Japanese encephalitis virus (JEV), a member of the *Japanese Encephalitis serocomplex* of 9 genetically and antigenically related viruses, some which are particularly severe in horses, and four known to infect humans[54]. To date, no trials on Japanese encephalitis have translated into improvements in treatment; however, in total, only 381 patients with proven Japanese encephalitis have been randomly assigned in treatment trials. Although vaccines for Japanese encephalitis are available, the disease will never be eradicated owing to its zoonotic cycle. Moreover, its propensity to cause unpredictable outbreaks in unexpected places make vaccination planning challenging, underscoring the need to develop treatments for this devastating condition. JEV is a single-stranded, positive-sense RNA virus[55], features that it shares in common with other flaviviruses.

It has been noted that Japanese encephalitis infects the lumen of the endoplasmic reticulum (ER)[56,57] and rapidly accumulates substantial amounts of viral proteins.

In order to determine whether DDX3X is involved in the JEV infection, the endogenous DDX3X expression was first silenced and found that JEV replication was significantly reduced. On these bases was determined that the helicase activity is crucial for JEV replication by studying the effects of the helicase dead DDX3X mutants and DDX3X inhibitor on virus replication. Furthermore, was also demonstrated that DDX3X could interact with JEV NS3, NS5 and found that DDX3X could bind to the JEV 5′and 3′un-translated regions (UTR) and colocalize with viral RNA during viral infection[58].

Antiviral drug resistance

Commonly, a virus is said susceptible to un antiviral drug when an antiviral drug itself is fully effective against it. Viruses are constantly changing and can sometimes modify in ways that might make antiviral drugs work less well or not work at all against these viruses. When a virus changes in the active site where an antiviral drug works, that virus shows reduced susceptibility to that antiviral drug. Reduced susceptibility can be a sign of potential antiviral drug resistance. Antiviral drugs may not work as well in viruses with reduced susceptibility.

A clear example of antiviral drug resistance is HIV. The treatment of HIV consists in a combination of drugs called antiretroviral therapy (ART), which work by stopping the virus replicating in the body. In this way the immune system can repair itself and prevent further damage. Because HIV can quickly adapt and become resistant, a combination of HIV drugs is used. The classes of anti-HIV drugs include:

- non-nucleoside reverse transcriptase inhibitors (NNRTIs) turn off a protein needed by HIV to make copies of itself. Examples include efavirenz (Sustiva), etravirine (Intelence) and nevirapine (Viramune).
- Nucleoside or nucleotide reverse transcriptase inhibitors (NRTIs) are faulty versions of the building blocks that HIV needs to make copies of itself. Examples include Abacavir (Ziagen), and the combination drugs emtricitabine/tenofovir (Truvada), Descovy (tenofovir alafenamide/emtricitabine), and lamivudine-zidovudine (Combivir).
- Protease inhibitors (PIs) inactivate HIV protease, another protein that HIV needs to make copies of itself. Examples include atazanavir (Reyataz), darunavir (Prezista), fosamprenavir (Lexiva) and indinavir (Crixivan).
- Entry or fusion inhibitors Tblock HIV's entry into CD4 T cells. Examples include enfuvirtide (Fuzeon) and maraviroc (Selzentry).

- Integrase inhibitors work by disabling a protein called integrase, which HIV uses to insert its genetic material into CD4 T cells. Examples include raltegravir (Isentress) and dolutegravir (Tivicay).

On these bases the development of novel antiviral agents with different mechanism of actions is necessary.
Considering that host cellular proteins are less prone to mutate than viral ones, this strategy will provide new targets of research in the field of antivirals, which could help to overcome the drug resistance issue[59].

DDX3X in cell cycle regulation and tumorigenesis

The eukaryotic cell cycle consists of four phases: G_1 phase, S phase (synthesis), G_2 phase (collectively known as interphase) and M phase (mitosis and cytokinesis). Activation of each phase is dependent on the proper progression and completion of the previous one.

The cell cycle is driven by a series of cyclin-dependent kinases (Cdks), which are activated via association with their respective cyclin partners. Cyclins D and E are specific for cell cycle progression from G_1 to S phase. DDX3X plays a crucial role in cell cycle control.

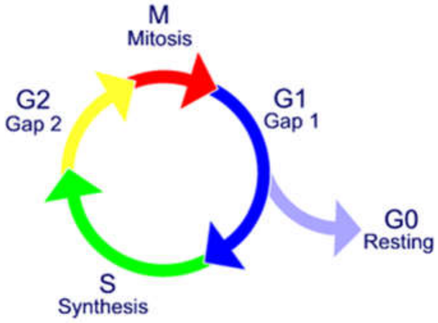

Figure 14
Cell cycle times for human cell. The figure shows the fraction of the cell cycle devoted to each of the primary stages of the cell cycle. The area of each chart is proportional to the overall cell cycle duration.

Lee group and Y-H Wu Lee group reported that knockdown of DDX3X expression reduces growth and proliferation, impeding the G1/S-phase transition of the cell cycle through cyclin D1 and cyclin E1 mRNA translation. This data apparently suggested that knockdown of DDX3 decelerated cell cycle progression by preventing entry into S phase.

Tumorigenesis

Recently, DDX3X is getting increasing attention due to its oncogenic roles in many cancer subtypes[60,61,62,63], anti-apoptotic properties[64,65] and to have a role in cell cycle progression[60,61], migration[66] and invasion[67].

Accordingly, DDX3X may be a new potential target for cancer biotherapy but, the roles of DDX3X in cancer development are rather complicated. As a ‘double-edged sword’ gene, DDX3X either promotes cancer progression or acts as a tumour suppressor in some cancer types. The biological roles of DDX3X in cancer development are conflicting. Notably, the dual roles of DDX3X are reported not only in different types of cancer but also in the same type of cancer. The divergent roles of DDX3X in multiple cancer progression (**Table 1**) are briefly discussed in the specific cancer as follows.

Table 1
Summary of DDX3 roles in cancer.

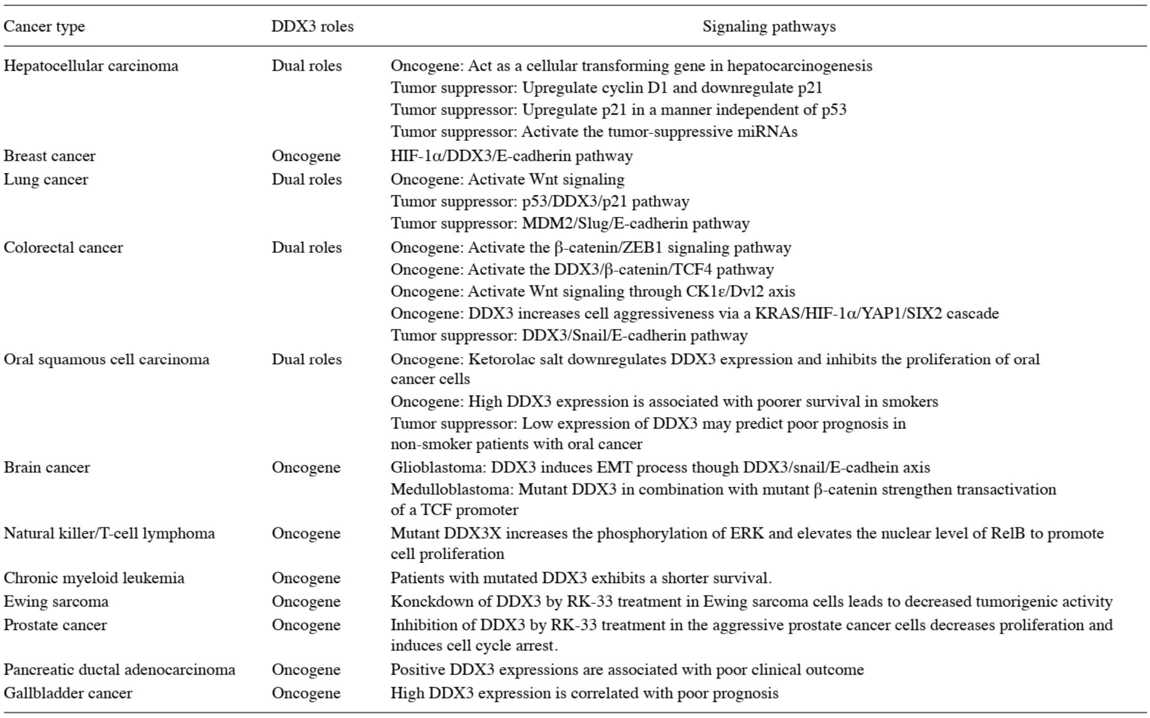

Cancer type	DDX3 roles	Signaling pathways
Hepatocellular carcinoma	Dual roles	Oncogene: Act as a cellular transforming gene in hepatocarcinogenesis Tumor suppressor: Upregulate cyclin D1 and downregulate p21 Tumor suppressor: Upregulate p21 in a manner independent of p53 Tumor suppressor: Activate the tumor-suppressive miRNAs
Breast cancer	Oncogene	HIF-1α/DDX3/E-cadherin pathway
Lung cancer	Dual roles	Oncogene: Activate Wnt signaling Tumor suppressor: p53/DDX3/p21 pathway Tumor suppressor: MDM2/Slug/E-cadherin pathway
Colorectal cancer	Dual roles	Oncogene: Activate the β-catenin/ZEB1 signaling pathway Oncogene: Activate the DDX3/β-catenin/TCF4 pathway Oncogene: Activate Wnt signaling through CK1ε/Dvl2 axis Oncogene: DDX3 increases cell aggressiveness via a KRAS/HIF-1α/YAP1/SIX2 cascade Tumor suppressor: DDX3/Snail/E-cadherin pathway
Oral squamous cell carcinoma	Dual roles	Oncogene: Ketorolac salt downregulates DDX3 expression and inhibits the proliferation of oral cancer cells Oncogene: High DDX3 expression is associated with poorer survival in smokers Tumor suppressor: Low expression of DDX3 may predict poor prognosis in non-smoker patients with oral cancer
Brain cancer	Oncogene	Glioblastoma: DDX3 induces EMT process though DDX3/snail/E-cadhein axis Medulloblastoma: Mutant DDX3 in combination with mutant β-catenin strengthen transactivation of a TCF promoter
Natural killer/T-cell lymphoma	Oncogene	Mutant DDX3X increases the phosphorylation of ERK and elevates the nuclear level of RelB to promote cell proliferation
Chronic myeloid leukemia	Oncogene	Patients with mutated DDX3 exhibits a shorter survival.
Ewing sarcoma	Oncogene	Konckdown of DDX3 by RK-33 treatment in Ewing sarcoma cells leads to decreased tumorigenic activity
Prostate cancer	Oncogene	Inhibition of DDX3 by RK-33 treatment in the aggressive prostate cancer cells decreases proliferation and induces cell cycle arrest.
Pancreatic ductal adenocarcinoma	Oncogene	Positive DDX3 expressions are associated with poor clinical outcome
Gallbladder cancer	Oncogene	High DDX3 expression is correlated with poor prognosis

Hepatocellular carcinoma (HCC). DDX3X is essential for the replication of hepatitis B virus (HBV) and hepatitis C virus (HCV) which are two types of hepatitis virus usually linked to hepatocellular carcinoma (HCC)[68,69]. DDX3X has diverse roles in HCC development. DDX3X overexpression was observed in HCC, and it was identified as a cellular transforming gene in hepatocarcinogenesis[70]. In contrast, Chang et al found that a decreased expression level of DDX3X is present in HBV-positive HCC patients, but not in the HCV-positive ones[60]. On these bases, they proposed a mechanism of DDX3X where the inhibition of DDX3X upregulates cyclin D1 and downregulates p21waf1/cip1, and thereby promotes S phase entry to facilitate tumour cell growth. Other research demonstrated that DDX3X inhibits cell colony formation ability of HCC HuH-7 cells by upregulating p21waf1/cip1 in a p53-independent manner[71]. A recent study supports DDX3 as a tumour suppressor in HCC, since DDX3X downregulation promotes stem cell-like properties and tumorigenesis by silencing the tumour-suppressive miRNAs in HepG2 cells[72]. In addition, the decrease of DDX3X correlates with poor prognosis of HCC patients.

Breast cancer. Upregulation of DDX3X can increase cell growth, proliferation and epithelial-mesenchymal-like transformation (EMT) in normal breast epithelial MCF10A cells[73]. In a similar way, HIF-1α induces the transcriptional activation of DDX3X via binding to the HIF responsive element located in the DDX3X promoter region in MCF10A cells[74]. Moreover, DDX3X is overexpressed in a large series of breast cancer patients[75], and DDX3X upregulation is correlated with distant metastases of breast cancer[76], while DDX3X knockdown decreases tumour volume and metastasis in vivo[77]. In addition, a combination treatment using DDX3X and PARP inhibitors induces cooperative therapeutic effects in BRCA1-proficient breast cancer[78]. Thus, DDX3X drives breast cancer carcinogenesis and it can be a potential treatment target for breast cancer.

Lung cancer. In lung cancer, DDX3X seems to have antitumor activity in human papillomavirus (HPV)-positive lung cancer. HPV E6 decreases DDX3X transcription to synergistically suppress p21 expression, thereby low level of DDX3X leads to a poor relapse-free survival (RFS) in early-stage lung cancer and non-small cell lung cancer patients[79]. Furthermore, loss of DDX3 suppressed E-cadherin by MDM2/Slug axis to promote tumour progression and metastasis in HPV-infected lung cancer cells[80]. However, DDX3X is also reported to overexpress in lung cancer, and DDX3X upregulation is related with shorter survival for lung cancer patients[81]. While DDX3X downregulation decreases colony formation in lung A549 cells. To date, DDX3X roles are variable in lung cancer. It is still likely that DDX3X should be considered as a drug target for lung cancer therapy.

Colorectal cancer. The conflicting role of DDX3X in colorectal cancer needs to be further explored: it is inaccurate to predict survival outcomes of colorectal cancer patients only using the protein DDX3X due to its multiple functions in cancer development. It seems more feasible to jointly analyse several proteins, including DDX3 and its associated molecules, with colorectal cancer progression and prognosis.

Other cancers. DDX3X is also usually increased in the Ewing sarcoma[82], prostate cancer[83], glioblastoma[84], pancreatic ductal adenocarcinoma[85] and gallbladder cancer[86]. However, the molecular mechanism of DDX3X using oncogenic functions in these cancers requires further study and discussion.

Concluding, DDX3X possesses several functional domains with kinase activities that allow to be designed as new drug targets by docking small molecular inhibitors[87]. In recent years there is a new increasing interest to develop more small molecular inhibitors targeting DDX3 as potential target chemical drugs for cancer therapy.

Hypoxia

The process of tumour progression is characterized by rapid cellular growth, displaying many structural and functional abnormalities leading to tumour hypoxia[88,89]. Hypoxia inducible factor-1 (HIF-1) is a transcription factor, crucial in cellular survival during hypoxia and is associated with tumour progression and metastasis in various solid tumours. The DDX3X promoter has three HIF-1 responsive elements (HRE)[75] to which HIF-1α binds. Under hypoxic conditions HIF-1α promotes DDX3X expression through promoter activation at the most proximal HRE to the transcriptional start site[83]. In breast cancer patient samples, DDX3X is strongly correlated to hypoxia markers, specifically HIF-1α.

Apoptosis

Only few studies have presented data concerning DDX3X's role in apoptosis. Chang et al.[90] observed that DDX3X downregulation promoted cell proliferation and anti-apoptosis. They also found that key elements of the intrinsic apoptotic pathway, caspase-6 and caspase-9, cannot be activated in the absence of DDX3X[90]. On the contrary Sun et al.[91], described an anti-apoptotic death receptor complex comprising glycogen synthase kinase-3 (GSK3), cellular inhibitor of apoptosis protein-1 (c-IAP1) and DDX3X. Stimulated death receptors can surmount this complex by inactivating GSK3 and cleaving DDX3X and c-IAP1, enabling progression of the apoptotic signalling cascade. This study also reported that DDX3X knockdown enhanced signalling through the death receptor TRAIL-R2 and activation of caspase-3[91].

Given this limitation, clarification of the role of DDX3X needs to be addresses by further studies.

State of the art

In the last decade Prof. M. Botta's research group has been involved in the study of new inhibitors of DDX3X protein.

DDX3X has multiple enzymatic activities (ATPase and RNA helicase) and functional domains that may be targeted by potential inhibitors[23,92]. Drug discovery activity in this area has been mostly oriented towards both ATPase inhibitors and RNA helicase inhibitors[47,50,93,94].

The structures of known DDX3X ATPase inhibitors are shown in **Figure 15.** The first ATPase DDX3X inhibitors have been discovered in 2008[46]. Among them, FE15 was identified through a virtual screening approach. This compound, characterized by a rhodanine scaffold, showed low micromolar potency of inhibition against the DDX3X ATPase activity and was able to inhibit the HIV-1 replication in MT4 cells with an EC_{50} of 86.7 μM, without showing cytotoxicity. Similarly, the ring expanded nucleosides (RENs) were found able to inhibit the ATP dependent activity of DDX3X and to suppress HIV-1 replication in T cells and monocyte-derived macrophages[95]. In 2011, through a hit optimization protocol the second generation of rhodanine DDX3X inhibitors were identified endowed with an improved activity profile (as an example FE109 showed a Ki of 0.2 μM) [96]. In parallel, some REN derivatives were synthesized, among them compound NZ51 has been reported to inhibit the ATP dependent helicase activity of DDX3X as well as the proliferation of cancer cells expressing high levels of DDX3X[77]. Raman and coworkers have recently reported compound RK-33 containing the diimidazo[4,5-d;4′,5′-*f*][1,3]diazepine ring. RK-33 has been extensively studied as an anticancer compound, and its spectrum of activity includes different tumor cell lines derived from lung (A-549 and H-460), prostate (PC-3), breast (MCF-7 and MDA-MB-231) and ovarian (OVCAR-3) cancers[63,97,98]. At the same time, ketorolac salt has been identified as a novel DDX3X inhibitor able to affect the ATPase activity and endowed with anticancer activity against oral squamous cell carcinoma (OSCC) cell lines[99].

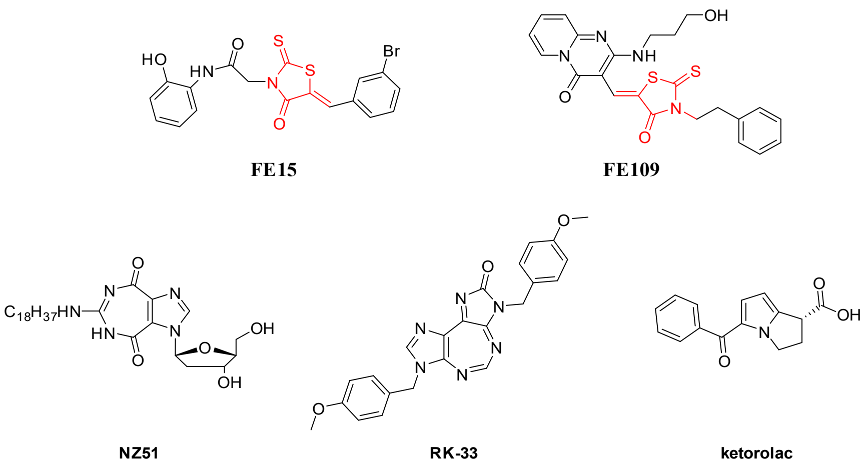

Figure 15

2D Structures of previously identified DDX3X ATPase inhibitors.

Docking simulations were performed on the known ATPase DDX3X inhibitors, RK33 and Ketorolac in order to study the key molecular interactions at the basis of their inhibitory activity and the predicted binding modes were compared to those previously published for the active rhodanine derivative FE15 as well as with that of the crystallized ligand AMP (**Figure 16**). Calculations were performed according with the protocol already published[46].

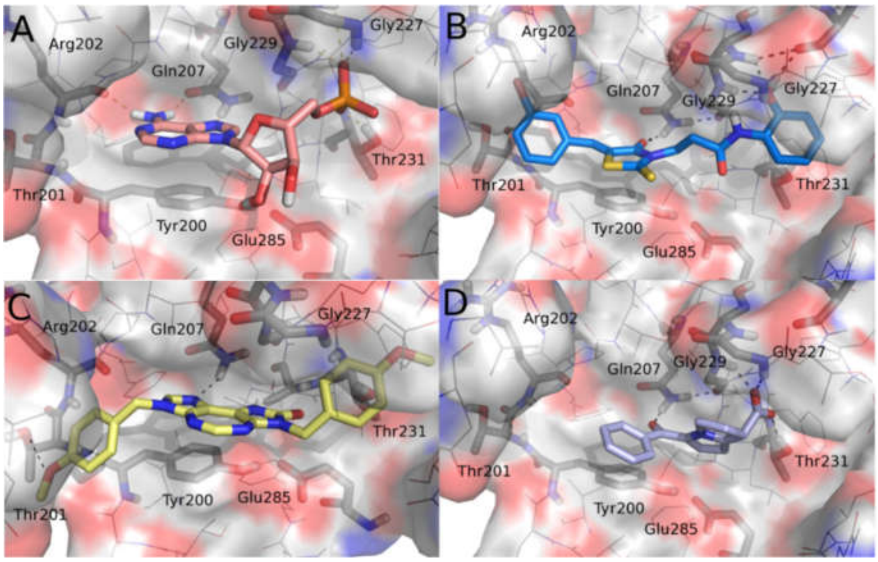

Figure 16

Binding poses of **A**) AMP (salmon), **B**) FE15 (blue), **C**) RK-33 (yellow) and **D**) ketorolac (periwinkle) into the ATP pocket of human DDX3X. For the sake of clarity, only a few key residues are labeled, hydrogen atoms are omitted, and hydrogen-bonding interactions are represented by black dashed lines. Compounds and key amino acids are in stick representation.

In detail, the studied inhibitors established a hydrogen bond with Gln207 and a π-π interaction with Tyr200 that thus resulted to be crucial for their inhibitory activity. Furthermore, FE15 and ketorolac made polar contacts with Gly227 and Gly229, mimicking the phosphate group of AMP. Ketorolac, being endowed with an acidic group, better reproduced the phosphate interactions and indeed additionally interacted with Thr231. Both FE15 and RK-33 also occupied a region delineated by the amino acids Thr201 and Arg202.

The rhodanine group included in the previous hit compound, FE15, was discarded. Indeed, rhodanine derivatives are promiscuous binders which have been associated with multiple biological activities. Furthermore, rhodanines have been described as PAINS and highly problematic frequent hitters[100,101].

As mentioned before[22], DDX3X needs to switch through three different conformational states to carry out its functions: in the first step, the open conformation is unsuitable to bind the RNA substrate; in the second step, after ATP-binding, a more stable conformation namely pre-RNA binding state is obtained. Finally, the last step occurs after RNA binding. This interaction stabilizes the closed conformation and allows the placement of the substrate.

In 2012 a theoretical 3D structure of human DDX3X in its pre-RNA binding conformation has been generated and was then used to perform a virtual screening approach, which led to the identification of the first human DDX3X helicase inhibitor EI01D able to inhibit the helicase activity of human DDX3X at low micromolar concentration.

Compound EI01D showed both antihelicase activity against DDX3X (IC_{50} = 1 μM) and inhibitory effects on HIV-1 replication in peripheral blood mononuclear cells [half-maximal effective concentration (EC_{50}) = 10 μM].

Because of the lack of a crystal structure of human DDX3 bound to RNA (closed conformation), an homology model was built using the closed conformation of *Drosophila Vasa* DEAD-box helicase (Protein Data Bank ID code 2DB3) as a template (**Figure 17**)[59].

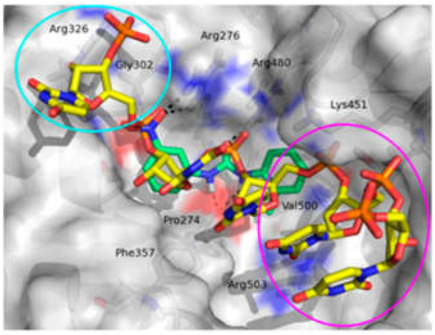

Figure 17
Graphical representation of the DDX3X RNA binding site. The RNA strand is represented as yellow carbon sticks. The binding mode of EI01D (green carbon sticks) was predicted by docking studies. Hydrogen bond interactions are visualized as black dashed lines. EI01D occupies a little part of the large pocket, and the two regions circled in magenta and cyan are unexplored by this ligand.

Like the RNA strand (**Figure 17**, yellow stick), compound EI01D (**Figure 17**, green stick) establishes polar contacts with Arg276, Arg480, and Pro274. Furthermore, it makes hydrophobic interactions with Phe357, His472, Lys451, and Val500. In addition, the modeling analysis revealed the presence in the binding pocket of two unexplored areas (**Figure 17,** cyan and magenta circles). A small library of compound EI01D derivatives has been designed and synthesized, introducing modifications to expand available structure–activity relationship (SAR) data. Substitutions have been made by inserting a substituted triazole ring instead of the nitro group, which allowed the exploration of additional interactions involving residues Arg326 and Gly302. The para position was predicted by docking studies as the most appropriate for such kinds of substitutions, and side chains at four positions were selected, considering the interactions into the pocket. Remarkably, the modifications aimed at optimizing the van der Waals contacts of the ligands with Arg276 and Arg326.

Pursuing this research line, compound EI02D resulted in an increase of the helicase inhibitory activity IC_{50} values of 0.3 μM.

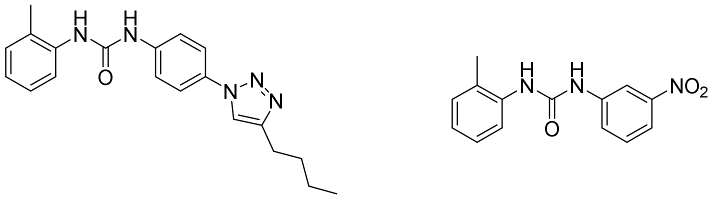

EI02D **EI01D**

Figure 18

2D Structures of previously identified DDX3X RNA helicase inhibitors

The predicted binding mode of EI02D within the DDX3X RNA binding pocket is shown in **Figure 19**. Some of the ligand contacts are coincident with the key interactions made by the parent compound EI01D. Indeed, the urea NH groups were involved in hydrogen bonds with the backbone carbonyl oxygen of Pro274, whereas the triazole ring interacted with the guanidine group of Arg276. Moreover, the tolyl terminus established hydrophobic interactions with residues Arg503 and Pro274, and the phenyl ring made hydrophobic contacts with the aromatic side chain of Phe357. Finally, the butyl substituent at the four position of the triazole ring made profitable interactions with residues Arg326 and Gly302, was unexploited by compound EI01D, and was probably responsible for the improved antihelicase activity[94].

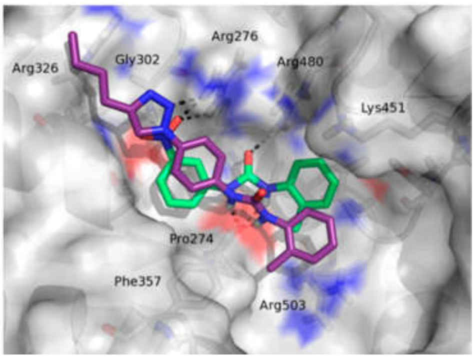

Figure 19
Binding mode of EI02D (purple sticks) and EI01D (green sticks).

Compound EI02D showed a broad spectrum of antiviral activity (HIV, HCV, DENV and WNV) in infected cells. Also active against HIV-1 drug-resistant strains, its aqueous (aq) solubility limited its bioavailability in preclinical models, causing its accumulation in fat tissues (Log S = -7.05).

Table 2
Antiviral activities of compound **EI02D**

Virus	**Strain**	**Cell type**	**EC_{50}(μM)**	**CC_{50}(μM)**
HIV*	NL4-3	PBMCs	1.1	>200
HCV†	Replicon	LucUbiNeo-ET	0.97	49.77
DENV‡	2, New Guinea C	Huh7	2.55	>200
WNV‡	NY99	Huh7	16.5	>200

CC_{50} half-maximal cytotoxic concentration; EC_{50} half-maximal concentration; PBMC, peripheral blood mononuclear cell.

*Evaluated in PBMCs.

†Evaluated in LUNET: LucUbiNeo-ET cells.

‡Evaluated in Huh7: Hepato cellular carcinoma cells.

Aim of the work

The aim of this PhD work was to improve the limits of both ATPase inhibitors and RNA helicase inhibitors.

ATPase inhibitors

The derivatives belonging to the first and second generation of ATPase inhibitors were characterized by the presence of the rhodanines group in their structure. Being the rhodanines promiscuous binders with poor selectivity and also considered Pan Assay Interference Compounds (PAINS)[100], the idea of replacing the rhodanine moiety with a different ring was pursued, trying to maintain profitable interactions within the ATP binding pocket of DDX3X. As a result, a new series of inhibitors of the ATPase activity of DDX3X was identified which showed good anti-HIV activity. Taken together, these results led to the identification of a new family of DDX3X inhibitors that can be used as a starting point to identify novel preclinical candidates to treat viral diseases caused by DDX3X dependent pathogens. Herein, docking studies were employed to guide the design of new DDX3X inhibitors endowed with a thiadiazole nucleus.

Furthermore, rhodanines have been described as PAINS and highly problematic frequent hitters[100,101]. Viceversa, the thiadiazole ring is an important framework in medicinal chemistry. Thiadiazole is a bioisostere of pyrimidine and oxadiazole and given the prevalence of pyrimidine in nature it is unsurprising that thiadiazoles exhibit significant therapeutic potential. Accordingly, a number of thiadiazole-containing drugs are currently on the market[102]. For the above reasons the rhodanine nucleus of the hit compound **FE15** was replaced with a 1,3,4-thiadiazole ring.

Docking studies predicted good poses for the novel series of compounds within the ATP binding pocket of DDX3X. The binding mode of compound **23** (as representative of the novel series, **Figure 20**) revealed its ability to establish, similarly to the active inhibitors RK33, ketorolac and FE15, hydrogen bond interactions with the crucial residues Gln207, Gly227, Gly229, Thr231, Thr201 and Arg202. Furthermore, its binding mode is stabilized by a π-π contact between the thiadiazole heterocycle and the side-chain of Tyr200. Starting from this result, a small library of 1,3,4-thiadiazole derivatives has been rationally designed and synthesized.

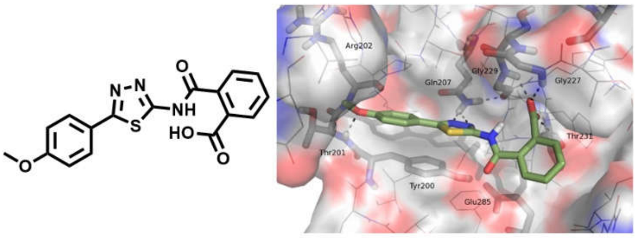

Figure 20
Binding mode of **23** within the ATP binding pocket of human DDX3.

RNA helicase inhibitors

In the contest of RNA helicase inhibitors my PhD work was directed by First Health Pharmaceuticals in collaboration with Prof. M. Botta.

In a recent work[94] was identified the first inhibitor of the helicase binding site of DDX3X, characterized by high selectivity and no cytotoxic effects in both *in vitro* and *in vivo* models. Compound EI02D, belonging to the urea series, was the first DDX3X inhibitor endowed with a broad spectrum of antiviral activity against HIV-1 (both wildtype and drug-resistant strains), HCV, and new emerging viruses (WNV and DENV)[94]. Despite EI02D representing the proof of concept that DDX3X inhibitors could be used as novel antivirals drugs, its poor aqueous (aq) solubility limited its bioavailability in preclinical models, causing its accumulation in fat tissues (Log S = -7.05).

With the attempt to enlarge the library of DDX3X inhibitors, a homology model-based virtual screening was performed and that[59] led to identify another small-molecule inhibitor of DDX3X helicase activity (compound EI03D) characterized by a sulfonamide moiety. Despite its low passive permeability, compound EI03D was characterized by a very good aqueous solubility and at the same time by a promising antienzymatic activity value of 0.36 μM[59]. Pursuing the research of novel druglike DDX3X inhibitors, a docking analysis of the two hit compounds EI02D and EI03D was performed. On the basis of the three-dimensional (3D) overlap of the two molecules within the biding site, were designed a new series of hybrid compounds by merging the key structural moieties of both able to interact with the main residues involved in the binding of both of them (Arg276, Pro274, and Arg480).

Novel compounds were then synthesized and validated against DDX3X enzyme and evaluated for their ability to inhibit WNV replication, leading to a small library of derivatives endowed with antiviral activities comparable or higher than the broad spectrum antiviral compound 1-β-D-ribofuranosyl-1,2,4-triazole-3-carboxamide (ribavirin).

With the purpose of identifying novel small-molecule inhibitors of the DDX3X helicase binding site, the docking poses of hit compounds EI02D and EI03D within the DDX3X RNA binding pocket was analysed. The 3D structure of DDX3X in its RNA-bound closed conformation previously generated by homology modeling[59] was used to perform these studies. As shown in **Figure 21A**, the docking analysis of compound EI03D highlighted favourable hydrogen bond interactions between the nitrobenzene oxygen atom and Arg276 and Gly325, as well as between the sulfonamide group and Pro274 and Arg480 whereas the hydroxyl substituent is engaged in profitable H-bond interactions with the residues Pro274 and Arg503. Furthermore, hydrophobic interactions were found with Phe357, Val500 and Arg503. The predicted binding mode of EI02D (**Figure 21A**) confirmed some key interactions, as seen for EI03D; more in detail, the triazole ring interacted with the guanidine group of Arg276, whereas the urea NH groups and carbonyl moiety were involved in hydrogen bonds with Pro274 and Arg480, respectively. Moreover, the butyl terminus established beneficial interactions with Arg326 and Gly302. Finally, the tolyl ring established hydrophobic contacts with Arg503 and Pro274 side chains and the phenyl ring made hydrophobic interactions with Phe357.

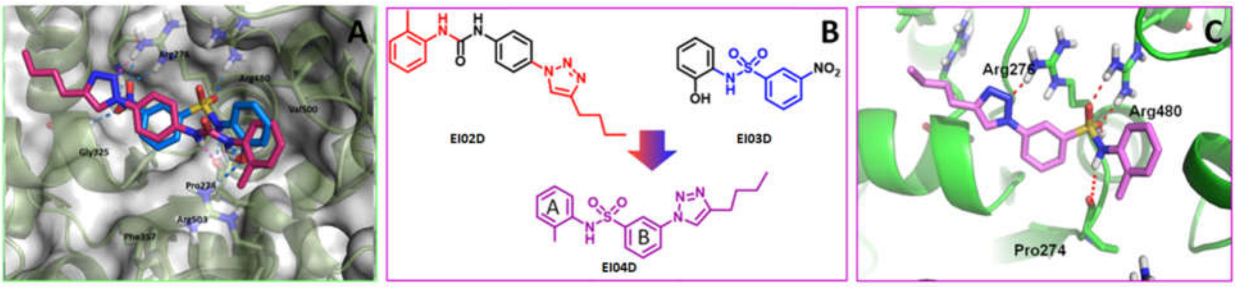

Figure 21

(A) Overlapped binding mode of compound EI02D (pink) and EI03D (blue marine) in DDX3X helicase pocket. Main interactions of both compounds with key residues of the active site are highlighted. Remarkably, Arg276, Arg480, and Gly302 make important contacts also with RNA phosphate backbone, whereas Gly325, Pro274, and Arg503 interact directly with the nucleobases. **(B)** Two-dimensional (2D) structure representation of the schematic idea behind the merged series design. **(C)** Proposed binding mode for merged derivative EI04D.

It is worthy to note that two compounds were both able to interact with Arg276 and Arg480 and also make profitable contacts with Gly325, Pro274, and Arg503, which our computational model[59] suggested to be important in RNA strand interactions into the helicase binding site. (**Figure 22**)

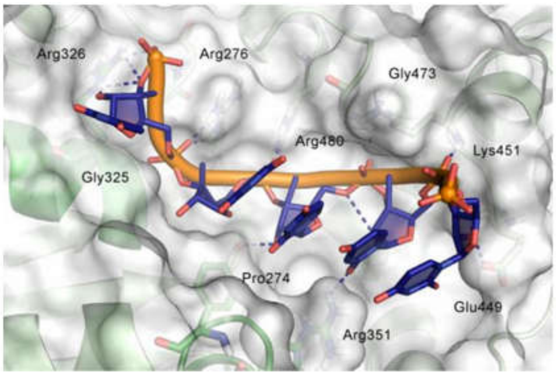

Figure 22
Surface and cartoon representation of RNA's main interactions within the helicase binding site of our homology model.

Starting from this analysis, the key structural units of EI02D[94] and EI03D[59] were mixed and was identified a new series of compounds able to interact at the same time with most of the residues involved in the binding of both of them, with particular attention to Arg276, Pro274, and Arg480, according to their suggested role in RNA strand binding. To this aim, as shown in **Figure 21B**, the n-alkyl substituted triazole group was selected from EI02D structure whereas the phenyl-substituted sulfonamide moiety was chosen from the structure of EI03D; the "hybrid" structure was finally composed by using the common aromatic ring **(B)** as a linker, and a small library of compounds were designed around this starting structure to explore the chemical space in relation to the activity against DDX3X.

Chapter 2

RESULTS AND DISCUSSION

Synthesis of Third Generation ATPase inhibitors

Chemistry

The synthesis of final compounds **23-28** and **29-32** first entailed the synthesis of the key intermediates **5-7** and **14-16**.

According to **Scheme 2**, **5**, **6** and **7** were obtained by condensation of the thiosemicarbazide **4** with the opportune benzoic acid **1-3**.

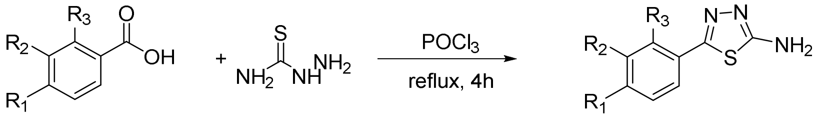

1 R_1=OCH_3 ; R_2=H; R_3=H;
2 R_1=OH ; R_2=H; R_3=H;
3 R_1=H ; R_2=H; R_3=Br;

4

5 R_1=OCH_3 ; R_2=H; R_3=H;
6 R_1=OH ; R_2=H; R_3=H;
7 R_1=H ; R_2=H; R_3=Br;

Scheme 2

Synthesis of intermediates **5-7**.

The synthesis of intermediates **14**, **15** and **16** was depicted in Scheme **3**. Aromatic aldehydes **8-10** reacted with thiosemicarbazide **4** to furnish thiosemicarbazones **11-13**. Subsequent cyclization in presence of $FeCl_3$ provides intermediates **14-16**.

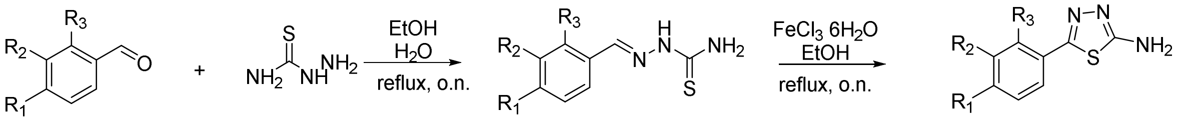

8 R_1=OCH_3 ; R_2=OCH_3; R_3=H;
9 R_1=$N(CH_3)_2$; R_2=H; R_3=H;
10 R_1=H ; R_2=H; R_3=NO_2;

4

11 R_1=OCH_3 ; R_2=OCH_3; R_3=H;
12 R_1=$N(CH_3)_2$; R_2=H; R_3=H;
13 R_1=H ; R_2=H; R_3=NO_2;

14 R_1=OCH_3 ; R_2=OCH_3; R_3=H;
15 R_1=$N(CH_3)_2$; R_2=H; R_3=H;
16 R_1=H ; R_2=H; R_3=NO_2;

Scheme 3

Synthesis of intermediates **14-16.**

Intermediates **5-7** and **14-16** were reacted with phtalimide to furnish compounds **17-22**. Subsequent hydrolysis in presence of LiOH provides final acids **23-28.** Esters **29-32** were synthesized by reaction of acids **23-28** with the opportune alcohoxydes. (**Scheme 4**).

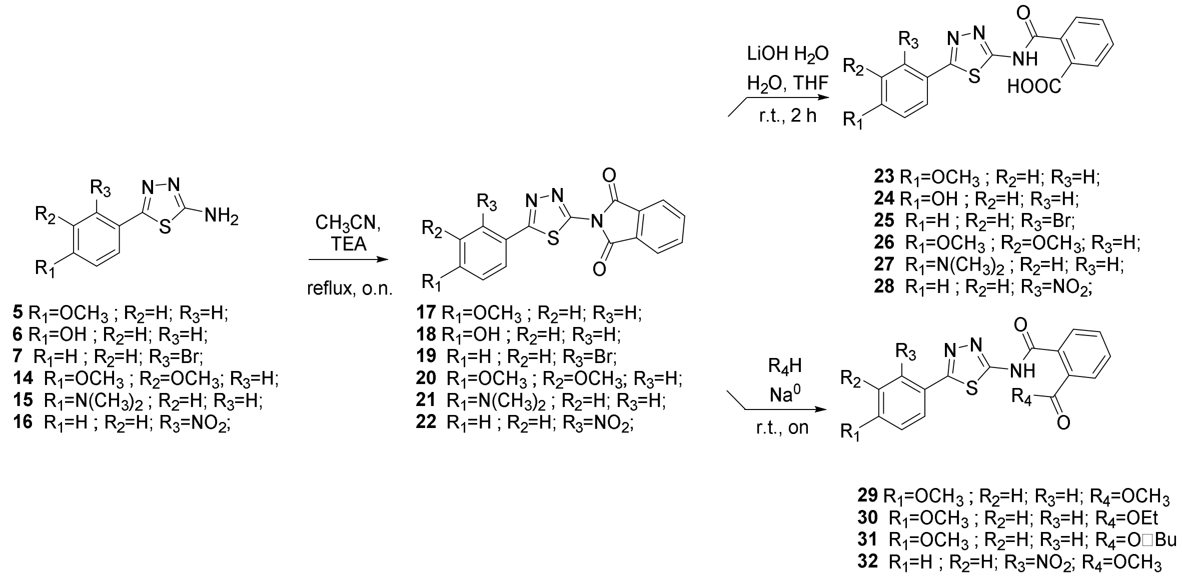

Scheme 4

Synthesis of final compounds **23-32**.

Biological evaluation

Derivatives **23-36** were next evaluated for their ability to inhibit the ATPase activity of DDX3X.

Table 3
Biological evaluation of selected compounds against DDX3X ATPase and HIV-1 infected cells[a].

Cpd ID	Structure	DDX3X ATPase	HIV-1 (NL4-3)	
		Ki[b]	IC50[b]	CC50[b]
17	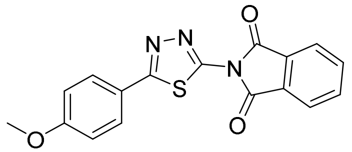	>50	NT	NT
23	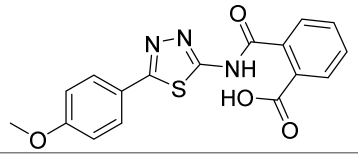	1.3±0.2	>50	>200
24	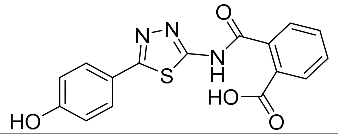	1.9±0.4	2.8±1.5	125

25	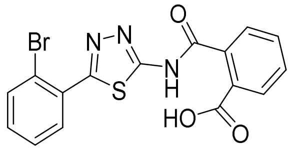	NA	NT	NT
26	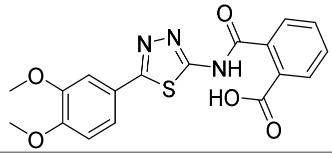	NA	NT	NT
27	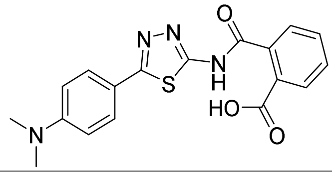	11.9±1.9	>50	130
28	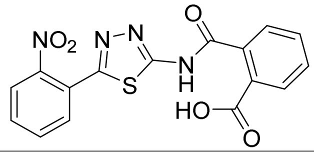	18.3±1.8	42.3±5.2	74
29	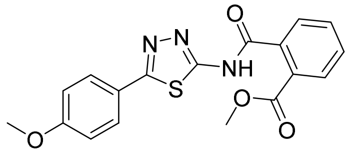	15.6	10	45
30	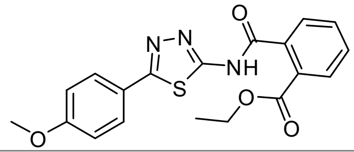	20.1±2.1	>50	>200
31	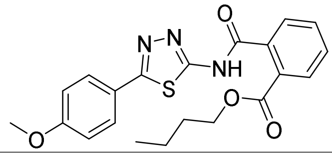	23.5±2.5	16.0±10	100
32	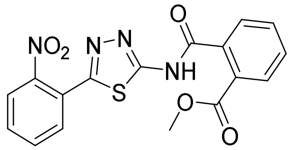	NA	NT	NT
33	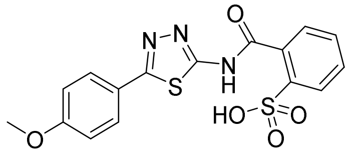	NA	NT	NT
34	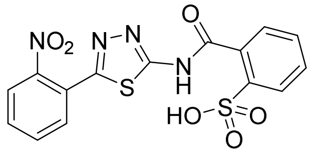	35.4±3.5	>50	110
35	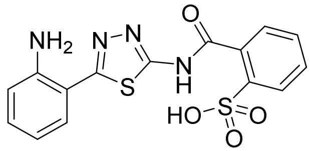	20.1±2.1	>50	130

36	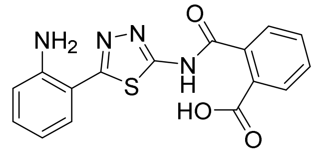	NA	NT	NT

[a] Data represent mean ± standard deviation of three experiments. [b] Ki, apparent dissociation constant for inhibitor binding; IC_{50}: half maximal inhibitory concentration or needed concentration to inhibit 50% viral replication. [c] CC_{50} Cytotoxic concentration 50 or needed concentration to induce 50% death of non-infected cells. [d] Evaluated on H9 cells. NA: not active; NT: not tested.

As reported in **Table 3**, compounds were characterized by Ki values in the low micromolar range against the ATPase binding site, confirming the validity of the reported approach. The phtalimido compound **17** was found completely inactive, probably due to its chemical instability. The para-methoxy derivative **23** and its corresponding phenol derivative **24** are endowed with the best affinity values (Ki) of 1.5 μM and 1.9 μM, respectively. Substitution of acidic function with ester slightly reduced the activities, being derivatives **29**, **30** and **31** respectively 12.5, 16.8 and 18.8 times less active than compound **23**. The introduction of electron withdrawing groups such as bromine and nitro in ortho position abolished (compound **25**) or reduced the activity (compound **28)**, despite even in this case the substitution of the carboxylic acid with a methyl ester (compound **32**) annulled enzymatic inhibition. The introduction of dimethylamino group in para position slightly decreased the activity in compound **27** (Ki= 11.9), while the introduction of amino group induced total loss of inhibitory capability of compound **36**. Finally, the replacement of the carboxylic group with sulfonic acid was detrimental for the activity of compounds **33**, **34** and **35**.

Compounds endowed of the best anti-enzymatic activity values were then essayed against HIV-1 in H9 cells. As reported in **Table 3**, esters derivatives **29** and **31** had promising antiviral activity values of 36 μM and 16 μM. Compound **28** had some antiviral activity that can however be attributable to its cytotoxic effect (SI=1.7). The best result is represented by compound **24**, characterized by a promising antiviral activity of 3.9 μM without signs of cytotoxicity (CC_{50}=125μM, SI=45). Strikingly, its p-methoxy derivative **23** was found inactive. The reasons are unknown and under investigation.

ADME assays

Selected compounds were then analysed *in vitro* for liver microsomal stability, membrane passive permeability and aqueous solubility at pH 7.4.

Microsomal metabolic stability was evaluated by incubating each compound at 37 °C for 60 minutes in phosphate buffer in presence of human liver microsomes. The reaction mixtures were then centrifuged, and the parent drug and metabolites were subsequently determined by LC-UV-MS. As reported in **Table 4**, compounds **23** and **24** had good metabolic stability, and only little percentage of the parent compound was metabolized into the dealkylated and into the oxidized derivatives. Contrary, esters **29-31** revealed low stability, and were rapidly converted into their corresponding carboxylic acids. In particular, compound **29** was rapidly converted into methoxy derivative **23** and phenol derivative **24**.

Kinetic solubility was calculated adding 1 mg of compound into 1 mL of water. After 24 h of stirring at 27°C, the mixture was filtered and the quantity of solubilized compound determined by LC-MS-MS. As reported in Table 3**,** compounds **23**, **24** and **29** showed very promising solubility values. By contrast, esters **30** and **31** due to their lipophilicity have values outside the recommended range (-2<LogS<-6).

Passive membrane permeability (AppP) using Parallel Artificial Membrane Permeability Assay (PAMPA) was also evaluated. The quantity of compound able to diffuse through a semipermeable artificial membrane, was calculated by LC-MS-MS. As reported in **Table 4** acids **23** and **24** showed low AppP, in contrast esters derivatives **29-31** possess very good permeability values, directly proportional to the length of their sidechains.

Table 4

In vitro ADME studies of selected compounds.

CPD ID	Methabolism		App P	Aq S
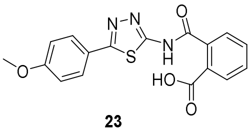 **23** P 98.1%	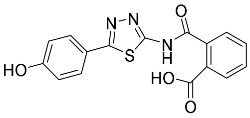 M_1 1.9%		<0.1 (0%)	3.3 (-5.03)
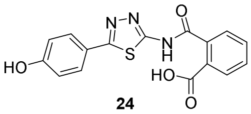 **24** P 98.8%	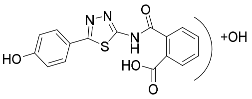 M_1 1.2%		<0.1 (0%)	27.8 (-4.08)
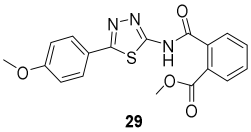 **29** P 25.3%	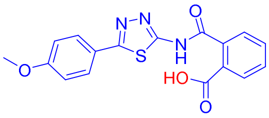 M_1 61.7%	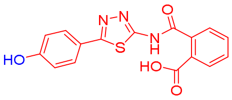 M_2 12.8%	0.7 (36%)	0.5 (-5.87)
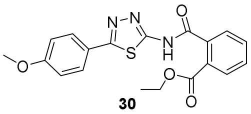 **30** P 75.7%	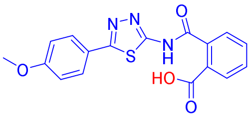 M_1 22.3	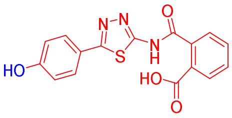 M_2 2.0	2.1 (4.6%)	<0.1 (>-6)
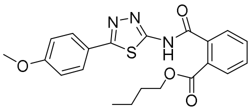 **31** P 53.8%	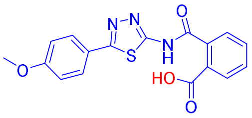 M_1 42.8%	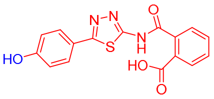 M_2 3.3%	6.1 (25.9%)	<0.1 (>-6)

[a] Human Liver Microsomal Metabolic Stability expressed as percentage of unmodified parent drug, methabolites M_1 and M_2 are reported. [b] Apparent permeability reported in $cm \cdot s^{-1}$. [c] Aqueous solubility expressed as µg/mL and as Log of molar concentration.

Conclusion

A new class of inhibitors of the ATPase activity of the human helicase DDX3X were designed, synthesized and biologically characterized. Compounds were designed starting from hits previously published, by replacing their rhodanine moiety, already reported in the list of PAINS, with the 1,3,4-thiadiazole ring. As a result, these new compounds showed promising anti- enzymatic activities varying from 1.5 μM to 35 μM. Compounds endowed of the most interesting activities against the enzyme, were then evaluated on HIV-1 infected H9 cells to discover potential antiviral drugs. The antiviral screening led to the identification of seven antiviral compounds endowed of activities ranging from 2.8 μM to 42 μM. Among them, compound **24** was characterized by the best anti-HIV-1 activity of 2.8 μM and by a promising selectivity index (CC_{50}=125μM, SI=45). ADME assays were finally performed to preliminary evaluate the pharmacokinetic parameters of compounds and to rationalize results. Acid derivatives showed very good metabolic stability, in contrast to their corresponding esters, which were rapidly metabolized into the acid precursors. The aqueous solubility was found very promising, in fact the values of the most active compounds were below 6, as recommended for drug candidates. Finally, compounds were characterized by low but not limiting passive permeability. Taking into account ADME results, the antiviral activities of the esters **29** and **31** is probably due to their enhanced membrane permeability, followed by a cellular conversion into compound **24**. Caco-2 experiments will be performed in the due time to evaluate the involvement of active transport mechanisms.

In conclusion, we have successfully replaced the rhodanine moiety of compound **FE15** with 1,3,4-thiadiazole ring. This approach is useful to reduce the interferences in assays that are generally associated with PAINS. The most promising derivative, compound **24**, is characterized by a good inhibition of the ATPase activity of DDX3X protein and by promising anti-HIV-1 activity in a reference virus-cell system without signs of *in vitro* cytotoxicity. These data, together with suitable *in vitro* PK properties, make inhibitor **24** a good starting point for further optimization.

Chapter 3

Experimental section

Synthetic procedures

Reagents were obtained from commercial suppliers (for example Sigma-Aldrich, Alfa Aesar). All commercially available chemicals were used as purchased without further purification. CH_2Cl_2 and MeOH were dried prior to use by distilling from calcium hydride or magnesium methoxide. Anhydrous reactions were run under a positive pressure of dry N_2 or argon. TLC was carried out using Merck TLC plates silica gel 60 F254. Chromatographic purifications were performed on columns packed with Merk 60 silica gel, 23-400 mesh, for flash technique.

All NMR spectra were recorded on Bruker Avance DPX400 spectrometer at 400 MHz for ^{1}H-NMR or 100 MHz for ^{13}C-NMR. Chemical shifts are reported relative to tetramethylsilane at 0.00 ppm. ^{1}H patterns are described using the following abbreviations: s = singlet, d = doublet, t = triplet, q = quartet, quint = quintet, sx = sextet, sept= septet, m = multiplet, br = broad signal, br s = broad singlet.

Mass spectra (MS) data were obtained using an Agilent 1100 LC/MSD VL system (G1946C) with a 0.4 mL/min flow rate using a binary solvent system 25 of 95:5 methyl alcohol/ water. UV detection was monitored at 254 nm. Mass spectra were acquired in positive and negative mode scanning over the mass range.

General procedure for the synthesis of amino thiazoles **5-7**

A mixture of the opportune substituted benzoic acid (6.57 mmol), thiosemicarbazide (9.85 mmol) and phosphorus oxychloride (5 mL) was stirred at 75°C for 4 h under N_2 atmosphere. After cooling to room temperature, water was added, the reaction mixture was further refluxed for 4 h. The mixture cooled and basified to pH 8 by addition of 1N NaOH(aq) solution. The resulting mixture was then extracted three times with EtOAc and washed with water. Organic layer was dried over Na_2SO_4 and evaporated under reduced pressure. The crude mass was recrystallized from EtOH. The compounds were obtained as light-yellow solids in a yield of 75%-80%.

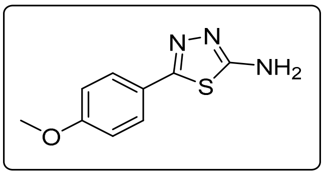

5-(4-methoxyphenyl)-1,3,4-thiadiazol-2-amine (5): crystallization in EtOH. Yellow solid, yield 75%.^{1}HNMR (400 MHz, Acetone): δ 7.73-7.71 (d, *J*=8.0 Hz, 2H), 7.01-6.99 (d, *J*=8.0 Hz, 2H), 6.56 (bs, 2H), 3.84 (s, 3H) ppm. LC-MS (ES): *m/z* 230 [M+Na]$^+$.

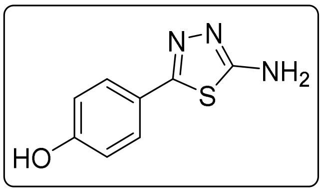

4-(5-amino-1,3,4-thiadiazol-2-yl)phenol (6): crystallization in EtOH. Yellow solid, yield 30%.^{1}HNMR (400 MHz, Acetone): δ8.88 (bs, 1H), 7.65-7.64 (d, *J*=5.2Hz, 2H), 6.92-6.91(d, *J*=5.2Hz, 2H), 6.57 (bs, 2H) ppm.

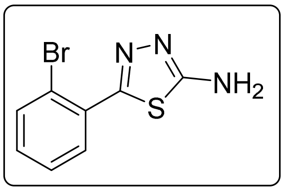

5-(2-bromophenyl)-1,3,4-thiadiazol-2-amine (7): Purification eluent DCM/MeOH 98:2, yield 50%, yellow solid. ^{1}HNMR (400 MHz, $CDCl_3$): δ7.95-7.93 (d, *J*=8.0 Hz, 1H), 7.68-7.66 (d, *J*=8.0 Hz, 1H), 7.42-7.38 (t, *J*=8.0 Hz, 1H), 7.32-7.30 (t, *J*=8.0Hz, 1H), 7.26 (bs, 2H) ppm.

General procedure for the synthesis of thiosemicarbazones **11-13**

The opportune aromatic aldehyde **8-10** (40 mmol) was dissolved in warm EtOH was added to an aqueous solution of thiosemicarbazide (40 mmol) with continuous stirring. After 1h, the white solid formed was filtered off as pure **11-13**.

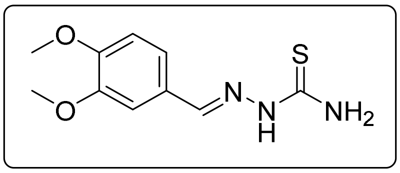

(**2-(3,4-dimethoxybenzylidene)hydrazine-1-carbothioamide (11):** crystallization in EtOH. Yellow solid, yield 60%.^{1}HNMR (400 MHz, DMSO-*d6*):δ 11.20 (bs, 1H), 8.07 (s, 1H),7.88 (s,1H), 7.43 (bs, 2H), 7.06-7.04 (d, *J*=8Hz, 1H), 6.88-6.86 (d, *J*=8Hz, 1H),3.73 (s, 3H), 3.70 (s,3H) ppm.

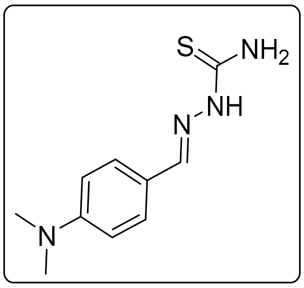

2-(4-(dimethylamino)benzylidene)hydrazine-1-carbothioamide (12): crystallization in EtOH, yellow solid, yield 50%, ^{1}HNMR (400 MHz, DMSO-*d6*): δ 12.3 (bs, 1H), 8.41 (s,1H), 7.75 (bs, 2H), 7.48-7.46 (d, *J*=8.0Hz, 2H), 6.81-6.6.79 (d, *J*=8.0Hz, 1H), 3.02 (s, 6H) ppm.

General procedure for the synthesis of thiadiazoles (**14-16**)

The opportune thiosemicarbazone (5 mmol) was suspended in EtOH, to this $FeCl_3.6H_2O$ (20 mmol) was added and the reaction mixture was stirred under reflux for further 12 hrs. The reaction mixture was quenched with aqueous $Na_2S_2O_3$, cooled to room temperature, poured into 30mL water under stirring, and extracted with CH_2Cl_2 (three times). The organic layer was dried over anhydrous Na_2SO_4. The organic solvent evaporated and the corresponding residue was purified by recrystallization from EtOH to afford the corresponding thiadiazoles **14-16**.

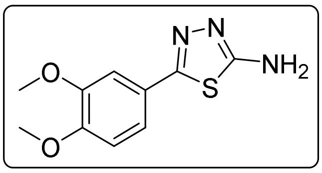

5-(3,4-dimethoxyphenyl)-1,3,4-thiadiazol-2-amine (14): crystallization in EtOH. Yellow solid, yield 44%.^{1}HNMR (400 MHz, DMSO-*d6*): δ 7.28 (s,1H), 7.22 (bs, 2H),7.13-7.12 (d, *J*=2.8Hz, 1H), 6.65- 6.64 (d, *J*=2.8Hz, 1H), 3.75 (s, 3H), 3.72 (s,3H) ppm.

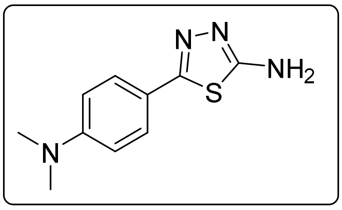

5-(4-(dimethylamino)phenyl)-1,3,4-thiadiazol-2-amine (15): crystallization in EtOH. yellow solid, yield 50%, ^{1}HNMR (400 MHz, DMSO-*d6*): δ7.72-7.70 (d, *J*=8.0Hz, 2H), 7.57 (bs, 2H), 6.90-6.88 (d, *J*=8.0Hz, 2H), 3.14 (s,6H) ppm.

General procedure for the synthesis of isoindoline-1,3-diones **17-22**

To a solution of substituted-1,3,4-thiadiazol-2-amine (0.48 mmol) in CH_3CN, phthalic anhydride (1.4 mmol) and triethylamine (1.05 mmol) were added, the corresponding mixture was stirred at reflux overnight under N_2 atmosphere. The product was filtered and washed with EtOAc to give a light yellow solid.

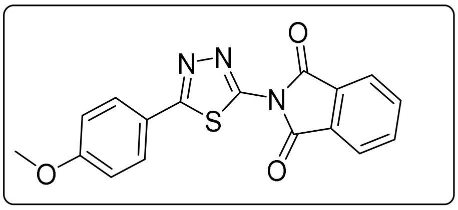

2-(5-(4-methoxyphenyl)-1,3,4-thiadiazol-2-yl)isoindoline-1,3-dione (17): Yellow solid, yield 78%. ^{1}HNMR (400 MHz, DMSO-*d6*): δ 8.06-8.04 (m, 2H), 7.98-7.96 (m, 4H, 7.12-7.10 (d,*J*= 8.0 Hz, 2H), 3.84 (s, 3H). ^{13}C-NMR (DMSO): δ 167.05, 164.74, 162.25, 152.88, 136.03, 131.59, 129.67, 124.74, 122.41, 115.95, 115.43, 114.87 ppm

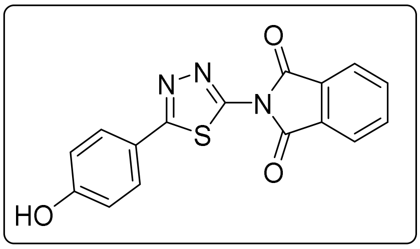

2-(5-(4-hydroxyphenyl)-1,3,4-thiadiazol-2-yl)isoindoline-1,3-dione (18): filtration, Yellow solid, yield 80%. ^{1}HNMR (400 MHz, DMSO-*d6*): δ10.23 (bs, 1H), 8.05-8.02 (m, 2H), 7.97-7.94 (m, 2H), 7.86-7.84 (d, *J*=8.0Hz, 2H), 6.93-6.91 (d, *J*=8.0Hz, 2H).

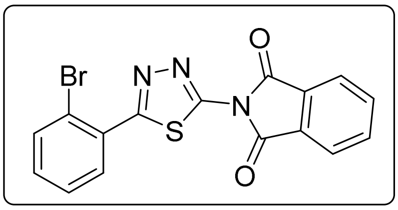

2-(5-(2-bromophenyl)-1,3,4-thiadiazol-2-yl)isoindoline-1,3-dione (19): filtration, Yellow solid, yield 45%. ^{1}HNMR (400 MHz, $CDCl_3$): δ 8.21-8.19 (d, *J*=8.0 Hz, 1H), 8.08-8.04 (m, 2H), 7.91-7.88 (m, 2H), 7.75-7.73 (d, *J*=8.0Hz, 1H), 7.49-7.46 (t, *J*=7.2 Hz, 1H), 7.38-7.34 (t, *J*=8.0Hz, 1H), 7.26 (s, 1H).

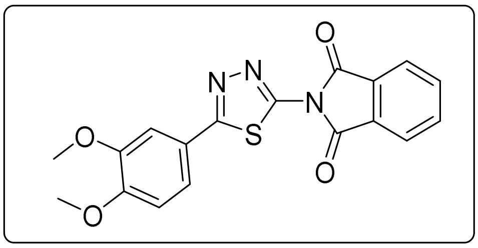

2-(5-(3,4-dimethoxyphenyl)-1,3,4-thiadiazol-2-yl)isoindoline-1,3-dione (20): filtration, Yellow solid, yield 63%. ^{1}HNMR (400 MHz, DMSO-*d6*): δ 8.08 (s,1H), 8.00-7.98 (d, *J*=8Hz, 1H), 7.91-7.89 (d, *J*=8.0Hz, 1H), 7.50 (s,1H), 7.42-7.40 (d, *J*=8.0 Hz, 1H), 7.07-7.05 (d, *J*=8.0 Hz 1H), 3.81 (s, 3H), 3.78 (s, 3H).

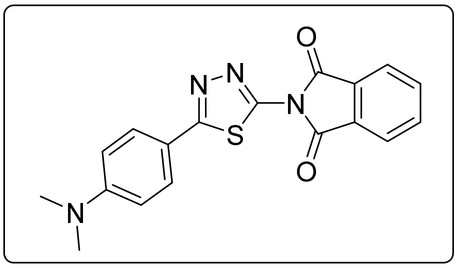

2-(5-(4-(dimethylamino)phenyl)-1,3,4-thiadiazol-2-yl)isoindoline-1,3-dione (21): filtration, Yellow solid, yield 45%. ^{1}HNMR (400 MHz, CDCl$_3$): δ8.06-8.08 (d, *J*=8.0Hz, 2H), 7.92-7.88 (m, 4H), 7.26-7.25 (d, *J*=3.2Hz, 1H), 6.92-6.91 (d, *J*=3.2Hz, 1H).

General procedure for the synthesis of acids **23-28**

Lithium hydroxide monohydrate (0.18 mmol) was added to a suspension of substituted-(1,3,4-thiadiazol-2-yl)isoindoline-1,3-dione (0.15 mmol) in a (1:1) mixture of H_2O:THF. The reaction mixture was stirred at room temperature for 2 h., then was acidified with HCl 1N and extracted 3 times with EtOAc. The organic layer was dried over anhydrous Na_2SO_4., and the solvent was removed at reduced pressure to provide the final product as white solid, that was used in the next step without further purification.

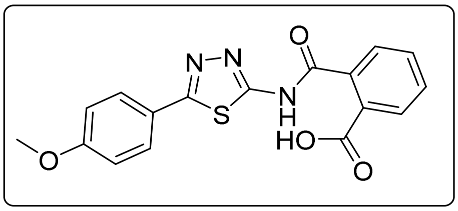

2-((5-(4-methoxyphenyl)-1,3,4-thiadiazol-2-yl)carbamoyl)benzoic acid (23): crystallization MeCN, yield 67% ^{1}H NMR (DMSO): δ 12.98 (s, 1H), 7.90-7.86 (m, 2H), 7.65-7.56 (m, 2H), 7.06-7.04 (m, 2H), 3.79 (s, 3H) ppm ^{13}C-NMR (DMSO): δ 167.55, 167.01, 161.76, 161.09, 158.06, 135.97, 131.87, 130.38, 130.30, 129.76, 128.56, 128.52, 128.48, 128.17, 122.17, 114.78, 55.42 ppm LC-MS(ES) m/z = 352.9 [M+H]+, m/z= 354.0 [M-H]$^-$.

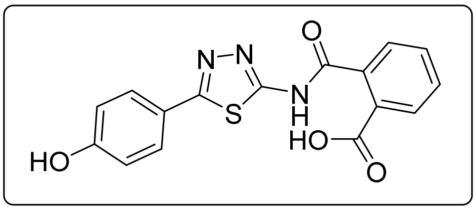

2-((5-(4-hydroxyphenyl)-1,3,4-thiadiazol-2-yl)carbamoyl)benzoic acid (24): crystallization in EtOH. white solid, yield 75%, [1]HNMR (400 MHz, DMSO-*d6*): δ13.16 (bs, 1H), 10.04 (s, 1H), 7.93-7.91 (d, *J*=8.0Hz, 1H), 7.79-7.77 (d, *J*=8.0Hz, 2H), 7.69-7.60 (m, 3H), 6.90-6.88 (d, *J*=8.oHz, 2H). [13]CNMR (100 MHz, DMSO-*D6*): δ167.96, 167.49, 162.60, 160.17, 158.21, 136.50, 132.32, 130.82, 130.22, 129.10, 128.64, 121.70, 116.56 ppm.

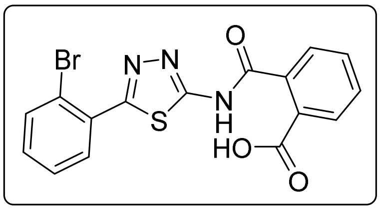

2-((5-(2-bromophenyl)-1,3,4-thiadiazol-2-yl)carbamoyl)benzoic acid (25): Purification eluent DCM/MeOH 96:4, yield 50%, white solid. [1]HNMR (400 MHz, DMSO-*d6*): δ 13.40 (bs, 1H), 7.97-7.93 (t, *J*=8.0Hz, 2H), 7.85-7.83 (d, *J*=8.0Hz, 1H), 7.68-7.61 (m, 3H), 7.58-7.54 (t, *J*=8.0 Hz, 1H), 7.49-7.45 (t, *J*=8.0Hz, 1H). [13]CNMR (100 MHz, DMSO-*d6*): δ168.18, 167.56, 160.70, 159.82, 136.20, 134.32, 132.44, 132.30, 132.21, 131.60, 130.96, 130.35, 128.79, 128.75, 121.89 ppm.

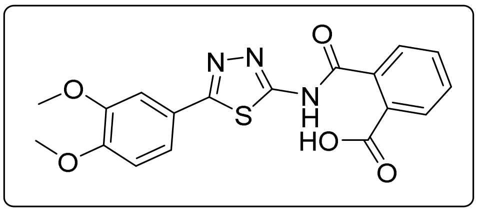

2-((5-(3,4-dimethoxyphenyl)-1,3,4-thiadiazol-2-yl)carbamoyl)benzoic acid (26): crystallization in EtOH. White solid, yield 60%.[1]HNMR (400 MHz, DMSO-*d6*):δ 7.87-7.85 (d, *J*=8 Hz, 1H), 7.64-7.54 (m, 3H), 7.45-7.41 (m, 2H), 7.04-7.02 (d, *J*=8Hz, 1H), 3.8 (s, 3H), 3.76 (s, 3H). [13]CNMR (100 MHz, $CDCl_3$): δ168.06, 167.43, 162.44, 158.58, 151.36, 149.65, 136.54, 132.41, 130.85, 130.61, 130.18, 128.60, 123.31, 120.86, 112.57 ppm.

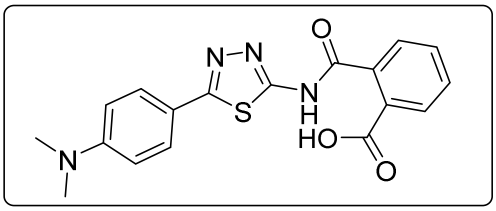

2-((5-(4-(dimethylamino)phenyl)-1,3,4-thiadiazol-2-yl)carbamoyl)benzoic acid (27): crystallization in EtOH. white solid, yield 98%, ^{1}HNMR (400 MHz, DMSO-*d6*): δ13.13 (bs, 1H), 7.92-7.90 (d, *J*=8.0Hz, 1H), 7.76-7.74 (d, *J*=8.0Hz, 2H), 7.96-7.59 (m, 3H), 6.80-6.68 (d, *J*=8.0Hz, 2H). ^{13}CNMR (100 MHz, DMSO-*D6*): δ167.86, 167.50, 163.07, 152.15, 136.62, 132.32, 130.77, 130.18, 128.62, 128.49, 117.90, 112.52 ppm.

General procedure for the synthesis of esters **29-32**

A mixture of substituted-(1,3,4-thiadiazol-2-yl)isoindoline-1,3-dione (0.29 mmol) and the opportune alcohoxide (0.29 mmol) was stirred at room temperature for 16 h under N_2 atmosphere. Mixture was diluted with diluted CH_3COOH, the residue was filtered and the solvent was evaporated at reduced pressure. The product was purified *via* flash chromatography on silica gel (eluent $CHCl_3$/EtOH, 98/2) to furnish a white solid product

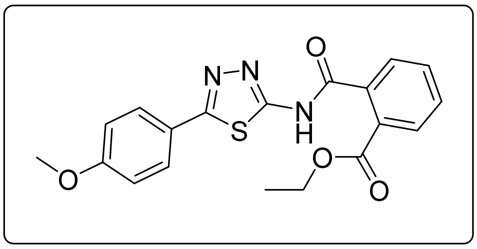

ethyl 2-((5-(4-methoxyphenyl)-1,3,4-thiadiazol-2-yl)carbamoyl)benzoate (30): Purification eluent $CHCl_3$/EtOH 98:2, yield 10%, white solid. ^{1}HNMR (400 MHz, $CDCl_3$):δ 8.00-7.98 (d, *J*= 8.0 Hz, 1H), 7.84-7.82 (d, *J*=8.0 Hz, 2H), 7.63-7.54 (m, 3H), 6.97-6.95 (d, *J*=8.0 Hz, 2H), 4.29-4.23 (q, *J*=7.2 Hz, 2H), 3.83 (s, 3H), 1.22-1.20 (t, *J*=8.0 Hz, 3H).^{13}CNMR (100 MHz, $CDCl_3$):δ167.48, 165.99, 164.74, 132.24, 130.68, 130.38, 129.43, 128.82, 127.85, 114.61, 61.82, 55.44, 13.87 ppm. LC-MS(ES) m/z = 384.2 $[M+H]^+$

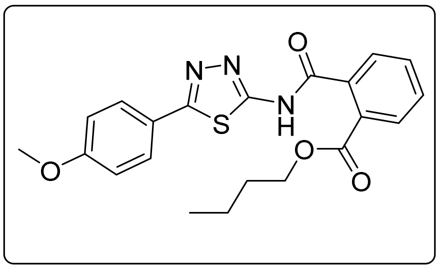

butyl 2-((5-(4-methoxyphenyl)-1,3,4-thiadiazol-2-yl)carbamoyl)benzoate (31): Purification eluent $CHCl_3$/EtOH 98:2, crystallization in EtOH, yield 23%, white solid. ^{1}HNMR (400 MHz, $CDCl_3$): δ 8.07-8.05 (d, *J*=8 Hz, 1H), 7.77-7.75 (d, *J*=8.0 Hz, 3H), 7.70-7.62 (m, 2H), 6.99-6.97 (d,*J*=8 Hz, 2H), 4.23-4.19 (t, *J*=6.8 Hz, 2H), 3.88 (s, 3H), 1.58-1.54 (q, *J*=6.8 Hz, 2H), 1-33-1.28 (q, *J*=7.6Hz, 2H), 0.82-0.79 (t, *J*=7.2Hz, 3H). ^{13}CNMR (100 MHz, $CDCl_3$): δ 167.44, 166.16, 162.39, 161.56, 159.59, 135.58, 132.19, 130.55, 130.39, 129.96, 128.60, 128.51, 123.11, 114.49, 65.57, 55.47, 53.43, 30.47, 19.15, 13.64 ppm. LC-MS(ES) m/z = 412.1 [M+H]+

Enzymatic assays

Protein expression and purification

Recombinant his-tagged human full length DDX3X was cloned into the *E. coli* expression vector pET-30a(+). Shuffle T7 *E. coli* cells were transformed with the plasmid and grown at 37°C up to OD_{600} = 0.7. DDX3X expression was induced with 0.5 mM IPTG at 15°C O/N. Cells were harvested by centrifugation, lysed and the crude extract centrifuged at 100.000xg for 60 min at 4°C in a Beckman centrifuge before being loaded onto a FPLC Ni-NTA column (GE Healthcare). Column was equilibrated in Buffer A (50 mM Tris-HCl pH 8.0, 250 mM NaCl, 25 mM Imidazole and 20% glycerol). After extensive washing in Buffer A, the column was eluted with a linear gradient in Buffer A from 25 mM to 250 mM Imidazole. Proteins in the eluted fractions were visualized on SDS-PAGE and tested for the presence of DDX3X by Western blot with anti-DDX3X A300-475A*(BETHYL)* at 1:2000 dilution in 5% milk. Fractions containing the purest DDX3X protein were pooled and stored at -80°C.

ATPase assay

The ATPase assay was carried out by using the commercial kit Promega ADP-Glo™ Kinase Assay. Reaction was performed in 30mM TrisHCl pH 8, 9 mM $MgCl_2$, 0.05mg/ml BSA, 50μM ATP and 4μM of recombinant DDX3X. Reaction was performed following the ADP-Glo™ Kinase Assay Protocol and luminescence was measured with MicroBeta TriLux (Perkin Elemer).

Antiviral assay

The antiviral activity was evaluated by measuring the half maximal inhibitory concentration (IC_{50}) values against the HIV-1 wild-type reference strain NL4-3 in a TZM-bl cell line based phenotypic assay named BiCycle Assay.[103] The method includes a first round of infection of human T cell lymphoma derived clone H9 at multiplicity of infection of 0.03 in presence of serial dilution of compounds in a 96-well plate. After 72 hours, 50 microliters of supernatants from each well were used to infect TZM-bl cell line, which allow the quantitative analysis of HIV infection by measuring the expression of the luciferase gene integrated in the genome of the cells under the control of HIV-1 LTR promoter. After 48 hours, dose-response curves were generated by measuring reporter gene expression in each well by using Bright-Glo Luciferase Assay (Promega) through the GloMax Discovery reader (Promega). Relative luminescence units measured in each well were elaborated with the GraphPad Software v.6.0 to calculate IC_{50} values. All viruses and cell lines were obtained through the NIH AIDS Reagent Program (www.aidsreagent.org).

Cytotoxicity assay

Cytotoxicity in H9 cells was determined by using the CellTiter-Glo 2.0 assay (Promega). H9 cells were seeded at 40,000 cells/well in duplicate in presence of serial 2-fold dilutions of compounds (range 200 – 1.56 μM) and incubated for 72 hours. Cell viability was calculated by measuring cellular ATP as a marker of metabolically active cells through a luciferase based chemical reaction and expressed as the concentration that reduce cell viability by 50%.

ADME assays

Chemicals. All solvents, reagents, were from Sigma-Aldrich Srl (Milan, Italy), Brain Polar Lipid Extract (Porcine) were from Avanti Polar Lipids, INC. (Alabama, USA). Dodecane was purchased from Fluka (Milan, Italy). Pooled Male Donors 20 mg/mL HLM were from

BD Gentest-Biosciences (San Jose, California). Milli-Q quality water (Millipore, Milford, MA, USA) was used. Hydrophobic filter plates (MultiScreen-IP, Clear Plates, 0.45 μm diameter pore size), 96-well microplates, and 96-well UV-transparent microplates were obtained from Millipore (Bedford, MA, USA).

Parallel artificial membrane permeability assay (PAMPA and PAMPA-BBB). Donor solution (0.5 mM) was prepared by diluting 1 mM dimethylsulfoxide (DMSO) compound stock solution using phosphate buffer (pH 7.4, 0.025 M). Filters were coated with 5 μL of a 1% (w/v) dodecane solution of phosphatidylcholine or 4 μL of brain polar lipid solution (20 mg/mL 16% $CHCl_3$, 84% dodecane) prepared from $CHCl_3$ solution 10% w/v, for intestinal permeability and BBB permeability, respectively. Donor solution (150 μL) was added to each well of the filter plate. To each well of the acceptor plate were added 300 μL of solution (50% DMSO in phosphate buffer). All compounds were tested in three different plates on different days. The sandwich was incubated for 5 h at room temperature under gentle shaking. After the incubation time, the plates were separated, and samples were taken from both receiver and donor sides and analyzed using LC with UV detection at 280 nm. LC analysis were performed with a PerkinElmer (series 200) instrument equipped with an UV detector (PerkinElmer 785A, UV/vis Detector). Chromatographic separation was conducted using a Polaris C18 column (150 - 4.6 mm, 5 μm particle size) at a flow rate of 0.8 mL min^{-1} with a mobile phase composed of 60% ACN/40% H_2O-formic acid 0.1% for all compounds. Permeability (P_{app}) was calculated according to the following equation with some modification in order to obtain permeability values in cm/s,

$$P_{app} = \frac{V_D V_A}{(V_D + V_A)At} - \ln{(1 - r)}$$

where V_A is the volume in the acceptor well, V_D is the volume in the donor well (cm^3), A is the “effective area” of the membrane (cm^2), t is the incubation time (s) and r the ratio between drug concentration in the acceptor and equilibrium concentration of the drug in the total volume(V_D+V_A). Drug concentration is estimated by using the peak area integration. Membrane retentions (%) were calculated according to the following equation:

$$\%MR = \frac{[r - (D + A)]100}{EQ}$$

where r is the ratio between drug concentration in the acceptor and equilibrium concentration, D, A, and EQ represented drug concentration in the donor, acceptor and equilibrium solution, respectively.

Water solubility assay. The appropriate (1 mg) was added to 1 mL of water. The sample was shaken in a shaker bath at room temperature for 24-36 h. The suspensions were filtered through a 0.45 μm nylon filter (Acrodisc), and the solubilized compound determined by LC-MS-MS assay. The determination was performed in triplicate. For the quantification was used an LC-MS system consisted of a Varian apparatus (Varian Inc) including a vacuum solvent degassing unit, two pumps (212-LC), a Triple Quadrupole MSD (Mod. 320-LC) mass spectrometer with ES interface and Varian MS Workstation System Control Vers. 6.9 software. Chromatographic separation was obtained using a Pursuit C18 column (50 x 2.0 mm) (Varian) with 3 μm particle size and gradient elution: eluent A being ACN and eluent B consisting of an aqueous solution of formic acid (0.1%). The analysis started with 0% of eluent A, which was linearly increased up to 70% in 10 min, then slowly increased up to 98% up to 15 min. The flow rate was 0.3 mL/min and injection volume was 5 μL. The instrument operated in positive mode and parameters were: detector 1850 V, drying gas pressure 25.0 psi, desolvation temperature 300.0 °C, nebulizing gas 45.0 psi, needle 5000 V and shield 600 V. Nitrogen was used as nebulizer gas and drying gas. Collision induced dissociation was performed using Argon as the collision gas at a pressure of 1.8 mTorr in the collision cell. Quantification of the single compound was made by comparison with apposite calibration curves realized with standard solutions in methanol.

Microsomal stability assay. Each compound in DMSO solution was incubated at 37 °C for 60 min in 125 mM phosphate buffer (pH 7.4), 5 μL of human liver microsomal protein (0.2 mg/mL), in the presence of a NADPH-generating system at a final volume of 0.5 mL (compounds' final concentration, 50 μM); DMSO did not exceed 2% (final solution). The reaction was stopped by cooling in ice and adding 1.0 mL of acetonitrile. The reaction mixtures were then centrifuged, and the parent drug and metabolites were subsequently determined by LC-UV-MS. Chromatographic analysis were performed with an Agilent

1100 LC/MSD VL system (G1946C) (Agilent Technologies, Palo Alto, CA) constituted by a vacuum solvent degassing unit, a binary high-pressure gradient pump, an 1100 series UV detector, and an 1100 MSD model VL benchtop mass spectrometer. Chromatographic separation was obtained using a Varian Polaris C18-A column (150 - 4.6 mm, 5 μm particle size) and gradient elution: eluent A being ACN and eluent B consisting of an aqueous solution of formic acid (0.1%). The analysis started with 2% of eluent A, which was rapidly increased up to 70% in 12 min, then slowly increased up to 98% in 20 min. The flow rate was 0.8 mL min^{-1} and injection volume was 20 μL. The Agilent 1100 series mass spectra detection (MSD) single-quadrupole instrument was equipped with the orthogonal spray API-ES (Agilent Technologies, Palo Alto, CA). Nitrogen was used as nebulizing and drying gas. The pressure of the nebulizing gas, the flow of the drying gas, the capillary voltage, the fragmentor voltage, and the vaporization temperature were set at 40 psi, 9 L/min, 3000 V, 70 V, and 350 °C, respectively. UV detection was monitored at 280 nm. The LC-ESI-MS determination was performed by operating the MSD in the positive ion mode. Spectra were acquired over the scan range m/z 100-1500 using a step size of 0.1 u. The percentage of not metabolized compound was calculated by comparison with reference solutions.

Chapter 4

RESULTS AND DISCUSSION

Synthesis of RNA helicase inhibitors

Chemistry

The synthesis of finals compounds was accomplished following the synthetic route reported in **Scheme 5**. Amino thiophenol **37** was first converted into azide **38** by diazotization; a subsequent click reaction with the alkyne **39** provides triazole **40**. Oxidative chlorination of thiols **40** led to the corresponding sulfonyl chloride intermediates that were immediately converted into final compounds by nucleophilic reaction with the opportune amines.

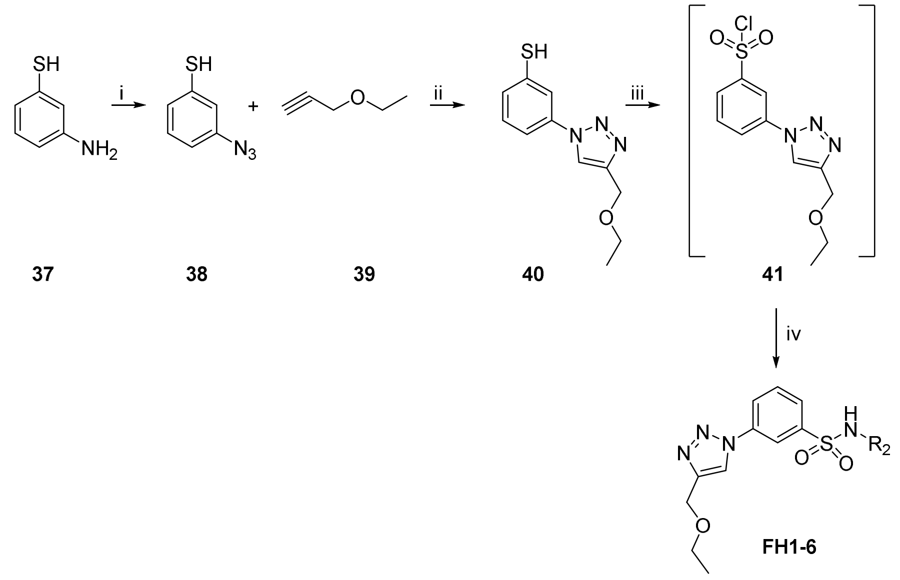

Scheme 5

Reagents and conditions: (i) (a) t-BuONO, acetonitrile (ACN), 20 min, 0 °C; (b) $TMSN_3$, ACN, 2 h, room temperature (r.t.); (ii) $CuSO_4$·5 H2O, sodium ascorbate, H_2O/t-BuOH (1:1), microwave (MW), 10 min, 120°C; (iii) H_2O_2, $SOCl_2$, ACN, from 0 °C to r.t., 15 min; (iv) opportune amine, pyridine (dry), 5 h, r.t

Terminal alkyne **39** was synthesized from propargyl alcohol **42** and diethylsulfate **43** by Haworth alkylation and purified by distillation (**Scheme 6**).

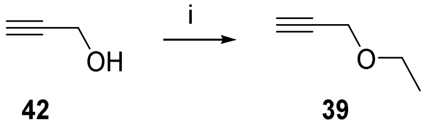

42 **39**

Scheme 6

Reagents and conditions: (i) (a) NaOH(aq) (6 M), 20 min, r.t; (b) diethylsulfate, 60 min, 50-55 °C.

The synthesis of final compounds **FH001**, **FH002**, **FH003**, **FH006** first entailed the synthesis of intermediates **49**,**55**,**59**,**63** respectively.

The synthesis of intermediate **48** provides the reaction between acrylonitrile **44** and hydrazine monohydrate **45** to obtain **46**; subsequent addition of tetrahydro-4H-pyran-4-one **47** provides intermediate **48**, which after intramolecular cyclization furnished amine **49** (**Scheme 7**).

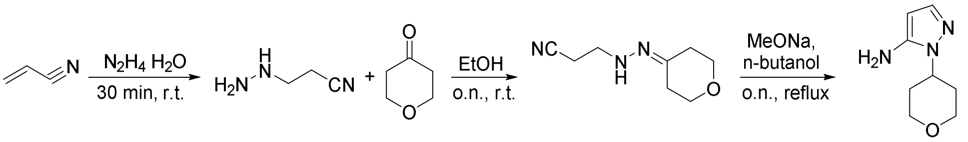

44 **46** **47** **48** **49**

Scheme 7

The synthesis of amines **55** and **59** starts from the same synthesis of chlorohydrate **53** shown in **Scheme 8**. Tetrahydro-4H-pyran-4-one **47** reacted with tert-butyl hydrazinecarboxylate **50** to furnish hydrazone **51**. Reduction with Sodium Cyanoborohydride led to corresponding intermediate **52**, which was subsequently deprotected to furnish chlorohydrate **53** (**Scheme 8)**.

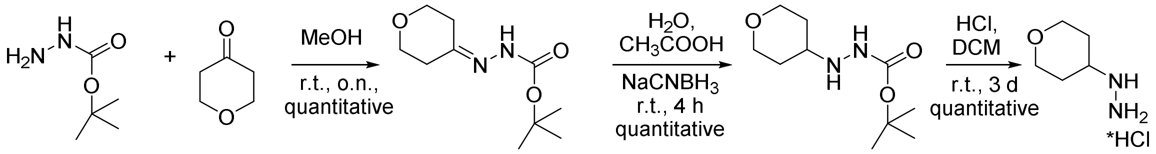

50 **47** **51** **52** **53**

Scheme 8

The synthesis of amines **55** and **59** were accomplished in a similar way: a reaction of condensation and cyclization between the intermediates **54** and **58** (respectively) and the salt **53** furnished the pyrazolos **55** and **59** (**Scheme 9**,**Scheme 10**).

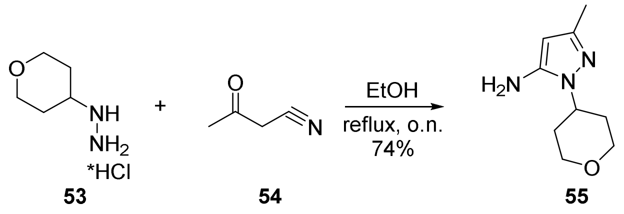

Scheme 9

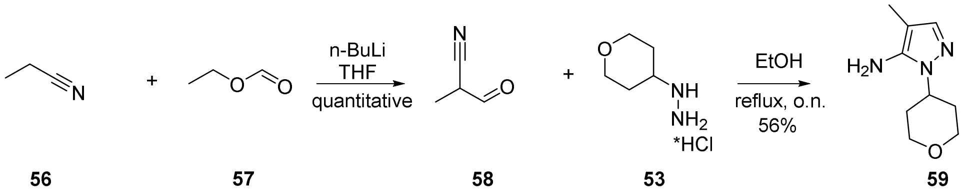

Scheme 10

Amine **63** was synthesized from pyridine **60** and boronic acid **61** by Suzuki reaction. Subsequently hydrogenation furnished amine **63** (**Scheme 11**)

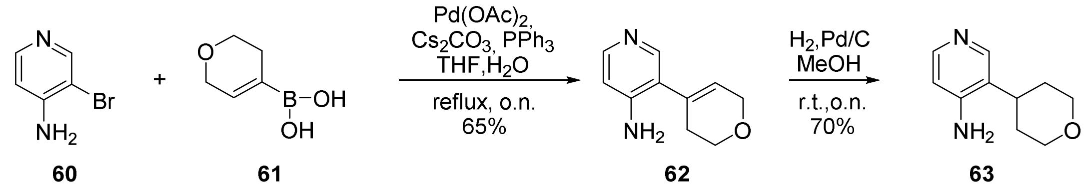

Scheme 11

Biological evaluation

Derivatives **64-82** were first evaluated for their ability to inhibit the helicase activity of DDX3X; results are reported in **Table 5**.

Table 5
DDX3 antienzimatic activity[a]

Cmp ID	Structure	Inhibition[b] (%)	Cmp ID	Structure	Inhibition[b] (%)
EI04D	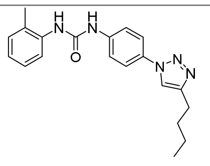	98±1	**73**	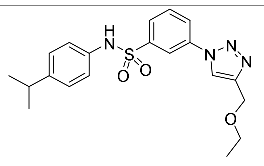	nd

EI03D	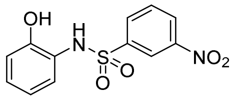	98±2	**74**	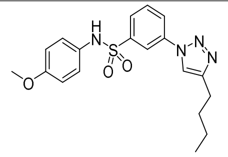	80±1
64	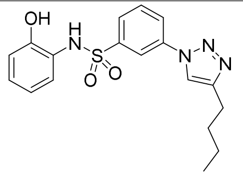	83±3	**75**	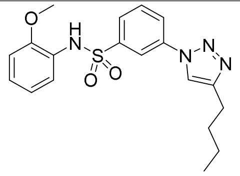	98±0.5
65	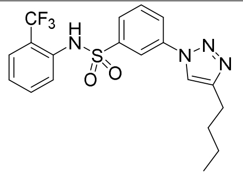	98±1	**76**	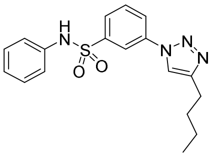	31±2
66	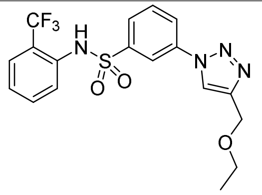	98±0.5	**77**	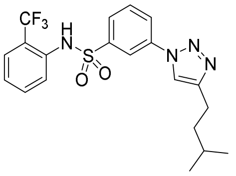	96±1
67	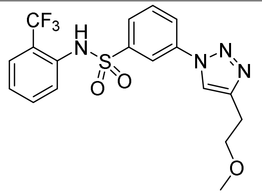	67±2	**78**	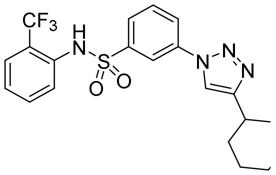	52±2
68	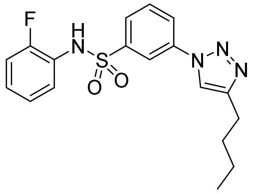	24±2	**79**	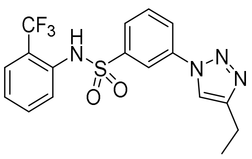	71±2
69	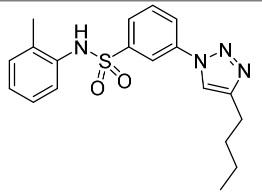	59±2	**80**	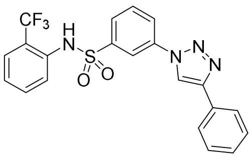	41±2.1
70	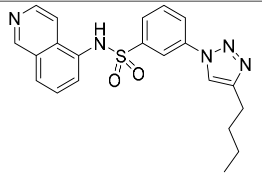	99±0.5	**81**	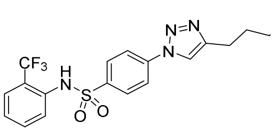	nd

71	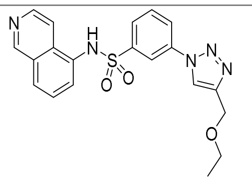	98±1	**82**	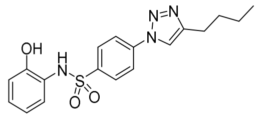	57±0.5
72	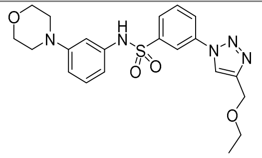	na[c]			

[a]Data represent mean two values of the least two experiments. [b]% inhibition at a fixed concentration of 20 μM. [c]na: not active. nd: not determined, compound precipitated from medium.

Seven compounds showed promising inhibitory values higher than of 80% (compounds **64-66**, **70**, **71**, **75**, and **77**). The meta substitution of triazole on ring B was more a favorite with respect to the para position, **82** being about 26% less active than the corresponding meta derivative **64**. This is also confirmed by the docking studies, due to the higher shape complementarity of the binding site and **64** with respect to **82**. Three-dimensional conformations of the latter results into being much more constrained within the pocket, and this is likely responsible for the lower activity. Replacement of triazole butyl chain with isopentyl was well tolerated (compound **77)**; when the length was reduced to two carbons, the activity decreased to about 25% in compound **79**, in line with a lower occupancy of the binding site and poorer complementarity between ligand and protein cavity, as also shown by the docking model. Yet, according to this observation, the introduction of bulkier substituents, such as cyclohexyl and phenyl, was detrimental for the activity, which decreased to 41 and 52% for compounds **80** and **78**, respectively. Alkyl chain of the triazole ring was also explored by checking the effect of introducing a polar atom. As a result, methyl-ethyl ether derivatives **66** and **71** retained their activities; in contrast, ethyl-methyl ether **67** was found 31% less active than the corresponding isomer **66**. According to our docking studies, the ether oxygen atom can establish a hydrogen bond interaction with Arg326. In fact, in the ethyl-methyl ether derivatives, the distance between the ether oxygen atom and its counterpart is less favourable to the hydrogen bond interaction. On the whole, pocket-hosting the substituted triazole moiety requires a precise spatial disposition (meta substitution preferred over the para one) while preferring more flexible, less constrained triazole substituents (butyl and isopentyl preferred over phenyl and cyclohexyl rings) occupying as much space as possible (lower activity in the presence of ethyl substituent). Polar atoms are tolerated, and a proper distance to efficiently interact with Arg326 appears to favour compound activity. Analogously, the pocket that houses the other terminal side of our compound series, i.e., ring A, also presents distinctive hallmarks. In particular, a proper combination of both polar and hydrophobic interactions appears to be beneficial to compounds' activity. Noteworthily, the presence of a hydrogen bond acceptor on ring A leads to a high percentage of DDX3X inhibition across this chemical series, hydrogen bond interactions being feasible with Pro274 and Arg503 of the binding pocket, as revealed by our docking studies. On confirmation of that, the introduction of an isoquinolyl-ring (compounds **70** and **71**) on ring A was well tolerated as well as the -OH and the -OCH3 ortho substitution (compounds **64** and **75**), all bearing hydrogen-bonding moieties. Also, compounds **65** and **66**, bearing the -CF_3 moiety at the ortho position of ring A, satisfy such requirements, being the trifluoromethyl group reported to have both hydrophobic and polar (hydrogen-bonding) properties[104]. Substitution of the trifluoromethyl or hydroxyl groups of compounds **64-66** with a methyl group (compound **69**), which shows only hydrophobic properties, leads to a lower DDX3X % of inhibition in the sulfonamide series. Activity further decreases in the presence of fluorine or hydrogen substituents (compounds **68** and **76**), which have similar percentage of inhibition. Lower activity of compound **68** is likely due to the lower occupancy combined with a less effective hydrogen-bonding interaction, both exerted by the fluorine atom; the unsubstituted derivative **76** likewise showed a reduced activity value of 31%. The abolishment of the activity for compound **72**, where a morpholine moiety was introduced on ring A, is explained by docking studies to be due to the spatial constraints of the region of the binding site, being able to accommodate the planar isoquinoline system but unfavorable in hosting the morpholine ring. Also, the ortho position of the substituents on ring A results in being preferred although the para-methoxy substitution of derivative **74** is tolerated with a slight loss of activity. Unfortunately, the low solubility of **73** and **81** limited their enzymatic evaluation.

The docking studies suggested that compounds could act as competitive inhibitors in the helicase binding site. To prove this hypothesis, a dose-response curves was generated, titrating compound **64** in DDX3X helicase assays, in the presence of increasing fixed concentrations of the RNA substrate. As shown in **Figure 23**, the inhibitory potency (ID_{50}) of the compound decreased (higher absolute values) as the RNA concentrations increased. This is consistent with the hypothesized competitive mechanism of inhibition, with respect to the RNA substrate.

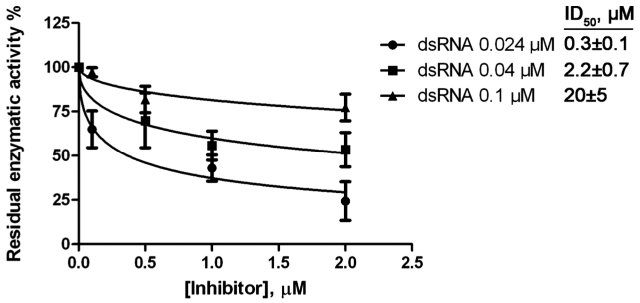

Figure 23

Increasing concentrations of the inhibitor **64** were titrated in helicase assays, in the presence of 30 pmol of DDX3X and increasing fixed concentrations of the dsRNA substrate. Values are the mean of three independent measurements ± standard deviation (S.D.). The residual enzymatic activity values were plotted as a function of the inhibitor concentrations, and the corresponding ID_{50} values calculated for each dsRNA concentration are indicated on the right side of the panel.

The compounds described here have been rationally designed to specifically target the helicase activity of DDX3X. To confirm the selectivity of our compounds, we tested the ability of **EI04D**, **EI03D**, **65**, and **70** to inhibit the ATPase activity of DDX3X and the helicase activity of the related human DEAD-box helicase DDX1. As shown in Table **6**, no inhibition was found with any compound concentration.

Table 6
Enzymatic data on selected compounds

Cpd ID	ATPase DDX3, IC_{50} (μM)	DDX1, IC_{50} (μM)
EI04D	>200[a]	>200[a]
EI03D	>200[a]	>200[a]
65	>200[a]	>200[a]
70	>200[a]	>200[a]

[a] The value >200 indicates that less than 20% of inhibition was observed at 200 μM, the highest concentration tested.

Then, the cellular concentrations of the protein DDX3X was quantified, to confirm the presence of the target before carrying out anti-WNV and cytotoxicity assays. As reported in **Table 7**, African green monkey kidney epithelial (VERO) cells are endowed by a DDX3X concentration of 421 nM, higher than adenocarcinomic human alveolar basal epithelial cells (A549) but lower than human hepatocellular carcinoma cell line Huh7 (respectively valued 103 and 755 nM).

Table 7
DDX3X cellular expression in Huh7, A549, and VERO[a]

	Huh7[b]	VERO[c]	A549[d]
DDX3(nM)	755±170	421±140	103±20

[a] Values represent mean ± S.D. of three independent experiments. [b] Evaluated in Huh7: hepatocellular carcinoma cells. [c] Evaluated in VERO: African green monkey kidney cells. [d] Evaluated in A549: adenocarcinomic human alveolar basal epithelial cells.

The three cell lines were infected with WNV at a multiplicity of infection (MOI) of 0.1, and the antiviral activity of compound **65** was assayed. As reported in **Table 8**, its activities seemed proportional to the DDX3X concentrations. Probably due to the DDX3X implications in pulmonary cancer[23], **65** showed a cytotoxic activity of 21.3 μM. For these reasons, to avoid interferences due to anticancer-related cytotoxic effects, the human Huh7 cells characterized by a higher DDX3X concentration of 755 nM were chosen to perform our studies.

Table 8
Comparison of antiviral activities of **65** in different cell lines infected with WNV

Cpd ID	**Huh7**^{d}		**VERO**^{e}		**A549**^{f}	
	EC_{50}^b(μM)	CC_{50}^c(μM)	EC_{50}^b(μM)	CC_{50}^c(μM)	EC_{50}^b(μM)	CC_{50}^c(μM)
65	23.1±0.4	>200	12±1.1	>200	3.4±0.8	21.3±1.1
rivabirin	90±2.5	>200	95±5.1	nt	46±2.3	nt

[a]Data represent the mean of two values of the least two experiments. [b]EC50: half-maximal effective concentration or the needed concentration to inhibit 50% viral-induced cell death. [c]CC50: cytotoxic concentration 50 or the needed concentration to induce 50% death of noninfected cells. [d]Evaluated in Huh7: hepatocellular carcinoma cells. [e]Evaluated in VERO: African green monkey kidney cells. [f]Evaluated in A549: adenocarcinomic human alveolar basal epithelial cells. Ribavirin was used as a reference compound. nt = not tested.

Subsequently, Huh7 cells were infected with WNV and compounds endowed with the best IC_{50}s against DDX3X were assayed for their antiviral properties.

Table 9
Antiviral activities and cytotoxicity of selected compounds against WNV-infected Huh7 cells[a]

Cpd ID	**WNV**^{d}	**Huh7**
	EC_{50}^b(μM)	CC_{50}^c(μM)
EI04D	8.8±0.2	>200
EI03D	120±5.2	175±11
64	2.3±0.5	>200
65	23.1±0.4	>200
66	65.9±2.3	>200
68	>200	>200

69	39.9±1.1	>200
70	55±1.1	>200
71	13±0.8	>200
ribavirin	95.5±3.2	>200

[a]Data represent mean ± standard deviation of three experiments. [b] EC50: half-maximal effective concentration or needed concentration to inhibit 50% viral-induced cell death. [c]CC50: cytotoxic concentration 50 or needed concentration to induce 50% death of noninfected cells. [d]evaluated in Huh7 cells. Ribavirin was used as a reference compound.

As reported in **Table 9**, compounds showed interesting antiviral activities, ranging from 2.3 to 65.9 μM, comparable or even higher than those of the broad spectrum antiviral ribavirin, which was used as a reference compound. Compound **64** showed the highest antiviral activity value of 2.3 μM, followed by **71**, **65**, **69**, **70**, and **66**. All of these compounds had comparable antienzymatic profiles; the overall trend of their cellular activities could be ascribed to their different physicochemical parameters, which may influence the cellular penetration and consequently antiviral effects. Compound **71** resulted to be particularly promising, since it showed good antiviral activity together with favorable aqueous solubility, 100 times higher than that of hit **EI04D**. **EI03D** showed the lowest activity, probably due to the limited cellular permeability (see ADME Assay and **Table 11**). The mild antiviral activity of **69** is in line with its % inhibition of about 60% against DDX3X and was considered not worthy of further investigation. Finally, compound **68** endowed with the worst DDX3X inhibitory activity was found to be inactive in the cell- based assay.

To better evaluate the antiviral activities of our compounds, we selected **65** as a representative of the series, to investigate the mechanism of action (**Figure 24**).

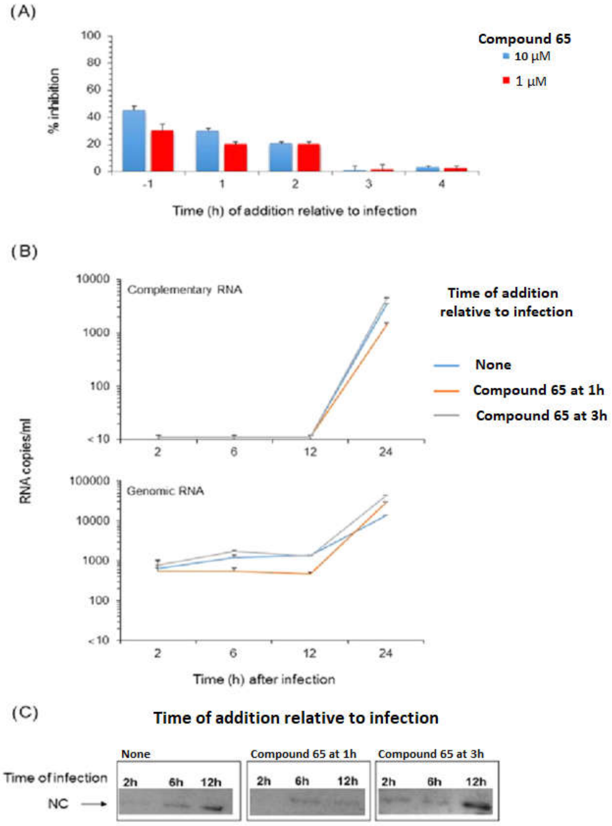

Figure 24

Effect of varying anti-DDX3X compound **65** at the time of administration on WNV replication. **(A)** WNV infection of Huh7 cells at MOI of 0.1 in presence of compound **65** at 1 and 10 µM added at the indicated time (h) relative to the infection and assayed with the viral plaque reduction assay. Data represent mean ± standard deviation. **(B)** WNV genomic and complementary viral RNA in Huh7 cells assayed after infection in absence or in presence of compound **65** at 1 µM added at 1 and 3 h of the infection. Data represent mean ± standard deviation. **(C)** WNV capsid protein electrophoretic mobility obtained from Huh7 cells after infection in absence or in presence of compound **65** at 1 µM added at 1 and 3 h of the infection. No compound **65** addition performed.

Time of addition studies, performed at compound inhibitory concentration near and under the IC_{50} values, clearly demonstrated that **65** acted in the first 2 h of the WNV life cycle, since the addition of **65** after 3 h post infection did not affect viral replication (**Figure 24A**). In particular, although an antiviral effect was visible when added before viral infection and cell entry occurred, the substantial activity of compound **65** after 2 h of infection also could indicate that its main target activity was in subsequent steps of the viral replication. Consequently, we evaluated the effect of **65** in the production of both genomic and complementary viral RNA. Importantly, our inhibitor was able to interfere with the concentration of genomic RNA at an early time of the infection (from 2 to 12 h post infection) only when added 1 h post infection and caused no significant changes when added 3 h post infection. Moreover, although the complementary RNA was not revealed up to 12 h post infection, 24 h post infection the quantity of complementary RNA was slightly lower after the addition of compound **65** 1 h post infection. Moreover, our inhibitor was able to interfere marginally with the concentration of genomic RNA, without significant changes in the quantity of the complementary noninfective RNA. Finally, we evaluated its effect on the production of WNV nucleocapsid (NC) protein. As highlighted in **Figure 24C**, the addition of **65** 1 h post infection significantly reduced the concentration of NC whereas according to the results shown in panel C, its addition after 3 h did not change NC concentration, which was comparable to the control. Overall, these results suggested a possible implication of **65** in the first phases of viral replication, probably during protein translation, after the entry process.

Derivatives **FH001**, **FH002**; **FH003** and **FH006** were assayed for their antiviral activity on HIV-1 infected cells.

Table 10
Antiviral activities and cytotoxicity of selected compounds against HIV-1 infected cells.

cpd ID		HIV (NL4-3)	H9
		IC_{50} (μM)[a]	CC_{50} (μM)[b,c]
FH001	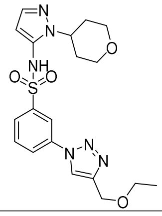	>100	50

FH002	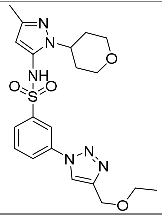	>100	>100
FH003	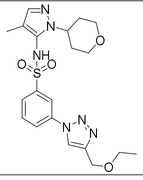	>100	>100
FH006	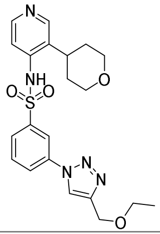	>100	>100

[a] IC_{50}: half maximal inhibitory concentration or needed concentration to inhibit 50% viral replication. [b] CC_{50} Cytotoxic concentration 50 or needed concentration to induce 50% death of non-infected cells. [c] Evaluated on H9 cells.

As reported in **Table 10** the introduction of pyrazolo ring for **FH001**, **FH002** and **FH003** induced no antiviral activity on HIV-1 infected cells. The introduction of methyl groups in **FH002** and **FH003** on pyrazolo ring reflected better profile of cytotoxicity.

In a similar way also the pyridinic ring of **FH006** revealed inactivity against HIV-1, but without signs of cytotoxicity (CC_{50} >100).

In vitro ADME analysis

Compounds **EI03D**, **64**, **65**, **66**, **70**, and **71** were *in vitro* profiled for aqueous solubility, liver microsomal stability, and membrane permeability. As reported in **Table 11**, compounds were characterized by improved aqueous solubility values, in particular, compounds **70**, **71**, and **66**, even if less active against WNV than compound **EI04D** and about 100 times more soluble than **EI04D** with Log *S* comparable to that of **EI03D**. Furthermore, passive membrane permeability assay (PAMPA) indicated nonlimiting values with the exception of hit compound **EI03D**, that showed a minor value of 0.1×10^{-6} cm s^{-1} that is probably the cause of its inactivity in antiviral assay. Finally, stability tests in human liver microsomes (HLM) disclosed that all selected compounds showed a high metabolic stability major of 95.6%.

Table 11
***In vitro* ADME analysis of selected compounds**

Cpd ID	P_{app}[a]	LogS[b]	HLM stability[c]
EI04D	2.86×10^{-6}	-7.05	99.0±0.6
EI03D	$<0.1 \times 10^{-6}$	-4.36	98.3±1.1
64	0.1×10^{-6}	-7.5	95.6±0.8
65	0.21×10^{-6}	-7.5	99.0±1.2
66	0.71×10^{-6}	-4.6	97.1±0.6
70	0.68×10^{-6}	-5.4	98.0±0.9
71	0.44×10^{-6}	-4.7	96.0±0.4

[a]Apparent permeability reported in cm s^{-1}. [b]Aqueous solubility expressed as Log of molar concentration. [c]Human liver microsomal (HLM) metabolic stability.

Conclusion

We identified a completely new family of selective inhibitors of the helicase activity of DDX3X. The compounds described here have been rationally designed to specifically target the helicase activity of DDX3X. Accordingly, they were inactive in the ATPase assay and in the helicase assay against the related human DEAD-box helicase DDX1. Future plans for improving the assessment of selectivity of our compounds include their evaluation on a broader panel of DDX-family helicases, as well as the exploitation of Huh7 cells with inducible silencing of DDX3X expression. Among the compounds reported, six of them (namely, compounds **64**, **65**, **66**, **69**, **70** and **71**) are characterized by promising antiviral activities against WNV, lower than those of the broad spectrum antiviral ribavirin, and more importantly without signs of cellular toxicities. It is worth pointing out that the antiviral activities are DDX3X-dependant, since compound **68,** endowed with the worst inhibitory activity, did not show any antiviral effect up to 200 μM. Furthermore, merged derivatives **66**, **70**, and **71**, even if less active against WNV than compound **EI04D**, are endowed with very good aqueous solubility, with values 100 times higher than those of the hit **EI04D**, thus overcoming an important limitation of the previously published compounds. Furthermore, the time of addition experiments is consistent with literature studies previously published on DDX3X recruitment on WNV replication site,[21] highlighting an involvement of our compounds in the first phases of WNV replication and suggesting their possible role in the step of protein translation, after the entry process. Noteworthily, although tolerability and bioavailability need to be proved in vivo, the effectiveness of the compounds also when added before viral cell infection suggests their possible use as prophylactic antiviral drugs. Even if we are aware that deep investigations are needed to elucidate the mechanism of action of our compounds, to date, the exact implications of our own target on the WNV life cycle remain poorly understood.

In the absence of any available antiviral compound for the treatment of WNV infection[24], the present study confirms our previous findings, suggesting that DDX3X helicase inhibitors can represent the Achilles' hell of viruses and that human proteins can be manipulated to fight novel emerging viral threats.

Chapter 5

Experimental section

Docking studies

All compounds studied herein were docked within the RNA binding site of the modeled human DDX3X closed conformation previously published[19] using the software package GOLD 4.1.[25,26] The pocket under investigation was inserted into a grid box centered on residue Phe357 and enclosing residues lying within 10 Å from such amino acid. The genetic algorithm parameter settings were employed using the search efficiency set at 100%, and 100 runs were carried out for each ligand. Chemscore was chosen as the fitness function. Finally, results differing by less than 1.5 Å in ligand-all atom root-mean-square deviation were clustered together. For each inhibitor, the first ranked solution was selected for further analysis. Pictures of the modeled ligand−enzyme complexes together with graphic manipulations were rendered using PyMOL molecular graphic system.[27]

Chemistry

Reagents were obtained from commercial suppliers (for example, Sigma-Aldrich, Alfa Aesar). All commercially available chemicals were used as purchased without further purification. CH_2Cl_2 and MeOH were dried prior to use by distilling from calcium hydride or magnesium methoxide. Anhydrous reactions were run under positive pressure of dry N_2 or argon. Thin-layer chromatography (TLC) was carried out using Merck TLC plate silica gel 60 F254. Chromatographic purifications were performed on columns packed with Merck 60 silica gel, 23−400 mesh, for the flash technique.

All NMR spectra were recorded on a Bruker Avance DPX400 spectrometer at 400 MHz for ^{1}H NMR or 100 MHz for ^{13}C NMR. Chemical shifts are reported relative to tetramethylsilane at 0.00 ppm.

^{1}H patterns are described using the following abbreviations: s = singlet, d = doublet, t = triplet, q = quartet, quint = quintet, sx = sextet, sept = septet, m = multiplet, br = broad signal, and br s = broad singlet.

Mass spectra (MS) data were obtained using an Agilent 1100 LC/ mass spectra detection (MSD) VL system (G1946C) with a 0.4 mL min^{-1} flow rate using a binary solvent system 25 of 95:5 methyl alcohol/ water ratio. UV detection was monitored at 254 nm. Mass spectra were acquired in positive and negative mode scanning over the mass range.

Microwave Irradiation Experiments. These were conducted using CEM Discover Synthesis Unit (CEM Corp., Matthews, NC). The machine consists of a continuous focused microwave power delivery system with operator selectable power output from 0 to 300 W. The temperature of the content vessels was monitored using a calibrated infrared temperature control mounted under the reaction vessel. All experiments were performed using a stirring option whereby the contents of the vessels are stirred by means of a rotating magnetic plate located below the floor of the microwave cavity and a Teflon-coated magnetic stir bar in the vessel.

UV/Layer Chromatography (LC)-MS Method. For the quanti- tative analysis, a UV/LC-MS system was used. LC analysis was performed by Agilent 1100 LC/MSD VL system (G1946C) (Agilent Technologies, Palo Alto, CA) constituted by a vacuum solvent degassing unit, a binary high-pressure gradient pump, and a 1100 series UV detector, and a 1100 MSD model VL benchtop mass spectrometer was used. The Agilent 1100 series mass spectra detection (MSD) single-quadrupole instrument was equipped with the orthogonal spray atmospheric pressure ionization electrospray (API- ES, Agilent Technologies, Palo Alto, CA). Nitrogen was used as nebulizing and drying gas. The pressure of the nebulizing gas, the flow of the drying gas, the capillary voltage, the fragmentor voltage, and the vaporization temperature were set at 40 psi, 9 L min^{-1}, 3000 V, 70 V, and 350 °C, respectively. UV detection was monitored at 280 nm. The LC-electrospray ionization (ESI)-MS determination was performed by operating the MSD in the positive-ion mode. Spectra were acquired over the scan range *m/z* 50−1500 using a step size of 0.1 u. Chromatographic analysis was performed using a Varian Polaris 5 C18- A column (150 × 4.6 mm^2, 5 μm particle size) at room temperature. Analysis was carried out using gradient elution of a binary solution; eluent A was ACN, whereas eluent B consisted of water. The analysis started at 0% A for 3 min, then rapidly increased up to 98% in 12 min, finally remaining at 98% A until 18 min. The analysis was performed at a flow rate of 0.8 mL min^{-1}, and the injection volume was 20 μL. LC retention times, molecular ion (*m*/*z*), and LC purity (by UV) were based on the method below. Purity of compounds (as measured by the peak area ratio) was >97%.

Procedure for the synthesis of 3-Azidobenzenethiol **38**

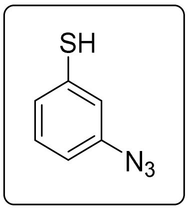

3-Azidobenzenethiol (38). 3-Aminothiophenol (2.0 g, 15.97 mmol) was dissolved in CH_3CN and cooled to 0 °C in an ice–salt bath. To this stirred solution was added *t*-BuONO (2.84 mL, 23.9 mmol), and the mixture was stirred for 10 min; after this time, $TMSN_3$ (2.53 mL, 19.17 mmol) was added dropwise, during 10 min, and the resulting brown solution was stirred at r.t. One hour later the solvent was removed at reduced pressure and the residue was purified by flash chromatography on silica gel. Purification eluent: EP/EA 8:2, yield 80%. Pale white solid. ^{1}H NMR (400 MHz, $CDCl_3$): δ 7.3–7.2 (m, 2H), 7.1 (s, 1H) 6.9 (d, *J* = 6.4 Hz, 1H) ppm.

Procedure for the synthesis of alkyne (39)

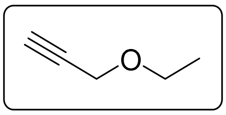

Ethoxyprop-1-yne (39). To a stirring solution of 200 g of NaOH in 300 mL of water (0.3 mol, 16.8 g) was added propargyl alcohol (2.5 mL, 33.02 mmol). To this was slowly added diethylsulfate (15 mmol, 2082 mg) in 2 h dropwise, and the mixture was heated at 50 °C. The final product was distilled off; the distillation was stopped at 95 °C; then, the content of the receiver was washed with cold NH_4Cl(aq) solution and separated. Yield 68% colorless oil. ^{1}H NMR (400 MHz, $CDCl_3$-*d*): δ 4.13–4.13 (d, *J* = 2.4 Hz, 2H), 3.60–3.55 (q, *J* = 6.9 Hz, 2H), 2.41–2.40 (t, *J* = 4.8 Hz, 1H), 1.24–1.22 (t, *J* = 6.9 Hz, 3H)ppm.

Procedure for the synthesis of Triazole 40

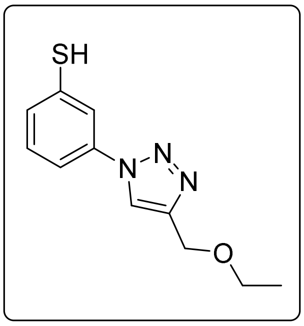

3-(4-(ethoxymethyl)-1H-1,2,3-triazol-1-yl)benzenethiol (40). The alkyne **39** (6.08 mmol) and the azide **38** (5.07 mmol) were suspended in a 1:1 mixture of water and *t*-BuOH (1.5 mL each) in a 10 mL glass vial equipped with a small magnetic stirring bar. To this was added sodium ascorbate (2.5 mmol) and copper(II) sulfate pentahydrate (2.50 mmol). The mixture was then heated for 10 min at 80 °C under microwave irradiation, using an irradiation power of 300 W. Thereafter, the solvent was removed at reduced pressure, water was added, and the mixture was extracted with EtOAc (3 × 20 mL). The organic layers were collected, washed with brine, and dried over Na_2SO_4. The crude was purified by flash chromatography on silica gel. Purification eluent: EP/EA 7:3, white solid, yield 62%. ^{1}H NMR (400 MHz, MeOD): δ 7.97 (s, 1H), 7.94 (s, 1H), 7.60 7.57 (m, 2H), 7.49 (t, J = 8.0 Hz, 1H), 4.70 (s, 2H), 3.66 (q, J = 6.8 Hz, 2H), 0.89 (t, J = 6.8 Hz, 3H) ppm.

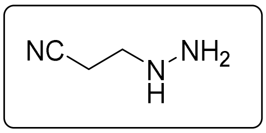

3-hydrazinylpropanenitrile 46. Acrylonitrile (18.85 mmol) was added dropwise to hydrazine hydrate (18.85 mmol) at 0°C and stirred at room temperature for thirty minutes. Solvent was removed at reduced pressure to provide the product as yellow oil, that was used in the next step without further purification. ^{1}HNMR (500 MHz, $CDCl_3$): δ4.1 (bs, 1H), 2.99 (bs, 2H), 2.72-2.70 (t, J=5.0 Hz, 2H), 2.32-2.30 (t, J=5.0 Hz, 2H) ppm.

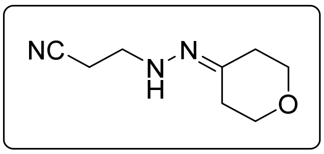

3-(2-(tetrahydro-4H-pyran-4-ylidene)hydrazinyl)propanenitrile 48 A solution of tetrahydro-4H-pyran-4-one(2.65 mmol) in EtOH was added dropwise to **46** (2.65 mmol) at 0°C. The mixture was stirred at room temperature for 12 h. Solvent was removed at reduced pressure to provide the product as yellow oil, that was used in the next step without further purification. ^{1}HNMR (500 MHz, CDCl$_3$): δ4.6 (bs, 1H), 4.05-4.03 (t, J=5.0 Hz, 2H), 4.01-3.98 (t, J=5.0 Hz, 2H),3.64-3.61 (t, J=5.0 Hz, 2H),2.90-2.87 (t, J=10 Hz, 2H), 2.62-2.59 (q, J=10.0 Hz, 2H) ppm.

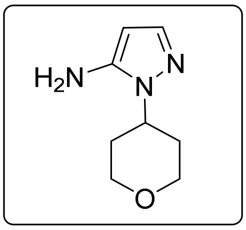

1-(tetrahydro-2H-pyran-4-yl)-1H-pyrazol-5-amine 49. 48 (5.08 mmol) was dissolved in butanol, MeONa (20.3 mmol) was added dropwise and the mixture was refluxed 12 h. The mixture was concentrated at reduced pressure. The residue was treated with sat. NH$_4$Cl. The resulting mixture was then extracted three times with DCM and washed with brine. Organic layer was dried over Na$_2$SO$_4$ and evaporated under reduced pressure. The product was purified *via* flash chromatography on silica gel (eluent EtOAc), to furnish a yellow solid in a yield of 23%. ^{1}HNMR (500 MHz, CDCl$_3$): δ7.21-7.17 (d, J=20 Hz, 1H), 5-47-5.43 (d, J=20 Hz, 1H), 4.08-4.0 (m, 3H), 3.45-3.37 (m, 4H), 2-20-2.12 (m, 2H), 1.76-1.74 (m, 2H) ppm.

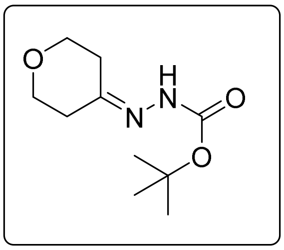

tert-butyl 2-(tetrahydro-4H-pyran-4-ylidene)hydrazine-1-carboxylate 51. To a solution of tetrahydro-4H-pyran-4-one (0.76 mmol) in MeOH, tert-butyl hydrazinecarboxylate (0.76

mmol) **50** was added dropwise at 0°C. The mixture was stirred at room temperature 12 h. Solvent was removed at reduced pressure to provide the product as white solid, that was used in the next step without further purification. ^{1}HNMR (400 MHz, $CDCl_3$): δ7.26 (bs, 1H), 3.76-3.73 (t, J=5.2 Hz, 2H), 3.69- 3.66 (t, J=5.2, 2H), 2.43-2.40 (t, J=11.2 Hz, 2H), 2.36-2.33 (t, J=11.2 Hz, 2H), 1.43 (s, 9H) ppm.

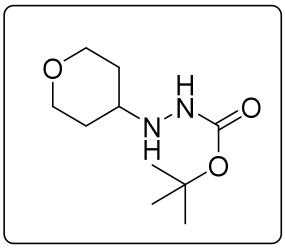

tert-butyl 2-(tetrahydro-2H-pyran-4-yl)hydrazine-1-carboxylate 52. To a suspension of **51** (0.23 mmol) in H_2O, CH_3COOH (2.76 mmol) was added and the reaction mixture was stirred at room temperature for 30 minutes to get a clear solution. To this solution $NaCNBH_3$ (0.23 mmol) was added portionwise and stirred at room temperature for 2 hours. The mixture was cooled to 0°C and quenched with 1N NaOH. The resulting mixture was then extracted three times with DCM and washed with brine. Organic layer was dried over Na_2SO_4 and evaporated under reduced pressure to provide the product as white solid, that was used in the next step without further purification. ^{1}HNMR (400 MHz, $CDCl_3$):δ6.32 (bs, 1H), 5.26 (bs, 1H), 3.93-3.90 (m, 2H), 3.38-3.33 (m, 2H), 3.03-2.98 (m, 1H), 1.74-1.71 (m, 1H), 1.47 (s, 9H), 0.89-0.85 (m, 2H) ppm.

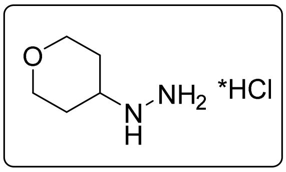

(tetrahydro-2H-pyran-4-yl)hydrazine hydrochloride 53. A solution of **52** in DCM was added to a solution of HCl in dioxane ant the mixture was stirred at room temperature for 3 days. Solvent was removed at reduced pressure to provide the product as white solid, that was used in the next step without further purification. ^{1}HNMR (400 MHz, $CDCl_3$): δ4.03 (bs, 1H), 3.67-3.57 (m, 4H), 3.35 (bs, 2H), 3.09-3.03 (m, 1H), 1.87-1.85 (m, 2H), 1.19-1.15 (m, 2H) ppm.

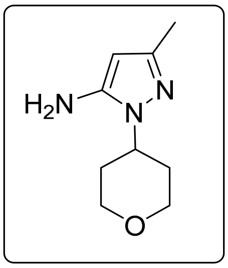

3-methyl-1-(tetrahydro-2H-pyran-4-yl)-1H-pyrazol-5-amine 55. To a solution of **53** (1.03 mmol) in EtOH, 3-oxo-butyronitrile (1.03 mmol) was added and the mixture was refluxed 12 h. Solvent was removed at reduced pressure and the product was purified *via* flash chromatography on silica gel (eluent DCM/MeOH 96/4), to furnish a white solid in a yield of 74%. ^{1}HNMR (400 MHz, $CDCl_3$): δ5.32 (s, 1H), 4.09-4.02 (m, 2H), 3.56 (bs, 2H), 3.49-3.43 (m, 1H), 3.09-3.03 (m, 2H), 2.30 (s, 3H), 2.17-2.15 (m, 2H), 1.19-1.13 (m, 2H) ppm.

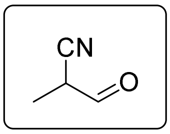

2-methyl-3-oxopropanenitrile 58. To a stirring solution of n-BuLi in THF (10 mmol) cooled to -78°C was added a solution of proprionitrile (9.1 mmol) in THF dropwise and the mixture was stirred for 1 hour. Ethyl formate (136 mmol) was added to the reaction mixture at -78°C. The reaction was warmed to room temperature over a period of 4 hours. pH 5 was achieved with HCl 1N, the resulting mixture was then extracted three times with Et_2O and washed with brine. Organic layer was dried over Na_2SO_4 and evaporated with air to provide the product as yellow oil, that was used in the next step without further purification. ^{1}HNMR (400 MHz, $CDCl_3$):δ7.98 (s, 1H), 4.067-4.01 (q, J= 6.8 Hz, 1H), 1.81 (s, 3H) ppm.

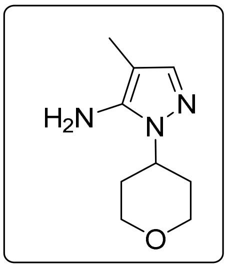

4-methyl-1-(tetrahydro-2H-pyran-4-yl)-1H-pyrazol-5-amine 59. To a solution of **53** (1.03 mmol) in EtOH, **58** (1.03 mmol) was added and the mixture was refluxed 12 h. Solvent was removed at reduced pressure and the product was purified *via* flash chromatography on silica gel (eluent DCM/MeOH 96/4), to furnish a white solid in a yield of 36%. ^{1}HNMR (400 MHz, $CDCl_3$): δ7.17 (s, 1H), 4.24-4.19 (m, 1H), 4.12-4.05 (m, 4H), 3.53-3.47 (m, 4H), 3.30 (bs, 2H), 1.89 (s, 3H), 1.82-1.79 (m, 2H), 1.25-1.21 (m, 2H) ppm.

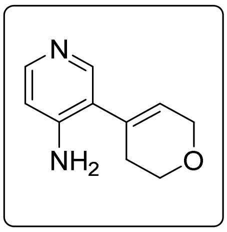

3-(3,6-dihydro-2H-pyran-4-yl)pyridin-4-amine 62. A mixture of 4-amino-3-bromopyridine (2.02 mmol) and (3,6-dihydro-2H-pyran-4-yl)boronic acid (3.03 mmol) were dissolved in THF/H_20 (6/1). Cs_2CO_3 (4.44 mmol), PPh_3 (0.20 mmol), $Pd(OAc)_2$ (0.20 mmol)were added and the mixture was stirred at reflux 16 hours under N_2 atmosphere. Water was added, then the resulting mixture was extracted three times with EtOAc. The organic layers were collected, washed with brine and dried over Na2SO4. The crude was purified by flash chromatography on silica gel usind DCM/MeOH 96/4 as eluent. White solid, yield 74%. ^{1}HNMR (400 MHz, MeOD): δ7.93 (s, 1H), 7.87-7.85 (d, J=4Hz, 1H), 6.63-6.61 (d, J=4 Hz, 1H), 5.48-5.45 (t, J=4Hz, 1H), 4.27-4.26 (d, J=4 Hz, 2H), 3.94-3.91 (t, J=4Hz, 2H), 2.34-2.31 (t, J=4Hz, 2H) ppm.

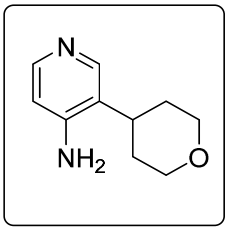

3-(tetrahydro-2H-pyran-4-yl)pyridin-4-amine 63. To a mixture of **62** (0.2 mmol) and Pd/C (10%) (0.02 mmol) in MeoH was added a balloon of H2, and the mixture was stirred at room temperature for 3 hours. The balloon was removed and the reaction mixture was filtered through a pad of celite. The filtrate was concentrated *in vacuo*. Yield 98%, white solid. ^{1}HNMR (400 MHz, MeOD): δ7.94 (s, 1H), 7.87-7.85 (d, J=4Hz, 1H), 6.63-6.61 (d, J=4Hz,1H), 4.05-4.02 (m, 2H), 3.63-3.57 (m, 2H), 2.87-2.83 (m, 1H), 1.78-1.71 (m, 4H) ppm.

General procedure for the synthesis of sulfonamides **FH001**, **FH002**, **FH003**. Benzenethiol **40** (0.43 mmol) was dissolved in 2 mL of acetonitrile; to this, 30% H_2O_2 (1.2 mmol, 133 µL) and $SOCl_2$ (0.43 mmol, 31 µL) were added and the corresponding solution was stirred at room temperature for 30 min. After this time, the reaction mixture was extracted with EtOAc (3 × 25 mL), washed with brine, and dried over Na_2SO_4. The solvent was removed at reduced pressure, and the resulting residue was dissolved in 5 mL of dichloromethane (DCM). To this, a solution of the opportune aromatic amine(0.43 mmol) in 1 mL of pyridine was added drop by drop. The resulting mixture was stirred at r.t. for 4 h. Thereafter, water was added and the mixture was extracted with DCM (6 × 30 mL), washed with brine, and dried over anhydrous Na_2SO_4. The corresponding residue was purified on silica with the opportune eluent.

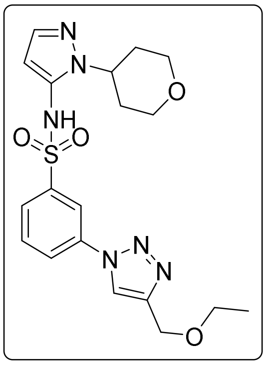

3-(4-(ethoxymethyl)-1H-1,2,3-triazol-1-yl)-N-(1-(tetrahydro-2H-pyran-4-yl)-1H-pyrazol-5-yl)benzenesulfonamide FH001. Purification eluent: DCM/MeOH 98/2, white solid, yield 41%. ^{1}HNMR (400 MHz, MeOD): δ8.40 (s, 1H), 7.51-7.49 (d, J=4 Hz, 2H), 7.41-7.38 (t, J=4Hz, 2H),7.14-7.12 (d, J= 8 Hz, 1H), 4.63 (s, 2H), 4.35-4.31 (m, 1H), 4.08-4.05 (q, J=4 Hz, 4 H), 2.17-2.12 (m, 2H), 1.88-1.85 (m, 2H), 1.22-1.19 (t, J=4 Hz, 3H) ppm. ^{13}C NMR (400 MHz, MeOD): 147.96, 144.21, 142.07, 140.85, 135.99, 128.31, 123.69, 120.16, 115.18, 114.98, 83.93, 65.24, 64.22, 61.50, 51.98, 30.09, 12.50, 6.36.

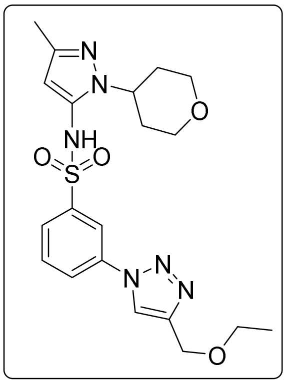

3-(4-(ethoxymethyl)-1H-1,2,3-triazol-1-yl)-N-(3-methyl-1-(tetrahydro-2H-pyran-4-yl)-1H-pyrazol-5-yl)benzenesulfonamide FH002. Purification eluent: EP/EA 3:7, white solid, yield 41%. ^{1}HNMR (400 MHz, MeOD): δ8.58 (s, 1H), 8.30 (s, 1H), 8.08-8.06 (d, J=7.6 Hz, 1H), 7.87-7.85 (d, J=8Hz, 1H), 7.75-7.71 (t, J=8 Hz, 1H), 5.47 (s, 1H), 4.66 (s, 2H), 4.50-4.44 (m, 1H), 4.11-4.05 (m, 1H), 3.98-3.94 (m, 1H), 3.64-3.50 (m, 1H), 3.47-3.41 (t, J=11.6 Hz, 2H), 2.06 (s, 3H), 2.04-1.99 (m, 2H), 1.27-1.24 (m, 2H), 1.23-1.21 (t, J=3.6 Hz, 3H) ppm. ^{13}C NMR (400 MHz, MeOD): 147.26, 146.17, 142.88, 137.30, 126.98, 123.64, 121.79, 118.60, 66.85, 65.75, 62.97, 60.14, 32.35, 14.00, 13.08, 12.29.

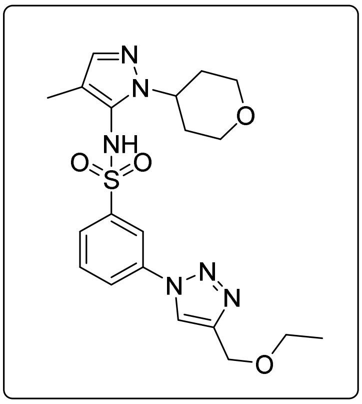

3-(4-(ethoxymethyl)-1H-1,2,3-triazol-1-yl)-N-(4-methyl-1-(tetrahydro-2H-pyran-4-yl)-1H-pyrazol-5-yl)benzenesulfonamide FH003. Purification eluent: EP/EA 3:7, white solid, yield 41%. ^{1}HNMR (400 MHz, MeOD): δ8.59 (s, 1H), 8.28 (s, 1H), 8.16-8.14 (d, J=7.6 Hz, 1H), 7.84-7.76 (m, 2H), 7.24 (s, 1H), 4.83 (s, 2H), 4.66-4.52 (m, 1H), 4.11-4.06 (m, 2H), 3.64-3.62 (9, J=6.8 Hz, 2H), 3.45-3.39 (m, 2H), 2.13-2.05 (m, 3H), 1.88-1.69 (m, 2H), 1.41 (s, 3H),1.33-1.30(t, J=4Hz, 3H) ppm. ^{13}C NMR (400 MHz, MeOD): 146.28, 142.09, 138.80, 137.63, 131.01, 130.51, 127.15, 124. 37, 121.76, 118.78, 112.39, 66.80, 65.79, 62.97, 60.12, 53.49, 32.46, 31.94, 19.48, 14.01, 13.08, 6.10

General procedure for the synthesis of sulphonamides **FH006**. Benzenethiol **40** (0.43 mmol) was dissolved in 2 mL of acetonitrile; to this, 30% H_2O_2 (1.2 mmol, 133 μL) and $SOCl_2$ (0.43 mmol, 31 μL) were added and the corresponding solution was stirred at room temperature for 30 min. After this time, the reaction mixture was extracted with EtOAc (3 × 25 mL), washed with brine, and dried over Na_2SO_4. The solvent was removed at reduced pressure, and the resulting residue was dissolved in 5 mL of dichloromethane (DCM). To this, a solution of the opportune aromatic amine(0.43 mmol) in 2 mL of triethylamine was added drop by drop. The resulting mixture was stirred at r.t. for 4 h. Solvent was removed at reduced pressure, the corresponding residue was purified on silica with the opportune eluent. The last step of synthesis for **FH006** was characterized by the use of triethylamine as base instead of pyridine as described for the other compounds considering the basicity of compounds **63**.

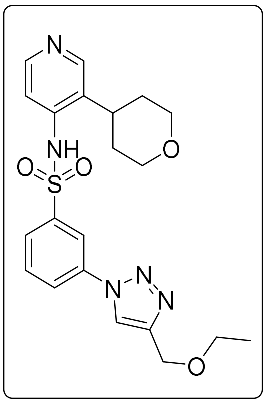

3-(4-(ethoxymethyl)-1H-1,2,3-triazol-1-yl)-N-(3-(tetrahydro-2H-pyran-4-yl)pyridin-4-yl)benzenesulfonamide FH006. Purification eluent: EP/EA 3:7, white solid, yield 4%. ^{1}HNMR (400 MHz, acetone): δ8.61 (s, 1H), 8,42 (s, 1H), 8.02-7.96 (m, 2H), 7.91-7.87 (t, J=7.2 Hz, 2H), 7.71-7.67 (t, J=8Hz, 1H), 7.51-7.50 (d, J=4Hz, 1H), 5.60 (s, 2H), 4.63 (s, 1H), 3.94-3.90 (m, 2H), 3.60-3.55 (m, 1H), 3.55-3.43 m(m, 2H), 3.30-3.27 (m, 2H), 1.58-1.54 (m, 2H), 1.51-1.54 (t, J=4.4 Hz, 3H) ppm. ^{13}C NMR (400 MHz, acetone): 156.5, 149.7, 147.1, 144.4, 139.7, 132.8, 129.0, 128.8, 127.3, 125.7, 124.3, 119.1, 109.5, 68.1, 66.6, 65.5, 40.6, 33.0, 32.8, 15.2.

Enzimatic assays

Protein expression and purification

Recombinant his-tagged human full length DDX3X was cloned in the *Escherichia coli* expression vector pET-30a(+). ShuffleT7 *E. coli* cells were transformed with the plasmid and grown at 37°C up to OD_{600} = 0.7. DDX3X expression was induced with 0.5 mM isopropyl β-D-1-thiogalactopyranoside at 15 °C O/N. Cells were harvested by centrifugation and lysed and the crude extract centrifuged at 100.000xg for 60 min at 4 °C in a Beckman centrifuge before being loaded onto a FPLC Ni-NTA column (GE Healthcare). The column was equilibrated in buffer A (50 mM Tris–HCl pH 8.0, 250 mM NaCl, 25 mM imidazole and 20% glycerol). After extensive washing in buffer A, the column was eluted with a linear gradient in buffer A from 25 to 250 mM imidazole. Proteins in the eluted fractions were visualized on a sodium dodecyl sulfate (SDS)-polyacrylamide gel electro- phoresis (PAGE) and tested for the presence of DDX3X by Western blot with anti-DDX3X A300-A450 (BETHYL) at 1:2000 dilution in 5% milk. Fractions containing the purest DDX3X protein were pooled and stored at −80 °C.

Helicase assay based on fluorescence resonance energy transfer

The dsRNA substrate for the helicase assay was prepared by hybridizing two ssRNA oligonucleotides with the following sequences:

Fluo-FAM 5′ UUUUUUUUUUUUUUAGUACCGC- CACCCUCAGAACC 3′
Qu-BHQ1 5′ GGUUCUGAGGGUGGCGGUACUA 3′ DNA capture 5′ TAGTACCGCCACCCTCAGAACC 3′

The sequence in Fluo-FAM complementary to Qu-BHQ1 is underlined. Flu-FAM carries a 6-carboxyfluorescein fluorophore at its 3′ end, whereas Qu-BHQ1 carries a Black Hole Quencher group at its 5′end. The DNA capture oligonucleotide is complementary to the Qu-BHQ1 oligonucleotide but bears no modifications.

Helicase assay using the dsRNA substrate was performed in 20 mM Tris–HCl (pH 8), 70 mM KCl, 2 mM $MgCl_2$, 2 mM dithiothreitol, 12 units RNasin, 2 mM ATP, 50 nM dsRNA, and 100 nM capture strand in 20 μL of reaction volume. The unwinding reaction was started by adding 60 pmol of DDX3X recombinant protein and carried out at 37 °C for 40 min using a LightCycler 480 (Roche). The fluorescence intensity was recorded every 30 s. Data of fluorescence signal were analyzed by linear interpolation, and the corresponding slope values were used to determine the apparent unwinding rate.

Kinetic Analysis. The IC_{50} values have been calculated from dose−response curves. Data (in triplicate) were plotted and analyzed by least-squares nonlinear regression, according to the method of Marquardt−Levenberg, with the computer program GraphPad Prism 6.0. Data were fitted to the following equation

$$E_{obs} = E_{max}/(1 + (IC_{50}/[I])^n)$$

where $E_{(obs)}$ is the observed enzymatic activity in the presence of each inhibitor dose [I], $E_{(max)}$ is the maximal enzymatic activity in the absence of the inhibitor, and n is an exponential term to take into account sigmoidal dose-response curves.

Cell extracts (CEs) and DDX3X quantification

Ten million cells were ruptured with a Dounce homogenizer in lysis buffer (50 mM Tris−HCl pH 8.0, 0.1% SDS, 350 mM NaCl, 0.25% Triton X-100, protease inhibitor cocktail (Sigma-Aldrich)). The lysate was incubated for 30 min on ice, sonicated for 5 min (at 30 s intervals), and centrifuged at 15.000xg for 10 min at 4 °C. The protein concentration in the supernatant (crude extract) was quantified with Bradford. For DDX3X quantification, increasing concentrations of crude extract (5, 10, 20, and 40 μg) were loaded on a SDS-PAGE alongside known concentrations (50, 100, 150, and 200 ng) of recombinant purified DDX3X. Separated proteins were subjected to Western blot analysis with anti-DDX3X A300-A450 (BETHYL) at 1:2000 dilution in 5% milk. The blot was next incubated with a horseradish peroxidase- conjugated secondary antibody, and the bands corresponding to DDX3X were visualized with enhanced chemiluminescent substrate (Westar Nova 2.0, Cyanagen) using a ChemiDoc XRS (Bio-Rad) apparatus. The intensity of the bands was measured by densitometry, and the values obtained for the purified DDX3X were plotted as a function of the protein concentration and analyzed by linear interpolation to derive a reference curve, whose slope corresponded to the estimated intensity (I) × ng^{-1} (DDX3X) value. This parameter was used to calculate the $I \times ng^{-1}$ values for the DDX3X in the cell extract, from the intensities of the DDX3X bands in the corresponding cell extract (CE) samples. The mean $I \times ng^{-1}$ (CE) value was used to calculate the ng of DDX3X × μL^{-1} of extract and then the total ng of DDX3X present in the extract. This value was divided for the total number of cells used (10^7), to derive the ng DDX3X/cell. On the basis of the known molecular weight of DDX3X, the Avogadro number, and assuming a mean cellular volume of 6.55×10^{-11} L, the final molar concentration of DDX3X per cell was calculated. Each experiment was repeated three times, with each blot carrying a reference curve alongside the extract samples, to account for variations in loading/transfer efficiency. The reference $I \times \text{ng}^{-1}$ (DDX3X) value obtained was anyway comparable across the different experiments (±20% variation).

ATPase assay

The ATPase assay was carried out by using the commercial kit Promega ADP-Glo Kinase Assay. The reaction was performed in 30 mM Tris−HCl, 9 mM $MgCl_2$, 0.05 mg mL^{-1} bovine serum albumin, 50 μM ATP, and 4 μM DDX3. The reaction was performed following the ADP-Glo Kinase Assay Protocol, and luminescence was measured with MicroBeta TriLux PerkinElmer.

The anti-DDX1 activity was evaluated as previously reported.[28]

Antiviral assay

WNV Inhibitory Viral Plaque Reduction Assay. Huh7 cells, derived from human hepatoma (kindly provided from Istituto Toscano Tumori, Core Research Laboratory, Siena, Italy) was used for the inhibitory viral plaque reduction assay. The cell propagation medium was Dulbecco's modified Eagle's medium (DMEM; Sigma, Milano, Italy) supplemented with 10% fetal bovine serum (Sigma) and 1% penicillin/streptomicin (Sigma). WNV (strain of lineage 2) viral stock, consisting of cell-free supernatants of acutely infected Huh7 cells, was aliquoted and stored at −80 °C until used. Titration of the viral stocks as a plaque forming unit (PFU) was carried out in Huh7 cells. WNV was used to infect Huh7 cell line in duplicate, and viral plaques were visualized 4 days following infection. Briefly, six-well plates were seeded with 2.5×10^5 cells in 3 mL of growth medium and kept overnight at 37 °C with 5% CO_2. On the day of infection, after removal of the growth medium, cell monolayers at 80−90% confluence were infected with WNV viral stock with a multiplicity of infection (MOI) of 0.1 in a final volume of 0.3 mL and incubated for 1 h at 37 °C with 5% CO_2. Then, cells were washed with phosphate-buffered saline (PBS) 1× and 30 μL of dimethyl sulfoxide (DMSO) alone (viral positive control) or with 10-fold serial dilutions of DDX3X inhibitory compounds immediately added in duplicates together with 300 μL of fresh DMEM complete medium (compound final concentrations of 100, 10, 1, 0.1, and 0.01 μM). 1-β-D- Ribofuranosyl-1,2,4-triazole-3-carboxamide (ribavirin; Sigma) diluted in DMSO was used as inhibitory reference control. Then, the overlay medium composed by 0.5% SeaPlaque Agarose (Lonza, Basel, Switzerland) diluted in propagation medium was added to each well. After 4 days (Huh7) of incubation at 37 °C, the monolayers were fixed with methanol (Carlo Erba Chemicals, Milan, Italy) and stained with 0.1% crystal violet (Carlo Erba Chemicals) and the viral titers were calculated by plaque forming unit (PFU) counting. The percent of plaque reduction activity was calculated by dividing the average PFU of treated samples by the average of DMSO-treated samples (viral positive control). Fifty percent inhibitory concentrations (IC_{50}) were calculated using the predicted exponential growth function in Microsoft Excel, which uses existing x–y data to estimate the corresponding anti-DDX3X compound concentration (x) from a known value (y), which in this case was 50% PFU. Mean IC_{50} ± standard deviations (S.D.) were calculated using all replicates. All experiments were repeated at least twice. All experimental procedures were conducted under biosafety level 3 containment.

Cytotoxicity assay

Monolayers of 2.5×10^4 Huh7 cells per well were kept in flat-bottom 96-well culture plates and allowed to adhere overnight. Then, when the cell layers were confluent, the medium was removed, the wells were washed twice with PBS, treated with 100 μL of DMEM, with 10 μL of DMSO alone (cell positive control), or with various concentrations of DDX3X inhibitory compounds under study (compound final concentrations of 100, 10, 1, 0.1, and 0.01 μM) and incubated for 3 days at 37 °C in a CO_2 atmosphere. After treatment, a 3-(4,5-dimethylthiazol-2-yl)-2,5-diphenyltetrazolium bromide kit (Roche, Milan, Italy) was used according to the supplier's instructions and the absorbance of each well was determined using a microplate spectrophotometer at a wavelength of 570 nm. Cytotoxicity was calculated by dividing the average optical density of treated samples by the average of DMSO-treated samples (cell positive control).

Virus RNA quantification and capsid protein detection assay

Total RNA was extracted and purified from infected and control cells using an RNAeasy mini Kit (Qiagen). Two hundred nanograms of total RNA of each sample in a 20 μL reaction mixture were reverse-transcribed by using the indicated primers (primer PROCf 5′ CCTgTgTgAgCTgACAAA CTT AgT 3′ for the transcription of WNV complementary RNA and primer PROCr 5′gCgT TTT AgCA TA TT gA CAgCC 3′ for the transcription of WNV genomic RNA) and amplified by real-time PCR in a Rotor-gene 3000 real-time thermal cycler (Corbett Research, Australia) with the following WNV specific primer and probe (primer PROCf 5′CCTgTgTgA gCTgA CAAACTTAgT 3′ and primer PROCr 5′gCgTTTTAg CAT A TTgACAgCC 3′, and probe PROC-TMD VIC-5′ CCTGGTTTCTTAGACATCGAGATCTTCGTGC 3′).[24] Plasmid calibration standards were used for quantification of the template concentration. The sensibility of the assay was 10 copies.

The specific WNV capsid protein was investigated with Western blot analysis of Huh7-infected cells electrophoresed on 10% SDS-PAGE and then probed with anticapsid protein polyclonal antibody followed by peroxidase-conjugated anti- rabbit IgG polyclonal antibody.

ADME assay

Chemicals. All solvents and reagents were from Sigma-Aldrich Srl (Milan, Italy), brain polar lipid extract (porcine) was from Avanti Polar Lipids, INC. (Alabama). Dodecane was purchased from Fluka (Milan, Italy). Pooled male donors 20 mg mL^{-1} HLM were from BD Gentest-Biosciences (San Jose, California). Milli-Q quality water (Millipore, Milford, MA) was used. Hydrophobic filter plates (MultiScreen-IP, Clear Plates, 0.45 μm diameter pore size), 96-well microplates, and 96- well UV-transparent microplates were obtained from Millipore (Bedford, MA).

Parallel Artificial Membrane Permeability Assay (PAMPA and PAMPA–Blood–Brain Barrier (BBB)). Donor solution (0.5 mM) was prepared by diluting 1 mM dimethyl sulfoxide (DMSO) compound stock solution using phosphate buffer (pH 7.4, 0.025 M). Filters were coated with

5 μL of a 1% (w/v) dodecane solution of phosphatidylcholine or 4 μL of brain polar lipid solution (20 mg mL^{-1} 16% $CHCl_3$, 84% dodecane) prepared from $CHCl_3$ solution 10% w/v, for intestinal permeability and BBB permeability, respectively. Donor solution (150 μL) was added to each well of the filter plate. To each well of the acceptor plate was added 300 μL of solution (50% DMSO in phosphate buffer). All compounds were tested in three different plates on different days. The sandwich was incubated for 5 h at room temperature under gentle shaking. After the incubation time, the plates were separated and samples were taken from both receiver and donor sides and analyzed using LC with UV detection at 280 nm. LC analysis was performed with a PerkinElmer (series 200) instrument equipped with an UV detector (PerkinElmer 785A, UV/vis detector). Chromatographic separation was conducted using a Polaris C18 column (150 × 4.6 mm^2, 5 μm particle size) at a flow rate of 0.8 mL min^{-1} with a mobile phase composed of 60% ACN/40% H_2O–formic acid 0.1% for all compounds. Permeability (P_{app}) was calculated according to the following equation with some modification to obtain permeability values in cm s^{-1}

$$P_{app} = \frac{V_D V_A}{(V_D + V_A)At} - \ln(1 - r)$$

where V_A is the volume in the acceptor well, V_D is the volume in the donor well (cm^3), A is the "effective area" of the membrane (cm^2), t is the incubation time (s), and r is the ratio between drug concentration in the acceptor and equilibrium concentration of the drug in the total volume(V_D + V_A). Drug concentration is estimated by using the peak area integration. Membrane retentions (%) were calculated according to the following equation

$$\%MR = \frac{[r - (D + A)]100}{EQ}$$

where r is the ratio between drug concentration in the acceptor and equilibrium concentration and D, A, and EQ represented drug concentration in the donor, acceptor and equilibrium solution, respectively.

Water Solubility Assay. Compound 1 (1 mg) was added to 1 mL of water. The sample was shaked in a shaker bath at room temperature for 24–36 h. The suspensions were filtered through a 0.45 μm nylon filter (Acrodisc) and the solubilized compound determined by LC-MS-MS assay. The determination was performed in triplicate. For the quantification was used an LC-MS system consisting of a Varian apparatus (Varian Inc.), including a vacuum solvent degassing unit, two pumps (212- LC), a Triple Quadrupole MSD (mod. 320-LC) mass spectrometer with ES interface and Varian MS Workstation System Control vers. 6.9 software. Chromatographic separation was obtained using a Pursuit C18 column (50 × 2.0 mm^2) (Varian) with 3 μm particle size and gradient elution: eluent A being ACN and eluent B consisting of an aqueous solution of formic acid (0.1%). The analysis started with 0% of eluent A, which was linearly increased up to 70% in 10 min, then slowly increased up to 98% up to 15 min. The flow rate was 0.3 mL min^{-1}, and the injection volume was 5 μL. The instrument operated in positive mode and parameters were: detector 1850 V, drying gas pressure 25.0 psi, desolvation temperature 300.0°C, nebulizing gas 45.0 psi, needle 5000 V, and shield 600 V. Nitrogen was used as nebulizer gas and drying gas. Collision-induced dissociation was performed using argon as the collision gas at a pressure of 1.8 mTorr in the collision cell. Quantification of the single compound was made by comparison with apposite calibration curves realized with standard solutions in methanol.

Microsomal Stability Assay. Each compound in DMSO solution was incubated at 37 °C for 60 min in 125 mM phosphate buffer (pH7.4) and 5 μL of human liver microsomal protein (0.2 mg mL^{-1}), in the presence of a NADPH-generating system at a final volume of 0.5 mL (compounds' final concentration, 50 μM); DMSO did not exceed 2% (final solution).The reaction was stopped by cooling in ice and adding 1.0 mL of acetonitrile. The reaction mixtures were then centrifuged, and the parent drug and metabolites were subsequently determined by LC-UV-MS. Chromatographic analysis was performed with an Agilent 1100 LC/MSD VL system (G1946C) (Agilent Technologies, Palo Alto, CA) constituted by a vacuum solvent degassing unit, a binary high- pressure gradient pump, an 1100 series UV detector, and an 1100 MSD model VL benchtop mass spectrometer. Chromatographic separation was obtained using a Varian Polaris C18-A column (150 × 4.6 mm^2, 5 μm particle size) and gradient elution: eluent A being ACN and eluent B consisting of an aqueous solution of formic acid (0.1%). The analysis started with 2% of eluent A, which was rapidly increased up to 70% in 12 min, then slowly increased up to 98% in 20 min. The flow rate was 0.8 mL min-1, and the injection volume was 20 μL. The Agilent 1100 series mass spectra detection (MSD) single quadrupole instrument was equipped with the orthogonal spray API-ES (Agilent Technologies, Palo Alto, CA). Nitrogen was used as nebulizing and drying gas. The pressure of the nebulizing gas, the flow of the drying gas, the capillary voltage, the fragmentor voltage, and the vaporization temperature were set at 40 psi, 9 L min-1, 3000 V, 70 V, and 350 °C, respectively. UV detection was monitored at 280 nm. The LC-ESI-MS determination was performed by operating the MSD in the positive-ion mode. Spectra were acquired over the scan range m/ z 100-1500 using a step size of 0.1 u. The percentage of a unmetabolized compound was calculated by comparison with reference solutions.

Abbreviation

DNA	Deoxyribonucleic acid
RNA	Ribonucleic acid
SF	Superfamily
DEAD	Aspartic acid- Glutamic acid- Alanine- Aspartic acid
ATP	Adenosine triphosphate
RNP	Ribonucleoprotein
snRNP	Small nuclear RNP
mRNA	Messenger RNA
RISC	RNA-induced silencing complex
ssRNA	Single stranded RNA
miRNA	microRNA
siRNA	Small interfering RNA
NMD	Nonsense mediated decay
PTC	Premature termination codon
EJC	Exon junction complex
Upf	Upstream frame shiftign
AZFa	Azoospermia factor a
ADP	Adenosine diphosphate
AMP	Adenosine monophosphate
HD	Hydrogen donor
HA	Hydrogen acceptor
CRM-1	Chromosome maintenance region 1
NES	Nuclear export signal
TAP	Tip-associated protein
RS	Arginine-serine rich
mRNP	Messenger RNP
IFNβ	Interferon β
NPC	Nuclear pore complex
rRNA	Ribosomal RNA
tRNA	Transfer RNA
Nups	Nucleoporins
HIV	Human immunodeficiency virus
AIDS	Acquired immunodeficiency syndrome
RRE	Rev responsive element
WNV	West nile virus
DENV	Dengue virus
JEV	Japanese encephalitis virus
YFV	Yellow fever virus
CDC	Centres for disease control prevention
WHO	World health organisation
ORF	Open reading frame
prM	Pre-membrane
NS	Non structural

ER	Endoplasmatic reticulum
UTR	Untraslated regions
ART	Antiretroviral therapy
NNRTI	Non-nucleoside reverse-transcriptase inhibitors
NRTI	Nucleoside reverse-transcriptase inhibitors
PI	Protease inhibitors
CdK	Cyclin-dependent kinases
HBV	Hepatitis B virus
HCV	Hepatitis C virus
HCC	Hepatocellular carcinoma
EMT	Epithelial -mesenkymal-like transformation
HIF	Hypoxia-inducible factor
HPV	Human papilloma virus infection
RFS	Relapse free survival
HRE	Hypoxia response element
EC_{50}	Half maximal effective concentration
REN	Ring expanded
PAINS	Pan-assay interference compounds
IC_{50}	Half maximal inhibitory concentration
SAR	Structure-activity relationship
CC_{50}	Cytotoxic concentration
PBMC	Peripheral blood mononuclear cell
o.n.	Overnight
TEA	Triethylamine
THF	Tetrahydrofuran
r.t.	Room temperature
ki	Inhibition constant
SI	Selectivity index
ADME	Absorption, distribution, metabolism excretion
AppP	Passive membrane permeability
PAMPA	Parallel artificial membrane permeability
TLC	Thin layer cromatography
NMR	Nuclear magnetic resonance
DMSO	Dimethylsulfoxide
DCM	Dichloromethane
ACN	Acetonitrile
n-BuLi	n-Buthyllithium solution
δ	Chemical shift
CE	Cell extract

Appendix I

Publications:

- **DDX3X Helicase Inhibitors as a New Strategy to Fight the West Nile Virus Infection.**
  Annalaura Brai; Francesco Martelli; Valentina Riva; Anna Garbelli; Roberta Fazi; Claudio Zamperini; Alessandro Pollutri; Lucia Falsitta; Stefania Ronzini; Laura Maccari; Giovanni Maga; Simone Giannecchini; Maurizio Botta.
  Journal of Medicinal Chemistry
  DOI: 10.1021/acs.jmedchem.8b01403
- **Synthesis and antiviral activity of novel 1,3,4-thiadiazole inhibitors of DDX3X.**

  Annalaura Brai, Stefania Ronzini, Valentina Riva, Lorenzo Botta, Claudio Zamperini, Matteo Borgini, Claudia Trivisani, Anna Garbelli, Carla Pennisi, Adele Boccuto, Francesco Saladini, Maurizio Zazzi, Giovanni Maga and Maurizio Botta.

  Molecules (Accepted)

Appendix II

Conferences and Presentations:

- Poster presentation on **"DDX3X Helicase Inhibitors as a New Strategy to Fight the West Nile Virus Infection"**, EFMC-ASMC 2019-9th Edition of EFMC International Symposium on Advances in Synthetic and Medicinal Chemistry, Athens (Greece), September 2019.
- Member of organizing committee of **VII EWDSy**–7th European Workshop in Drug Synthesis, Siena (Italy), (May 2018).
- Poster presentation on "**Human DDX3X Protein: A New Valuable Target to Develop Broad Spectrum Antiviral Agents**", VII EWDSy, 7th European Workshop in Drug Design and Synthesis, Siena (Italy), May 2018.
- Poster presentation on **"Design and Synthesis of new HIV-1 Reverse Transcriptase Dimerization Inhibitors"**, MYCS–Merck Young Chemists Symposium, Milano Marittima (Italy), November 2017.

Bibliography

1. Abdel-Monem, M, Durwald, H. & Hoffmann-Berling, H. Enzymic Unwinding of DNA. 2. Chain Separation by an ATP-Dependent DNA Unwinding Enzyme. *Eur. J. Biochem.* **65**, 441–449 (1976).

2. Jankowsky, E. RNA helicases at work: Binding and rearranging. *Trends Biochem. Sci.* **36**, 19–29 (2011).

3. Brosh, R. M. & Bohr, V. A. Human premature aging, DNA repair and RecQ helicases. *Nucleic Acids Res.* **35**, 7527–7544 (2007).

4. Pyle, A. M. Translocation and Unwinding Mechanisms of RNA and DNA Helicases. *Annu. Rev. Biophys.* **37**, 317–336 (2008).

5. Umate, P., Tuteja, N. & Tuteja, R. Genome-wide comprehensive analysis of human helicases. *Commun. Integr. Biol.* **4**, 118–37 (2011).

6. Jankowsky, E. & Fairman, M. E. RNA helicases--one fold for many functions. *Curr. Opin. Struct. Biol.* **17**, 316–24 (2007).

7. Kadaré, G. & Haenni, A. L. Virus-encoded RNA helicases. *J. Virol.* **71**, 2583–90 (1997).

8. Abdelhaleem, M. Do human RNA helicases have a role in cancer? *Biochim. Biophys. Acta* **1704**, 37–46 (2004).

9. Hanada, K. & Hickson, I. D. Molecular genetics of RecQ helicase disorders. *Cell. Mol. Life Sci.* **64**, 2306–22 (2007).

10. Singleton, M. R., Dillingham, M. S. & Wigley, D. B. Structure and Mechanism of Helicases and Nucleic Acid Translocases. *Annu. Rev. Biochem.* **76**, 23–50 (2007).

11. Gorbalenya, A. E. & Koonin, E. V. Helicases: amino acid sequence comparisons and structure-function relationships. *Curr. Opin. Struct. Biol.* **3**, 419–429 (1993).

12. Xing, Z., Ma, W. K. & Tran, E. J. The DDX5/Dbp2 subfamily of DEAD-box RNA helicases. *Wiley Interdisciplinary Reviews: RNA* **10**, (2019).

13. Tanner, N. K. & Linder, P. ScienceDirect - Molecular Cell : DExD/H Box RNA Helicases: From Generic Motors to Specific Dissociation Functions. *Mol. Cell* **8**, 251–262 (2001).

14. Gillian, A. L. & Svaren, J. The Ddx20/DP103 Dead Box Protein Represses Transcriptional Activation by Egr2/Krox-20. *J. Biol. Chem.* **279**, 9056–9063 (2004).

15. Cordin, O., Banroques, J., Tanner, N. K. & Linder, P. The DEAD-box protein family of RNA helicases. *Gene* **367**, 17–37 (2006).

16. Linder, P. & Stutz, F. mRNA export: Travelling with DEAD box proteins. *Current Biology* **11**, (2001).

17. Tseng, S. S. I. *et al.* Dbp5p, a cytosolic RNA helicase, is required for poly(A)+ RNA export. *EMBO J.* **17**, 2651–2662 (1998).

18. Kim, Y. S., Lee, S. G., Park, S. H. & Song, K. Gene structure of the human DDX3 and chromosome mapping of its related sequences. *Mol. Cells* **12**, 209–14 (2001).

19. Foresta, C., Ferlin, A. & Moro, E. Deletion and expression analysis of AZFa genes on the human Y chromosome revealed a major role for DBY in male infertility. *Hum. Mol. Genet.* **9**, 1161–9 (2000).

20. Ditton, H. J., Zimmer, J., Kamp, C., Rajpert-De Meyts, E. & Vogt, P. H. The AZFa gene DBY (DDX3Y) is widely transcribed but the protein is limited to the male germ cells by translation control. *Hum. Mol. Genet.* **13**, 2333–2341 (2004).

21. Bol, G. M., Xie, M. & Raman, V. DDX3, a potential target for cancer treatment. *Mol. Cancer* **14**, 188 (2015).

22. Schütz, P. *et al.* Comparative structural analysis of human DEAD-Box RNA helicases. *PLoS One* **5**, 1–11 (2010).

23. Högbom, M. *et al.* Crystal Structure of Conserved Domains 1 and 2 of the Human DEAD-box Helicase DDX3X in Complex with the Mononucleotide AMP. *J. Mol. Biol.* **372**, 150–159 (2007).

24. Brennan, R. *et al.* Investigating nucleo-cytoplasmic shuttling of the human DEAD-box helicase DDX3. *Eur. J. Cell Biol.* **97**, 501–511 (2018).

25. Lai, M.-C., Lee, Y.-H. W. & Tarn, W.-Y. The DEAD-box RNA helicase DDX3 associates with export messenger ribonucleoproteins as well as tip-associated protein and participates in translational control. *Mol. Biol. Cell* **19**, 3847–58 (2008).

26. Yedavalli, V. S. R. K., Neuveut, C., Chi, Y. H., Kleiman, L. & Jeang, K. T. Requirement of DDX3 DEAD box RNA helicase for HIV-1 Rev-RRE export function. *Cell* **119**, 381–392 (2004).

27. Schröder, M., Baran, M. & Bowie, A. G. Viral targeting of DEAD box protein 3 reveals its role in TBK1/IKKε-mediated IRF activation. *EMBO J.* **27**, 2147–2157 (2008).

28. Sekiguchi, T., Iida, H., Fukumura, J. & Nishimoto, T. Human DDX3Y, the Y-encoded isoform of RNA helicase DDX3, rescues a hamster temperature-sensitive ET24 mutant cell line with a DDX3X mutation. *Exp. Cell Res.* **300**, 213–222 (2004).

29. Lai, M. C., Lee, Y. H. W. & Tarn, W. Y. The DEAD-box RNA helicase DDX3 associates with export messenger ribonucleoproteins as well as tip-associated protein and participates in translational control. *Mol. Biol. Cell* **19**, 3847–3858 (2008).

30. Chao, C.-H. *et al.* DDX3, a DEAD box RNA helicase with tumor growth-suppressive property and transcriptional regulation activity of the p21waf1/cip1 promoter, is a candidate tumor suppressor. *Cancer Res.* **66**, 6579–88 (2006).

31. Yang, Q. & Jankowsky, E. The DEAD-box protein Ded1 unwinds RNA duplexes by a mode distinct from translocating helicases. *Nat. Struct. Mol. Biol.* **13**, 981–6 (2006).

32. Tarn, W. Y. & Chang, T. H. The current understanding of Ded1p/DDX3 homologs from yeast to human. *RNA Biology* **6**, 17–20 (2009).

33. Owsianka, A. M. & Patel, A. H. Hepatitis C virus core protein interacts with a human DEAD box protein DDX3. *Virology* **257**, 330–40 (1999).

34. Merz, C., Urlaub, H., Will, C. L., Lu¨hrmann, R. & Lu¨hrmann, L. Protein composition of human mRNPs spliced in vitro and differential requirements for mRNP protein

recruitment.

35. Shih, J.-W., Tsai, T.-Y., Chao, C.-H. & Wu Lee, Y.-H. Candidate tumor suppressor DDX3 RNA helicase specifically represses cap-dependent translation by acting as an eIF4E inhibitory protein. *Oncogene* **27**, 700–14 (2008).

36. Lee, C.-S. *et al.* Human DDX3 functions in translation and interacts with the translation initiation factor eIF3. *Nucleic Acids Res.* **36**, 4708–18 (2008).

37. Okamura, M., Inose, H. & Masuda, S. RNA export through the NPC in eukaryotes. *Genes (Basel).* **6**, 124–149 (2015).

38. Köhler, A. & Hurt, E. Exporting RNA from the nucleus to the cytoplasm. *Nat. Rev. Mol. Cell Biol.* **8**, 761–73 (2007).

39. Fairman-Williams, M. E., Guenther, U. P. & Jankowsky, E. SF1 and SF2 helicases: Family matters. *Current Opinion in Structural Biology* **20**, 313–324 (2010).

40. Ranji, A. & Boris-Lawrie, K. RNA helicases: Emerging roles in viral replication and the host innate response. *RNA Biology* **7**, 775–787 (2010).

41. Kwong, A. D., Rao, B. G. & Jeang, K.-T. Viral and cellular RNA helicases as antiviral targets. *Nat. Rev. Drug Discov.* **4**, 845–53 (2005).

42. Schröder, M. Viruses and the human DEAD-box helicase DDX3: inhibition or exploitation? *Biochem. Soc. Trans.* **39**, 679–83 (2011).

43. Mabuka, J., Nduati, R., Odem-Davis, K., Peterson, D. & Overbaugh, J. HIV-specific antibodies capable of ADCC are common in breastmilk and are associated with reduced risk of transmission in women with high viral loads. *PLoS Pathog.* **8**, (2012).

44. Hahn, R. A. & Inhorn, M. C. Anthropology and Public Health: Bridging Differences in Culture and Society. Anthropology and Public Health: Bridging Differences in Culture and Society (Oxford University Press, 2009).

45. Ishaq, M. *et al.* Knockdown of cellular RNA helicase DDX3 by short hairpin RNAs suppresses HIV-1 viral replication without inducing apoptosis. *Mol. Biotechnol.* **39**,

231–8 (2008).

46. Maga, G. *et al.* Pharmacophore modeling and molecular docking led to the discovery of inhibitors of human immunodeficiency virus-1 replication targeting the human cellular aspartic acid-glutamic acid-alanine-aspartic acid box polypeptide 3. *J. Med. Chem.* **51**, 6635–8 (2008).

47. Radi, M. *et al.* Discovery of the first small molecule inhibitor of human DDX3 specifically designed to target the RNA binding site: Towards the next generation HIV-1 inhibitors. *Bioorganic Med. Chem. Lett.* **22**, 2094–2098 (2012).

48. Shi, P.-Y. Molecular virology and control of flaviviruses. (Caister Academic Press, 2012).

49. Rice, C. M. *et al.* Nucleotide sequence of yellow fever virus: Implications for flavivirus gene expression and evolution. *Science (80-.).* **229**, 726–733 (1985).

50. Brai, A. *et al.* DDX3X Helicase Inhibitors as a New Strategy To Fight the West Nile Virus Infection. *J. Med. Chem.* **62**, 2333–2347 (2019).

51. Dwivedi, V. D., Tripathi, I. P., Tripathi, R. C., Bharadwaj, S. & Mishra, S. K. Genomics, proteomics and evolution of dengue virus. *Brief. Funct. Genomics* **16**, 217–227 (2017).

52. Rodenhuis-Zybert, I. A., Wilschut, J. & Smit, J. M. Dengue virus life cycle: Viral and host factors modulating infectivity. *Cell. Mol. Life Sci.* **67**, 2773–2786 (2010).

53. Bhatt, S. *et al.* The global distribution and burden of dengue. *Nature* **496**, 504–507 (2013).

54. Kumar, R., Singh, N., Abdin, M. Z., Patel, A. H. & Medigeshi, G. R. Dengue virus capsid interacts with DDX3X-A potential mechanism for suppression of antiviral functions in dengue infection. *Cell. Infect. Microbiol.* **7**, (2018).

55. Sumiyoshi, H. *et al.* Complete nucleotide sequence of the Japanese encephalitis virus genome RNA. *Virology* **161**, 497–510 (1987).

56. He, B. Viruses, endoplasmic reticulum stress, and interferon responses. *Cell Death Differ.* **13**, 393–403 (2006).

57. Su, H.-L., Liao, C.-L. & Lin, Y.-L. Japanese encephalitis virus infection initiates endoplasmic reticulum stress and an unfolded protein response. *J. Virol.* **76**, 4162–71 (2002).

58. Li, C. *et al.* Cellular DDX3 regulates Japanese encephalitis virus replication by interacting with viral un-translated regions. *Virology* **449**, 70–81 (2014).

59. Fazi, R. *et al.* Homology Model-Based Virtual Screening for the Identification of Human Helicase DDX3 Inhibitors. *J. Chem. Inf. Model.* **55**, 2443–54 (2015).

60. Bol, G. M. *et al.* Targeting DDX 3 with a small molecule inhibitor for lung cancer therapy . *EMBO Mol. Med.* **7**, 648–669 (2015).

61. Heerma van Voss, M. R. *et al.* Identification of the DEAD box RNA helicase DDX3 as a therapeutic target in colorectal cancer. *Oncotarget* **6**, 28312–26 (2015).

62. Wilky, B. A. *et al.* RNA helicase DDX3: A novel therapeutic target in Ewing sarcoma. *Oncogene* **35**, 2574–2583 (2016).

63. Xie, M. *et al.* RK-33 Radiosensitizes Prostate Cancer Cells by Blocking the RNA Helicase DDX3. *Cancer Res.* **76**, 6340–6350 (2016).

64. Li, Y. *et al.* Inducible resistance of tumor cells to tumor necrosis factor-related apoptosis-inducing ligand receptor 2-mediated apoptosis by generation of a blockade at the death domain function. *Cancer Res.* **66**, 8520–8 (2006).

65. Shih, J.-W. *et al.* Critical roles of RNA helicase DDX3 and its interactions with eIF4E/PABP1 in stress granule assembly and stress response. *Biochem. J.* **441**, 119–29 (2012).

66. Botlagunta, M. *et al.* Oncogenic role of DDX3 in breast cancer biogenesis. *Oncogene* **27**, 3912–22 (2008).

67. Chen, H.-H., Yu, H.-I., Cho, W.-C. & Tarn, W.-Y. DDX3 modulates cell adhesion and

motility and cancer cell metastasis via Rac1-mediated signaling pathway. *Oncogene* **34**, 2790–800 (2015).

68. Wang, H. & Ryu, W.-S. Hepatitis B virus polymerase blocks pattern recognition receptor signaling via interaction with DDX3: implications for immune evasion. *PLoS Pathog.* **6**, e1000986 (2010).

69. Angus, A. G. et al. Requirement of cellular DDX3 for hepatitis C virus replication is unrelated to its interaction with the viral core protein. *J. Gen. Virol.* **91**, 122–132 (2010).

70. Huang, J.-S. et al. Diverse cellular transformation capability of overexpressed genes in human hepatocellular carcinoma. *Biochem. Biophys. Res. Commun.* **315**, 950–8 (2004).

71. Chao, C.-H. et al. DDX3, a DEAD box RNA helicase with tumor growth-suppressive property and transcriptional regulation activity of the p21waf1/cip1 promoter, is a candidate tumor suppressor. *Cancer Res.* **66**, 6579–88 (2006).

72. Li, H.-K. et al. DDX3 Represses Stemness by Epigenetically Modulating Tumor-suppressive miRNAs in Hepatocellular Carcinoma. *Sci. Rep.* **6**, 28637 (2016).

73. Botlagunta, M. *et al.* Oncogenic role of DDX3 in breast cancer biogenesis. *Oncogene* **27**, 3912–22 (2008).

74. Botlagunta, M. *et al.* Expression of DDX3 is directly modulated by hypoxia inducible factor-1 alpha in breast epithelial cells. *PLoS One* **6**, e17563 (2011).

75. Bol, G. M. *et al.* Expression of the RNA helicase DDX3 and the hypoxia response in breast cancer. *PLoS One* **8**, e63548 (2013).

76. Heerma van Voss, M. R. *et al.* The prognostic effect of DDX3 upregulation in distant breast cancer metastases. *Clin. Exp. Metastasis* **34**, 85–92 (2017).

77. Xie, M. *et al.* NZ51, a ring-expanded nucleoside analog, inhibits motility and viability of breast cancer cells by targeting the RNA helicase DDX3. *Oncotarget* **6**, 29901–13 (2015).

78. Heerma van Voss, M. R. *et al.* Combination treatment using DDX3 and PARP inhibitors induces synthetic lethality in BRCA1-proficient breast cancer. *Med. Oncol.* **34**, 33 (2017).

79. Wu, D.-W. *et al.* Reduced p21(WAF1/CIP1) via alteration of p53-DDX3 pathway is associated with poor relapse-free survival in early-stage human papillomavirus-associated lung cancer. *Clin. Cancer Res.* **17**, 1895–905 (2011).

80. Wu, D.-W. *et al.* DDX3 loss by p53 inactivation promotes tumor malignancy via the MDM2/Slug/E-cadherin pathway and poor patient outcome in non-small-cell lung cancer. *Oncogene* **33**, 1515–26 (2014).

81. Bol, G. M. *et al.* Targeting DDX3 with a small molecule inhibitor for lung cancer therapy. *EMBO Mol. Med.* **7**, 648–69 (2015).

82. Wilky, B. A. *et al.* RNA helicase DDX3: a novel therapeutic target in Ewing sarcoma. *Oncogene* **35**, 2574–83 (2016).

83. Xie, M. *et al.* RK-33 Radiosensitizes Prostate Cancer Cells by Blocking the RNA Helicase DDX3. *Cancer Res.* **76**, 6340–6350 (2016).

84. Sun, M., Song, L., Zhou, T., Gillespie, G. Y. & Jope, R. S. The role of DDX3 in regulating Snail. *Biochim. Biophys. Acta* **1813**, 438–47 (2011).

85. Liang, S. *et al.* The Clinical and Pathological Significance of Nectin-2 and DDX3 Expression in Pancreatic Ductal Adenocarcinomas. *Dis. Markers* **2015**, 379568 (2015).

86. Miao, X. *et al.* Nectin-2 and DDX3 are biomarkers for metastasis and poor prognosis of squamous cell/adenosquamous carcinomas and adenocarcinoma of gallbladder. *Int. J. Clin. Exp. Pathol.* **6**, 179–90 (2013).

87. Backus, K. M. *et al.* Proteome-wide covalent ligand discovery in native biological systems. *Nature* **534**, 570–4 (2016).

88. Brown, J. M. & Giaccia, A. J. The unique physiology of solid tumors: opportunities (and problems) for cancer therapy. *Cancer Res.* **58**, 1408–16 (1998).

89. Vaupel, P., Kallinowski, F. & Okunieff, P. Blood flow, oxygen and nutrient supply, and metabolic microenvironment of human tumors: a review. *Cancer Res.* **49**, 6449–65 (1989).

90. Chang, P. C. *et al.* DDX3, a DEAD box RNA helicase, is deregulated in hepatitis virus-associated hepatocellular carcinoma and is involved in cell growth control. *Oncogene* **25**, 1991–2003 (2006).

91. Sun, M., Song, L., Li, Y., Zhou, T. & Jope, R. S. Identification of an antiapoptotic protein complex at death receptors. *Cell Death Differ.* **15**, 1887–1900 (2008).

92. Park, S. H., Lee, S. G., Kim, Y. & Song, K. Assignment of a human putative RNA helicase gene, DDX3, to human X chromosome bands p11.3-->p11.23. *Cytogenet. Cell Genet.* **81**, 178–9 (1998).

93. Fazi, R. *et al.* Homology Model-Based Virtual Screening for the Identification of Human Helicase DDX3 Inhibitors. *J. Chem. Inf. Model.* **55**, 2443–2454 (2015).

94. Brai, A. *et al.* Human DDX3 protein is a valuable target to develop broad spectrum antiviral agents. *Proc. Natl. Acad. Sci. U. S. A.* **113**, 5388–93 (2016).

95. Yedavalli, V. S. R. K. *et al.* Ring expanded nucleoside analogues inhibit RNA helicase and intracellular human immunodeficiency virus type 1 replication. *J. Med. Chem.* **51**, 5043–51 (2008).

96. Maga, G. *et al.* Toward the Discovery of Novel Anti-HIV Drugs. Second-Generation Inhibitors of the Cellular ATPase DDX3 with Improved Anti-HIV Activity: Synthesis, Structure-Activity Relationship Analysis, Cytotoxicity Studies, and Target Validation. *ChemMedChem* **6**, 1371–1389 (2011).

97. Bol, G. M. *et al.* Targeting DDX3 with a small molecule inhibitor for lung cancer therapy. *EMBO Mol. Med.* **7**, 648–669 (2015).

98. Kondaskar, A. *et al.* Novel, Broad Spectrum Anticancer Agents Containing the Tricyclic 5:7:5-Fused Diimidazodiazepine Ring System. *ACS Med. Chem. Lett.* **2**, 252–256 (2011).

99. Samal, S. K., Routray, S., Veeramachaneni, G. K., Dash, R. & Botlagunta, M. Ketorolac salt is a newly discovered DDX3 inhibitor to treat oral cancer. *Sci. Rep.* **5**, 9982 (2015).

100. Baell, J. B. & Holloway, G. A. New substructure filters for removal of pan assay interference compounds (PAINS) from screening libraries and for their exclusion in bioassays. *J. Med. Chem.* **53**, 2719–40 (2010).

101. Tomašić, T. & Peterlin Mašič, L. Rhodanine as a scaffold in drug discovery: a critical review of its biological activities and mechanisms of target modulation. *Expert Opin. Drug Discov.* **7**, 549–560 (2012).

102. Li, Y., Geng, J., Liu, Y., Yu, S. & Zhao, G. Thiadiazole-a promising structure in medicinal chemistry. *ChemMedChem* **8**, 27–41 (2013).

103. Saladini, F., Giannini, A., Boccuto, A., Vicenti, I. & Zazzi, M. Agreement between an in-house replication competent and a reference replication defective recombinant virus assay for measuring phenotypic resistance to HIV-1 protease, reverse transcriptase, and integrase inhibitors. *J. Clin. Lab. Anal.* **32**, e22206 (2018).

104. Chaudhari, S. R., Mogurampelly, S. & Suryaprakash, N. Engagement of CF3 group in N-H···F-C hydrogen bond in the solution state: NMR spectroscopy and MD simulation studies. *J. Phys. Chem. B* **117**, 1123–9 (2013).